BASIN ANALYSIS AND HYDROCARBON POTENTIAL OF THE BALI BASIN WITH EXPANDED GEOTHERMAL HEAT FLOW MAP OF INDONESIA

A THESIS SUBMITTED TO THE GRADUATE SCHOOL

IN PARTIAL FULFILLMENT OF THE REQUIREMENTS

FOR THE DEGREE

MASTER OF SCIENCE

BY

MARK INGRAM

DR. RICHARD FLUEGEMAN – ADVISOR

BALL STATE UNIVERSITY

MUNCIE, INDIANA

AUGUST 2018

Table of Contents

List of Figures

List of Appendices

Basin analysis and hydrocarbon potential of the Bali Basin with expanded geothermal heat flow map of Indonesia

Mark Ingram

Ball State University, Department of Geological Sciences, Fine Arts Building, AR 117, Muncie, IN 47306

This project was made possible by data contained in the L. Bogue Hunt database belonging to the Department of Geological Sciences at Ball State University and by funding from the American Chemical Society Petroleum Research Fund grant to K. Nicholson.

Introduction

Statement of the Problem

The Bali Basin is a back-arc basin located on the mid-Sunda Arc, a chain of island volcanoes extending over 5,000 km throughout Southeast Asia (Kundu and Gahalaut, 2011). The Sunda Arc is a tectonically diverse feature; containing regions of right lateral transform motion as well as both normal and oblique subduction zones. This convergence is responsible for the formation of deep ocean trenches, high volcanic activity, and, most importantly to this study, a number of back-arc basins (Hamilton, 1979). The thermal conditions found in many of these basins support the generation of hydrocarbons, while subsequent tectonic motion along the Sunda Arc can send faults into motion that create hydrocarbon traps (Doust and Noble, 2007). For this reason, Indonesia is one of the world's top oil producing

countries, ranking 24th in oil production at 785,900 barrels produced per day (BBL/day) and with nearly 3.7 billion barrels of oil (BBO) in reserve as of 2015 (cia.gov).

Figure 1) Satellite image of Indonesia. Red box outlines study area (Google Earth, 2018).

The sources of Indonesian oil are located almost entirely in large oil fields on the islands of Sumatra and Java, such as the Minas, Rokan, Duri, and Cepu fields (Steinshouer et al., 1997; Van Gorsel, 2016). The Northeast and Northwest Java Basins, as well as the South, Central, and North Sumatra Basins host hundreds of wells, many of which are productive, and contain rich seismic data which has been used to closely constrain the history, structure, and hydrocarbon prospectivity of these locations (Doust and Noble, 2007; Hamilton, 1979; Van Gorsel, 2016).

Immediately east of the East Java Basin is the Bali Basin and the primary focus of this study. It is here that the high oil and gas production seen in plays on

Sumatra and Java comes to an abrupt halt for the remainder of the Sunda Arc (Steinshouer et al., 1997). Only a handful of exploratory wells have been drilled and even fewer seismic surveys have been conducted in the Bali Basin; additionally, the data that has been collected only covers a portion of the basin. Although literature has explored the broad-scale characteristics of the Bali Basin and its immediate geological surroundings (Fainstein, 1997; Kusnida et al., 1995; McGaffey and Nabelek, 1987; Prasetyo, 1992; Silver et al., 1983; Xue et al., 2002) and the basin's stratigraphy has been peripherally examined (Doust and Noble, 2007; Johansen, 2003; Kaldi et al., 1997; Matthews and Bransden, 1995; Posamentier et al., 2010; Sharaf et al., 2005; Sharaf et al., 2006; Susilohadi, 1995), a lack of empirical information regarding the Bali Basin leaves the causes for its low hydrocarbon

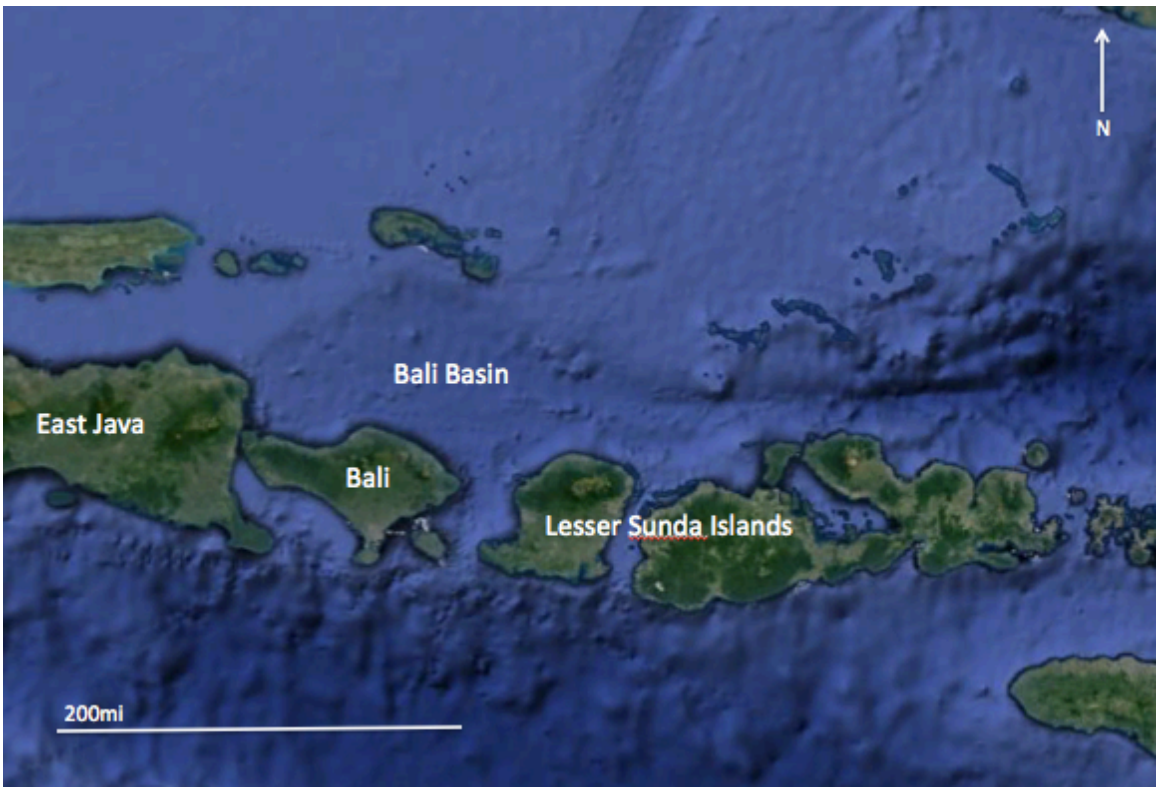

production in question.

Figure 2) Satellite image of the Bali Basin and its surrounding islands (Google Earth, 2018).

Being a frontier basin located directly adjacent to a trend of high hydrocarbon production, it would be expected that the Bali Basin would share some of its neighboring region's economic successes. The Bali Basin shares geologic formations with and has a similar geologic history to productive areas in the Java Sea and Northeast Java Basin, directly west (Doust and Noble, 2007; Johansen, 2003). Even with this knowledge, exploration of the Bali Basin has been limited to its northern margin, with minimal exploration of the center of the basin (Kaldi, 1997; Steinshouer et al., 1997). A petroleum system model created using the data that has been collected, in combination with a comprehensive comparison to locally productive areas could help in determining potential production issues in the Bali Basin. Hydrocarbon generation and maturation is dependent on the surrounding thermal characteristics. For this reason, an examination of the local thermal regime could help to extrapolate the true hydrocarbon potential of the Bali Basin.

This study will help to increase existing knowledge on the nature of hydrocarbon production along the mid-Sunda Arc, as well as constrain the most probable location of hydrocarbons that may be found in the Bali Basin. Expansion of this study's heat flow analysis to include all of Indonesia will help to understand the thermal characteristics of the Sunda Arc and the effect on hydrocarbon generation. Although the scope of this paper is focused on the Bali Basin, the data gathered by this project can be used by future studies with broader ranges.

Previous Work

Oil seeps in East and Central Java were first documented in the mid nineteenth century (Junghuhn, 1854) and by 1871 the first exploratory well was drilled in Central Java. The first productive well was drilled in 1888; the discovery was made in the Kuti field of Northwest Java and was to be followed by many other successful wells, some of which are still producing. Indonesian oil exploration began to decline by 1920 until it experienced a second peak in the 1980's (Van Gorsel, 2016).

Verbeek and Fennema (1896) conducted one of the earliest all-inclusive studies of the Indonesian islands of Java and Madura. Their text, simply titled "Geology of Java and Madura" is one of the earliest examinations of the lithology and structure of the islands and included several large atlases of the region (Van Gorsel, 2016). A half century later, van Bemmelen (1949) broadened the range of this type of study in a report on the general geology on all of Indonesia. These papers find their way into the reference pages of numerous geologic studies over the Indonesian islands; however, Hamilton (1979) conducted the most laterally extensive review of the geology of the Southeast Pacific Region in a USGS tectonic survey of the area, including the geomorphology, biostratigraphy, seismology, and geologic history of Indonesia, New Guinea, the Philippine islands, and Australia, as well as the surrounding marine regions. Hamilton (1979) includes hundreds of geologic and isopach maps, seismic reflection profiles, cross sectional diagrams, tectonic maps, and Landsat images. The report also covers the history of geologic principles and

how they relate to the region, including: geosynclinal cycles, plate tectonics, gravity surveys, and Beinioff zones.

Further large-scale information regarding Indonesia and the Southeast Pacific Region can be found in the works of Hall (1997, 2002 (b), 2011, 2014) and Metcalfe (2011). Using computer modeling and animation to conduct a plate reconstruction and tectonic evolution of Southeast Asia through the Cenozoic these authors describe the earlier regional geologic history of Southeast Asia and the mechanisms at work to shape the origins of Sundaland. These works describe the amalgamation of Sundaland to have occurred in many, chronologically extensive steps that assembled Gondwonan and Australian allocthons with Southeast Asian continental crust beginning in the Paleozoic and reaching completion about 80Ma.

Free gravity anomaly data has been collected and analyzed (Kusnida et al., 1995) in order to investigate the nature of the geological transition between the Sunda Shelf and Bali Trough. Kusnida et al. (1995) identify a distinct transition from low to high gravity readings along the 150m bathymetric contour between the Kangean Block and Bali Sea. They interpret the Sunda Shelf to consist of rhyolitic, continental crust, whereas the Bali Sea contains gabbroic crust of oceanic origin. This difference in crustal origin plays a key role in the development of an additional subduction zone, opposing that of the Australian-Eurasian Plate margin (Hamilton, 1979; Zubaidah et al., 2013).

Back-arc thrusting along the eastern Sunda Arc as a result of continued northward movement of the Australian continent (Keep et al., 2003) is an important mechanism to the structural characteristics of the Bali-Flores Basins. By

interpreting seismic profiles, Silver et al. (1983) determined that although the Bali Basin is well west of the collision zone, the Flores Thrust has laterally propagated into the basin. Four broad folds are identified that represent compression along the fault in this area. McGaffey and Nabelek (1987) conclude that the Bali Basin is a down warp in the crust of the Sunda Shelf maintained by thrusting along the Flores Thrust Zone. They recognize the Bali Basin as part of a nascent fold thrust belt developing on the continental side of an arc trench system at which oceanic lithosphere is being subducted; comparable to the early forelands of the Andes or Western North America (McGaffey and Nabelek, 1987).

Petroleum systems elements can be linked to common stages in the geological evolution of synrift to postrift Tertiary basins. Doust and Noble (2007) identify four petroleum system types (PST) based on the four stages of geodynamic basin development: (i) an oil-prone early synrift lacustrine PST, found in the Eocene to Oligocene deeper parts of the synrift grabens, (ii) an oil and gas-prone late synrift transgressive deltaic PST, located in the shallower Oligocene to Early Miocene portions of the synrift grabens, (iii) a gas-prone early postrift marine PST, characteristic of the Early Miocene transgressive period, and (iv) an oil and gas-prone late postrift regressive deltaic PST, forming the shallowest Late Tertiary basin fills. Using seismic and drill hole data, Prasetyo (1992) also supported a step-by-step characterization of the tectonic history of the Bali and Flores Basins described by four major phases:

1. Paleocene extension and normal faulting with thick Paleocene to Miocene sediments filling the downthrown areas.

2. Collision of a continental fragment and the Sulawesi Arc to the north resulting in regional compression and wrench faulting. These compressional forces inverted the basin in the Miocene, causing uplift of basement rocks and the basin floor, as well as folding deformation of basin fill sediments.
3. Downward flexure of the Sunda Shelf beneath the basin sediments and island volcanics due to compressional loading through the Miocene to present day, which makes up most or all of the Bali Basin's modern relief.
4. Paleogene to Neogene transpression, which causes basin inversion coupled with transform motion along some reactivated faults.

Well and seismic data has been used to define the East Java Sea Basin's stratigraphy by breaking the units into three megasequences underlain by a metamorphic basement complex (Matthews and Bransden, 1995). The Upper Cretaceous marine sediments of megasequence 1 and Lower Eocene-Miocene transgressive sediment packages of megasequence 2 are separated by an Early Eocene regional unconformity formed by contraction and near peneplanation of megasequence 1 and the underlying basement. This unconformity records the collision of the Indian microcontinent with Asia in the closing of the Tethy's Ocean (Hutchinson, 1992). Inversion of these fault controlled sub-basin deposits commenced in the Early Miocene and continues today; the resulting syn-inversion sediments comprise megasequence 3 (Matthews and Bransden, 1995). Regional subsidence occurring throughout the inversion process has resulted in the gradual reversal of depocenter locality and the most recent (Pleistocene to present time) depositional history shows record of rapid relative sea-level changes. Alternating

extension and contraction throughout the East Java Sea resulted in primarily dip slip fault movement and basin-scale cross-sectional geometries resembling positive flower structures resulting from the reverse reactivation of these fault systems could potentially act as hydrocarbon traps (Matthews and Bransden, 1995). Fainstein (1997), through seismic interpretation, identified several traps off north shore Madura Island that related to these regional inversion tectonics. The traps were found where zones of inversion created broad young anticlines containing shale and limestone and on stratigraphic structures located on the upthrown blocks of inverted half grabens. Additional Eocene shale plays were identified along structural closures and where stratigraphic wedges onlapped basement rocks. By analyzing seismic data, Xue et al. (2002) identified 14 additional structural and stratigraphic hydrocarbon traps off north shore Bali formed by the reverse reactivation of extensional faults, where low-lying strata were thrust above overlying layers.

Kaldi et al. (1997) examine the seal capacities of various formations in the Pagerungan gas field, a small but productive area off-shore of the western Kangean Islands, along the northern margin of the Bali Basin. Using techniques described in Downy (1984) and Vavra et al. (1992), Kaldi et al. (1997) calculated the amount of gas that could be contained by the Paciran Formation and the Ngimbang Shale, Carbonate, and Clastic Members. They conclude these formations to be capable of holding a gas column of 300, 700, 100, and 95 feet respectively, decisively making the Ngimbang Shale Member the most effective sealing formation analyzed by the study. Kaldi et al. (1997) estimate the Pagerungan gas column to be 1,200 feet, 500

feet in excess of the best seal's retention capacity. Capillary failure of the primary seal has led to the charging of shallow reservoirs and the development of gas chimneys characteristic to the Pagerungan field. It is also concluded that the Pagerungan system is dynamic and that gas will continue to migrate upwards, at geologic rates, until the system has reached equilibrium. The information reported by Kaldi et al. (1997) indicates not only that the Bali Basin is capable of producing hydrocarbons, but that it is currently doing so in excess of a primary seal's retention capacity.

Geologic Setting

Regional Tectonics

The Bali Basin is a small back-arc basin located along the mid-Sunda Arc. The Sunda Arc is a chain of island volcanoes that formed as a result of the Indo-Australian Plate subducting beneath the Eurasian Plate; it extends 5200km from the Andaman Sea and northwestern Sumatra to the island of Flores, where it becomes the Banda Arc (Kundu and Gahalaut, 2011). The currently active, convergent boundary was initiated in the Late Oligocene and is responsible for high levels of volcanism and seismicity along the Indonesian southern margin (Hamilton, 1979).

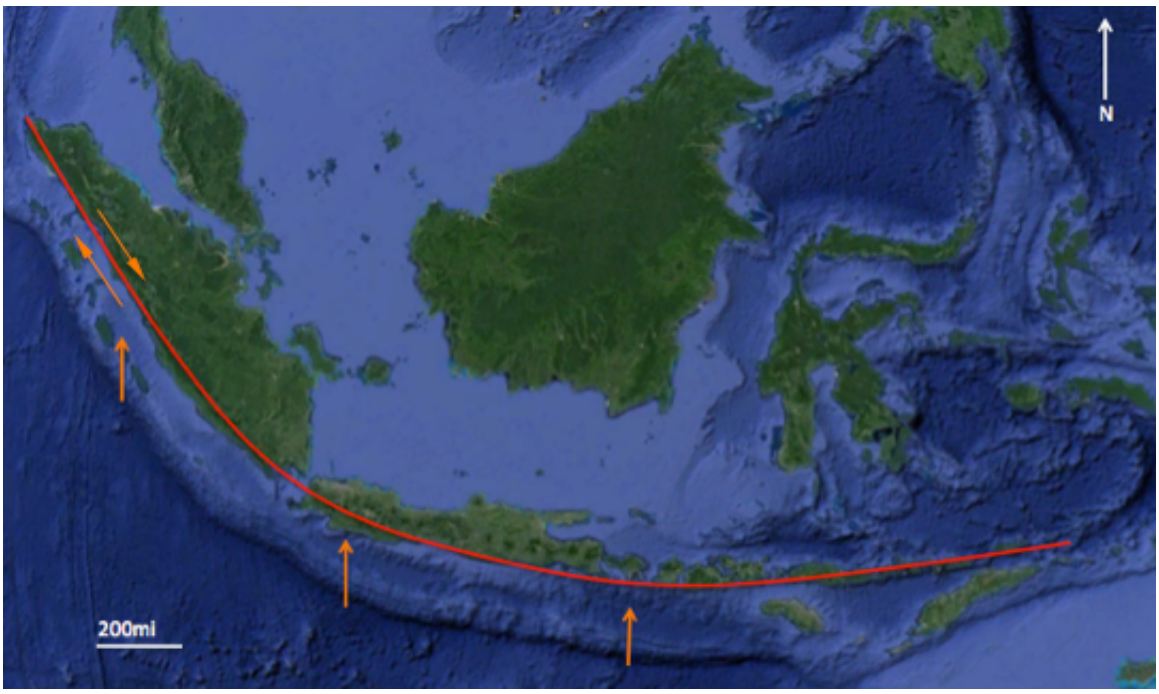

Figure 3) Satellite image of Indonesia with the Sunda Arc outlined in red. Orange arrows indicate relative motion along the plate boundary (Google Earth, 2018).

Sundaland describes the geographic and geologic area encompassing the continental region of Southeast Asia, now mostly submerged by a shallow sea. Indonesia, Malaysia, the Philippine Islands, the Thai Malay Peninsula, and parts of Indo-China, including Thailand, Cambodia, and Vietnam, currently occupy the areas of Sundaland that lie above sea level (Hall, 2011; Hall, 2014). The assemblage of Sundaland began in the Paleozoic, with the initial separation of large continental allocthons from Gondwana. These blocks collided with the autochthonous Southeast Asian continent in the Triassic. Following this initial amalgamation, continental fragments separated from Australia in the Jurassic and began accreting to the southeastern Sundaland margin in the Cretaceous (Hall, 2014). For this reason, the northwestern reaches of Sundaland, nearest the Asian continent sit on old, stable Gondwanan basement rocks, whereas sediments along the south-

southeastern portions of Sundaland overlie Mesozoic allochthonous basement rocks (Hall, 2011; Hall, 2014; Metcalfe, 2011).

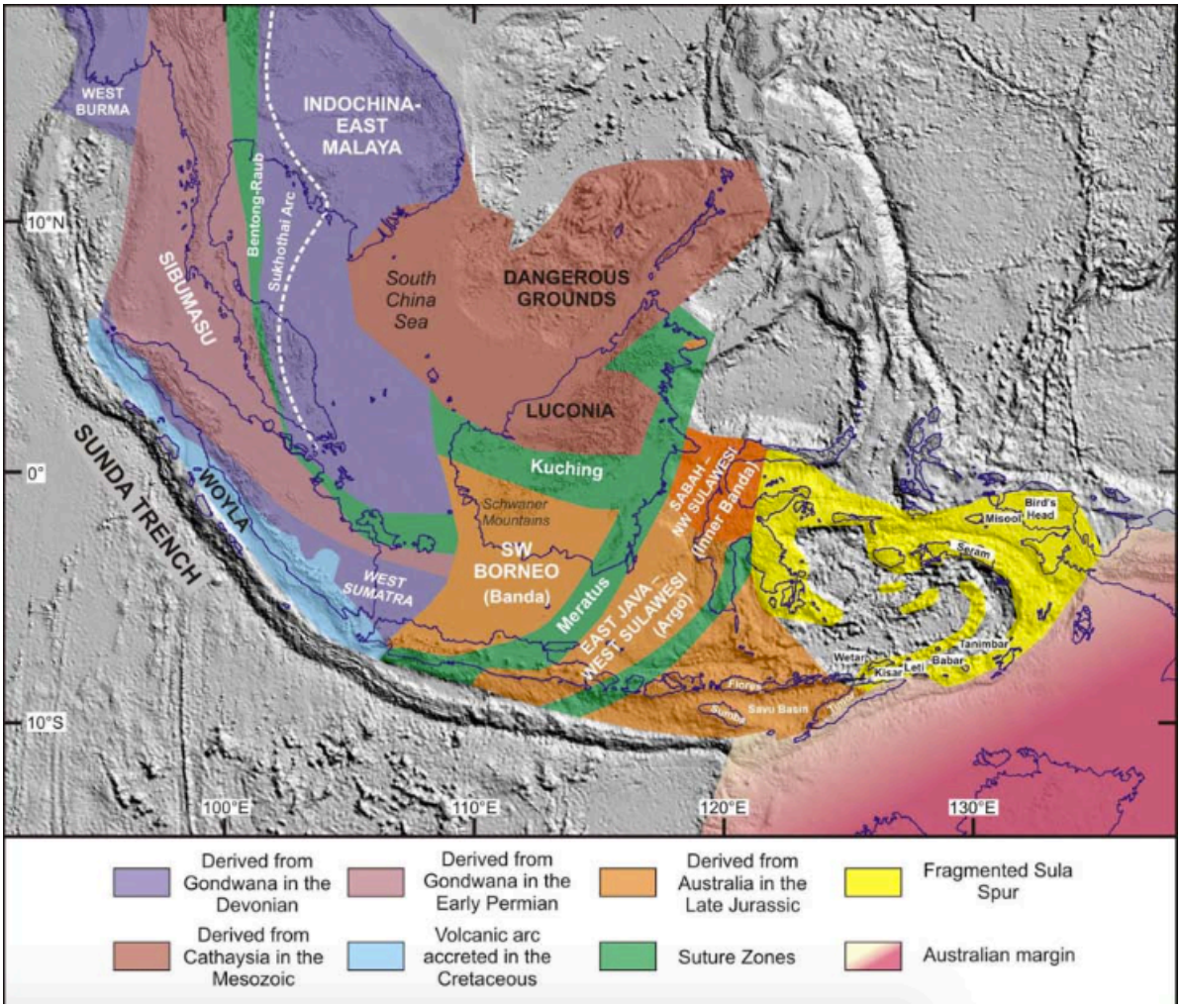

Figure 4) Regional map showing the age and origin of the various Sundaland geologic components (Hall, 2014).

West of Java tectonic activity becomes more complicated as convergence becomes oblique around Sumatra and eventually transitions to dextral strike slip displacement (Newcomb and McCann, 1987). This right lateral transform system can be broken into as many as 20 separate en echelon segments (Tjia, 1978) and extends through Sumatra to join the fracture zones of a back-arc spreading center in

the Andaman Basin (Curray et al., 1978). Vertical deformation in the western Sunda Arc shows crustal thinning in the back-arc and crustal thickening in the forearc. Oblique convergence, partial subduction, and transtensional back-arc spreading are the controlling factors of tectonics in the western Sunda Arc (Krishna and Sanu, 2002).

East of Flores the Sunda Arc turns into the Banda Arc and tectonic activity is largely influenced by convergence of the Australian continent to the south and subduction of the Philippine and Pacific Plates to the north. Most of the thrusting in this area occurs in the fore-arc (Timor Sea), with some thrusting in the back-arc (Banda Sea). Northward movement of the Banda Arc in this region is roughly equivalent to that of Australia, suggesting that subduction has ceased and the Australian continent is currently accreting onto Southeast Asia. This accretion is responsible for the Flores Thrust Zone (Keep et al., 2003).

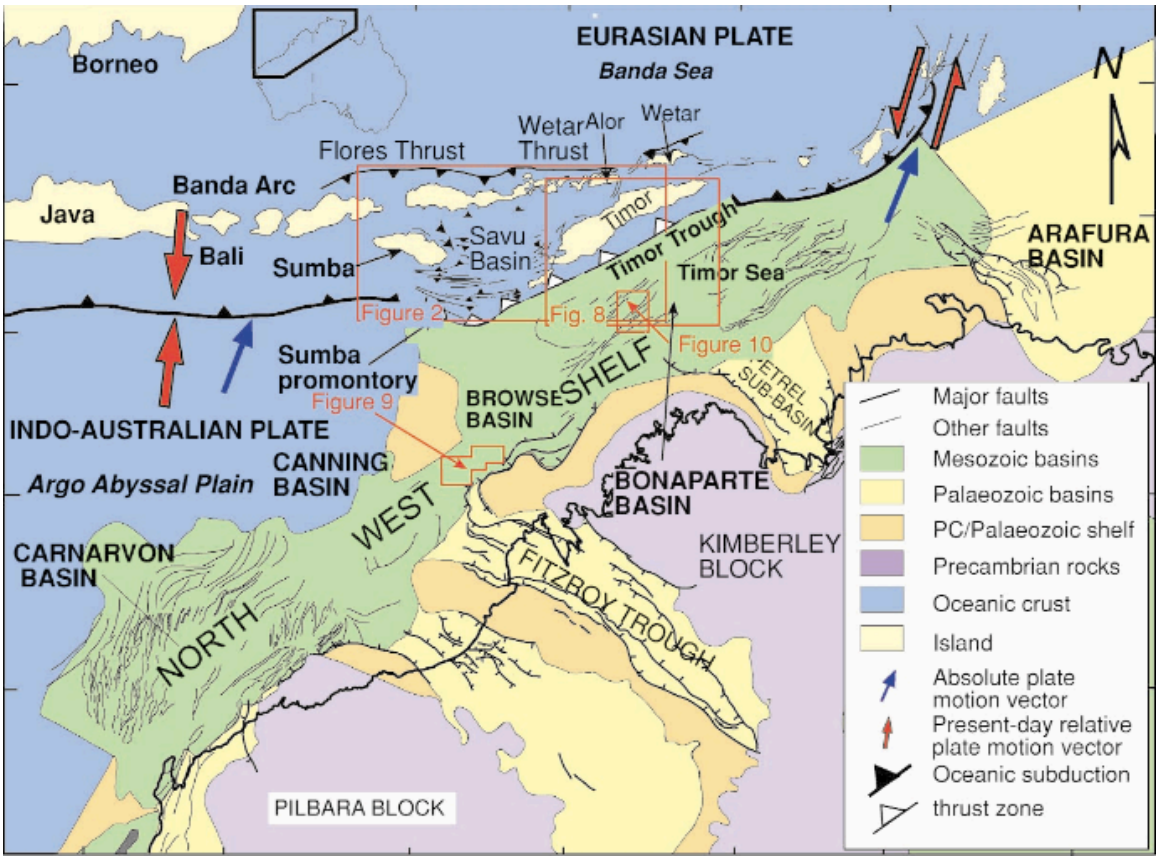

Figure 5) Map showing the plate motions and basic structural and geologic components of Northwest Australia and the Banda Arc (Keep et al., 2003).

Accretion of the Australian continent to Sundaland is locally responsible for the uplift of the Sumba ridge, development of the Savu Basin, and propagation of the Flores Thrust Zone into the Bali Basin (Silver et al., 1983; Keep et al., 2003; Hall, 2011; Lüschen et al., 2011). Continued convergence of the Australian Plate with Southeast Asia has formed a back-arc subduction zone opposite the Java Trench where oceanic crust of the Bali-Flores Basin is forced beneath elevated continental crust of the Flores Thrust Zone (Zubaidah et al., 2013).

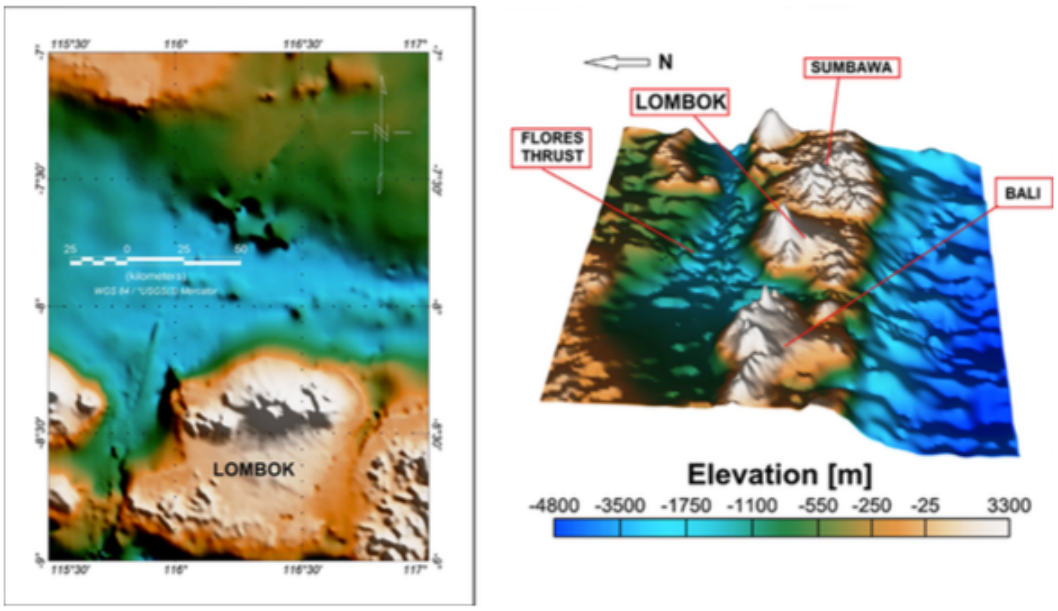

Figure 6) Map (left) and 2D model (right) showing elevation around the islands of Lombok and Bali. Where the elevated Flores Thrust meets oceanic crust in the Lombok back-arc is where opposing subduction begins (Zubaidah et al., 2013).

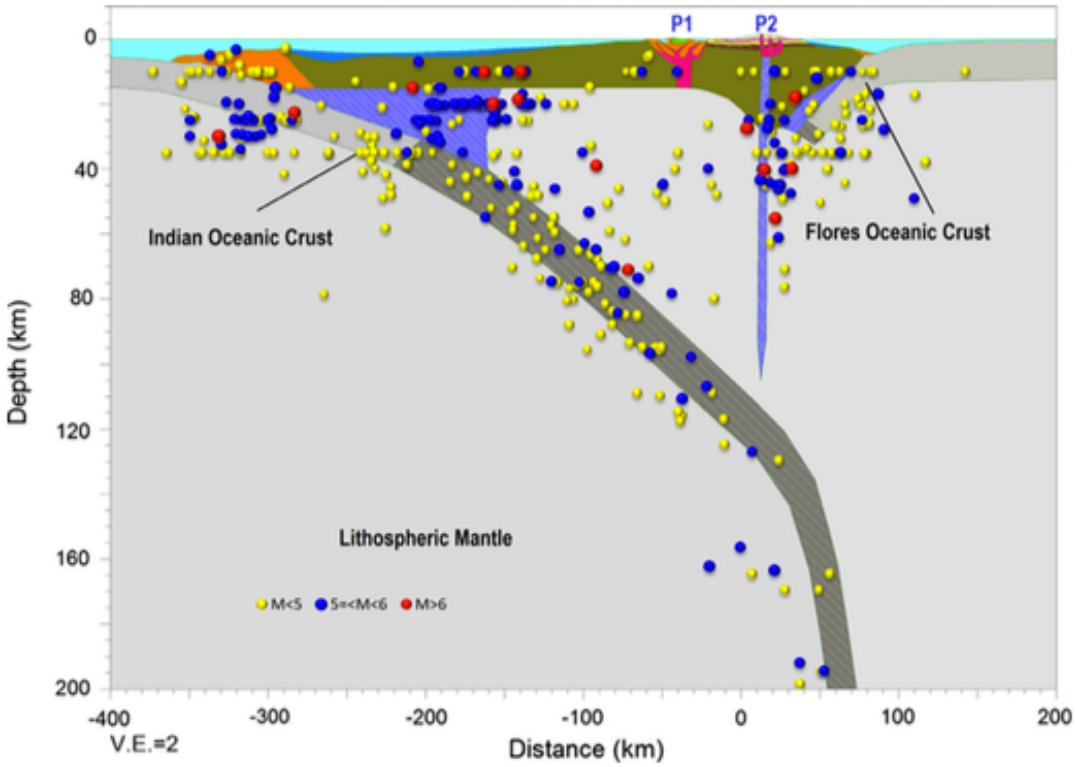

Figure 7) Cross section across Lombok and the Flores Thrust (Figure 6) showing the depth and magnitude of recorded earthquakes. Primary subduction of the Indo-Australian oceanic crust is located to the left (south) and opposing back-arc subduction of the Flores oceanic crust is to the right (north) (Zubaidah et al., 2013).

The partial melting and upwelling of upper mantle material caused by the introduction of oceanic lithosphere to the asthenosphere results in areas of high heat flow concentrated along the volcanic arcs and back-arc basins created by subduction zones (Hyndman et al., 2005). As a back-arc basin positioned directly adjacent to an island arc system and containing an additional subduction zone, the Bali Basin can be expected to have particularly high heat flow. This higher than average heat flow has the potential to crack the kerogen contained in source rocks into petroleum and natural gas (Rullkötter, 1993).

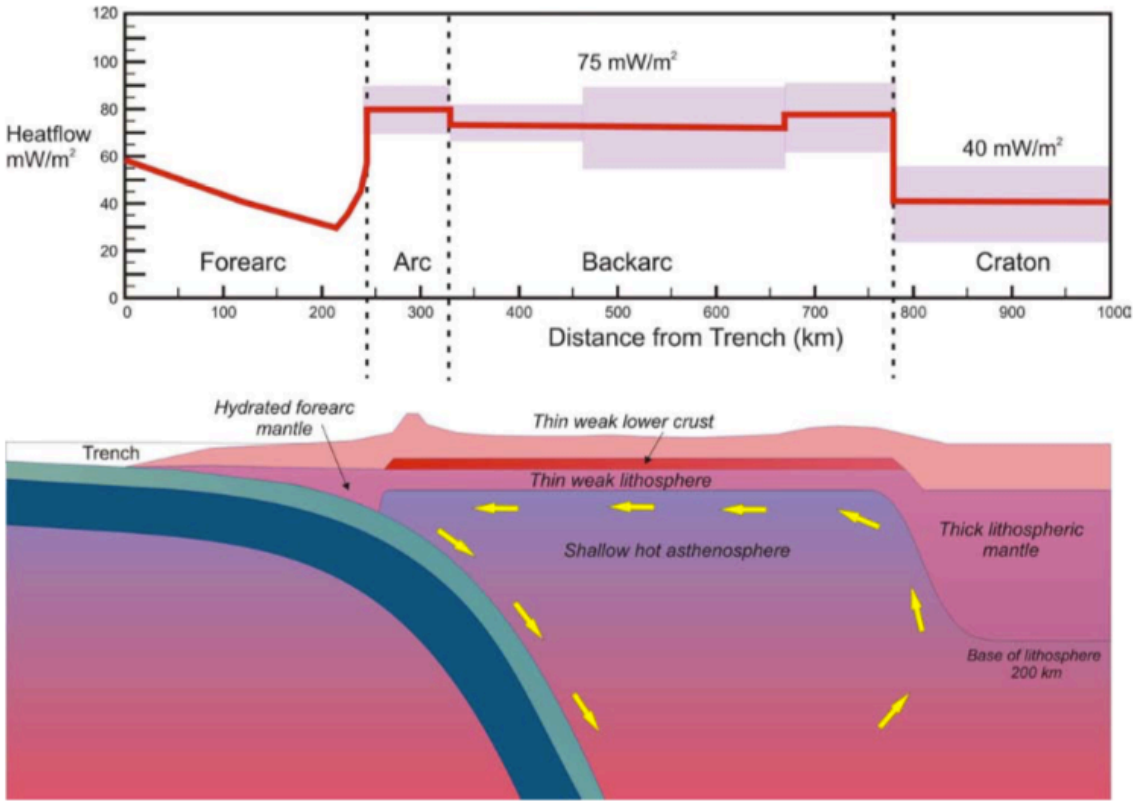

Figure 8) Illustration describing the amount of heat flow to be expected across a typical subduction zone. Image taken from Hall (2014) based on modeling by Hyndman et al. (2005).

The subducting Indo-Australian Plate can be broken into three distinct structural and compositional zones: the Roo Rise, Argal Abyssal Plain, and Scott Plateau. The Roo Rise is a portion of continental crust standing 1,500m above the surrounding sea floor, located along the Sunda forearc south of Java. The Argal Abyssal Plain describes the bathymetric low (5,500m water depth) that separates the Roo Rise from the Scott Plateau, which marks the northwestern margin of the Australian continent (Lüschen et al., 2011).

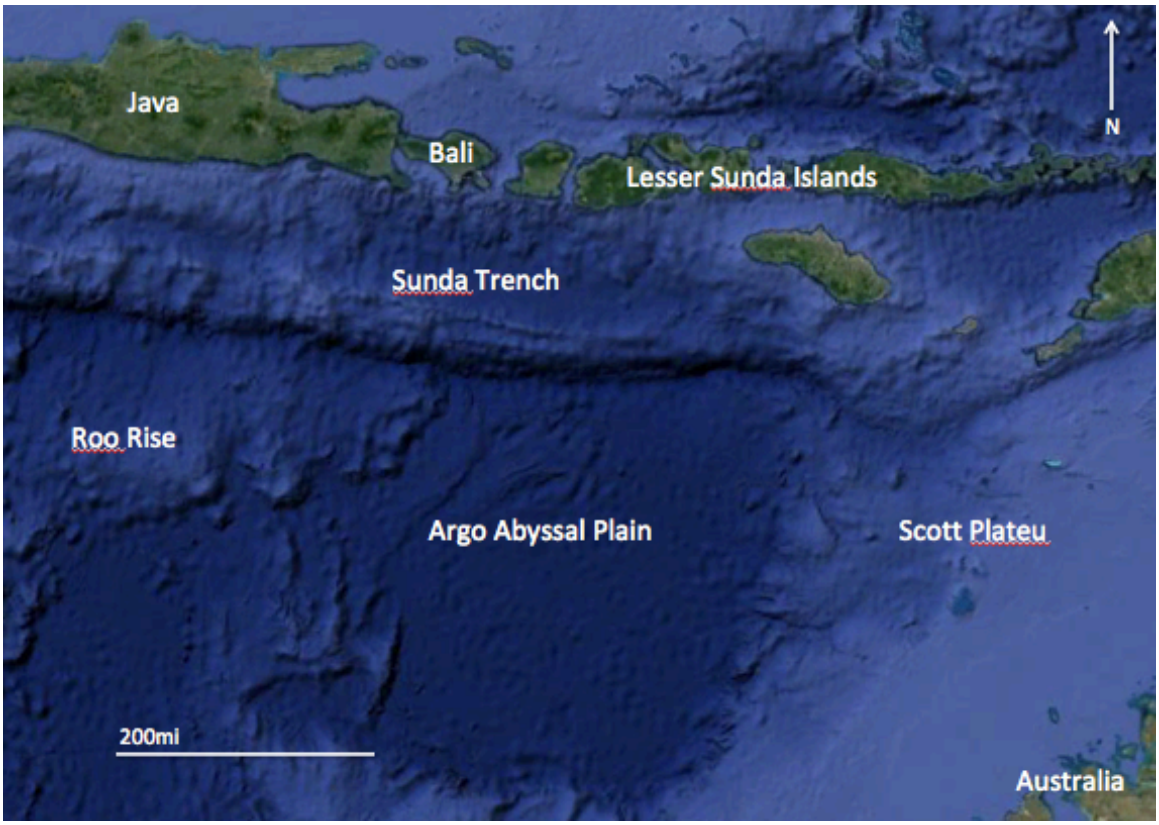

Figure 9) Satellite image of the Indo-Australian Plate south of the study area (Google Earth, 2018).

Areas north of Lombok and the Flores Thrust Zone show broad asymmetric folding, with south dipping thrust faults truncating the steeper limbs; this geometry is analogous to model subduction (McGaffey and Nabelek, 1987). Increasing dip

with depth in this area indicates the deformation occurred concurrent to sedimentation (McGaffey and Nabelek, 1987). To the west, the Flores Thrust Zone loses these characteristics at the surface but maintains broad folding throughout the entire sedimentary section, suggesting the presence of sub-sediment detachment faulting (Silver, et. al., 1983).

Local Tectonics

The Bali Basin is an east-west trending, half circle shaped basin located under the Bali Sea. It is bound to the north by the Kangean-Sepanjang Ridge, an east-west trending submarine ridge that rises above sea level to form the Kangean Islands on the southern margin of the Sunda Shelf. To the east, the Bali Basin merges with the Lombok Trough, which separates the Bali and Flores Basins. To the west, the Bali Basin is terminated by the easternmost expression of the Madura Straight and Northeast Java Basin. To the south, Bali, a volcanic island located along the mid-Sunda Arc, binds the Bali Basin (Prasetyo, 1992).

The Bali Basin is positioned on the southeastern Sunda Shelf along the eastern Sunda Arc, where convergence of oceanic Indo-Australian crust is perpendicular to the overriding continental crust from Java to Flores and back-arc subduction has been identified along the Flores Thrust (Hamilton, 1979; Zubaidah et al., 2013). The area marks the plate margin transition between two subduction zones of similar kinetics. To the west, old (>150Ma) Indian oceanic crust subducts beneath the Eurasian continental margin. To the east, the Australian continental margin also subducts beneath Eurasian Plate margin, until a point at which subduction turns to accretion. These mechanics are responsible for the ongoing

closure of the Bali Basin, making it an excellent example of a nascent fold thrust belt (Prasetyo, 1992).

The southern reaches of the Sunda Shelf are covered by an average 200m of water and 1-3km of sediment (Ben Avraham and Emery, 1973; Kusnida et al., 1995), but sediment thicknesses in the Bali Basin are estimated to be ~6km (McGaffrey and Nabelek, 1987). Along this area's margin, subduction is deep reaching, with a trench that reaches 8km and a Wadati-Benioff zone of 600km (Lüschen et al., 2011). Subduction in this area began in the late Oligocene and the rate of convergence has increased by 2cm/yr over the last 10 million years (DeMets et al., 2010).

Seismic reflection profiles record a compressional, fold thrust tectonic regime that includes segments of uplifted basement. The basement, as a western extension of the oceanic Flores Basin (Ben-Avraham and Emery, 1973) is dense and contributes to the Bali Basin's high gravity anomaly (Kusnida et al., 1995; Prasetyo, 1992). Reflectors representing the Sunda Shelf beneath the Bali Basin can be traced from the deepest reaches of the basin's southern margin to shallower depths along the basin's northern margin, beneath the Kangean-Sepanjang Ridge. The continual arching of the Sunda Shelf beneath the Bali Basin fill suggests that the basin's bathymetry is almost entirely due to downward flexure of the Sunda Shelf, as opposed to crustal thinning (Prasetyo, 1992).

Compressional deformation along the southern margin is the primary expression of the Indo-Australian Plate's northward migration in the Bali Basin. This zone of deformation is termed the Bali Fold and is expressed throughout the entire sedimentary column. Untruncated folds toward the north of the basin, which

include the entire sedimentary section, are interpreted to have been caused by the Flores Thrust Zone, the secondary compressional expression of the Indo-Australian-Eurasian Plate boundary in the Bali Basin. To the basin's west, the Bali Fold loses surface expression, indicating compressional stress in the Bali Basin to decrease from east to west (Prasetyo, 1992).

Regional Petroleum Systems Formation

Tectonic stress and extension caused by the northward migration of the Australian and Indian Plates, coupled with counterclockwise rotation of Borneo, formed a series of north-south oriented rift basins and half graben complexes along the southern margin of the Sunda Shelf in Eocene to Oligocene time (Bishop, 2000; Hall, 1997; Longley, 1997). The rotational direction of Borneo has been disputed (Murphy, 1998), but the nature and formation of these Tertiary rift basins remains unchanged.

Regional clastic sedimentation derived from the Sunda Shelf to the north filled the half grabens as they subsided during a post rifting Late Oligocene to Early Miocene sag phase. These structural lows became the depocenters for essential lacustrine source rocks, whereas structural highs would later host carbonate facies buildups. Increased erosion and dissolution of these reefs during intermittent lowstand periods created areas of enhanced porosity, making excellent hydrocarbon reservoirs, whereas widespread highstands deposited regional shales and calcareous clays that would become impermeable seal formations. The stress regime switched to compressional in the Late Oligocene (Hamilton, 1979), causing regional basin inversion and creating fault migration pathways and hydrocarbon

traps in the Miocene. This compressional tectonic regime has continued intermittently through the Pliocene and into current time (Bishop, 2000; Johansen, 2003).

Local Petroleum Systems Formation

Linear belts of extensional faulting across the Southeast Sunda Shelf in the Paleocene opened up the Bali-Flores basin in what was to become a rifted back-arc passive margin. Through the Eocene, this margin accumulated organic-rich terrestrial and shallow marine shales that would become source rocks (Prasetyo, 1992).

In the Late Oligocene, the tectonic regime shifted from extension to compression, initiating the Indo-Australian-Eurasian subduction zone; the continuation of this convergence resulted in basin-wide inversion tectonics in the Miocene (Hamilton et al., 1979). This inversion resulted in the creation of hydrocarbon traps by the reverse reactivation of pre-existing normal faults (Fainstein, 1997; Xue et al., 2002). Additionally, the thrusting and concomitant uplift due to compression resulted in regressive conditions (Prasetyo, 1992). The shallow water limestones and siltstones that were deposited as a result of this relative fall in sea level would soon become reservoirs for potentially generated hydrocarbons (Bishop, 2000; Johansen, 2003; Posamentier et al., 2010). Regional compression continued and significantly increased when the Australian continental margin ceased to subduct any further and instead began to accrete onto the Banda Arc during Upper Miocene time (Keep et al., 2003). This directly caused propagation of the Flores Thrust Zone into the Bali Basin, forming a second zone of

subduction opposing the plate boundary and further increasing thrusting and uplift (Hamilton, 1979; Zubaidah et al., 2013). This supplied additional heat flow to the basin and forced significant down warping along the southern margin of the Sunda Shelf, resulting in the current bathymetry of the Bali Basin (Prasetyo, 1992).

The deposition of marine carbonates and siliciclastics continued through the Miocene, including carbonaceous shales to seal hydrocarbons that would have begun to be generated as the Eocene shales reached depth and were heated by ongoing subduction (Posamentier et al., 2010; Sharaf et al., 2005; Sharaf et al., 2006). Porous sandstones and impermeable clays were subsequently deposited in the Pliocene, providing a potential secondary reservoir and seal (Pringgopriwiro, 1983).

A tectonic history of brief extension followed by consistent compression makes the most likely location for hydrocarbon entrapment in the Bali Basin where underlying strata have been forced above overlying layers by the reverse reactivation of normal faults; this would allow for potential hydrocarbons to be trapped in between the imbricated thrust sheets (Fainstein, 1997; Xue et al., 2002).

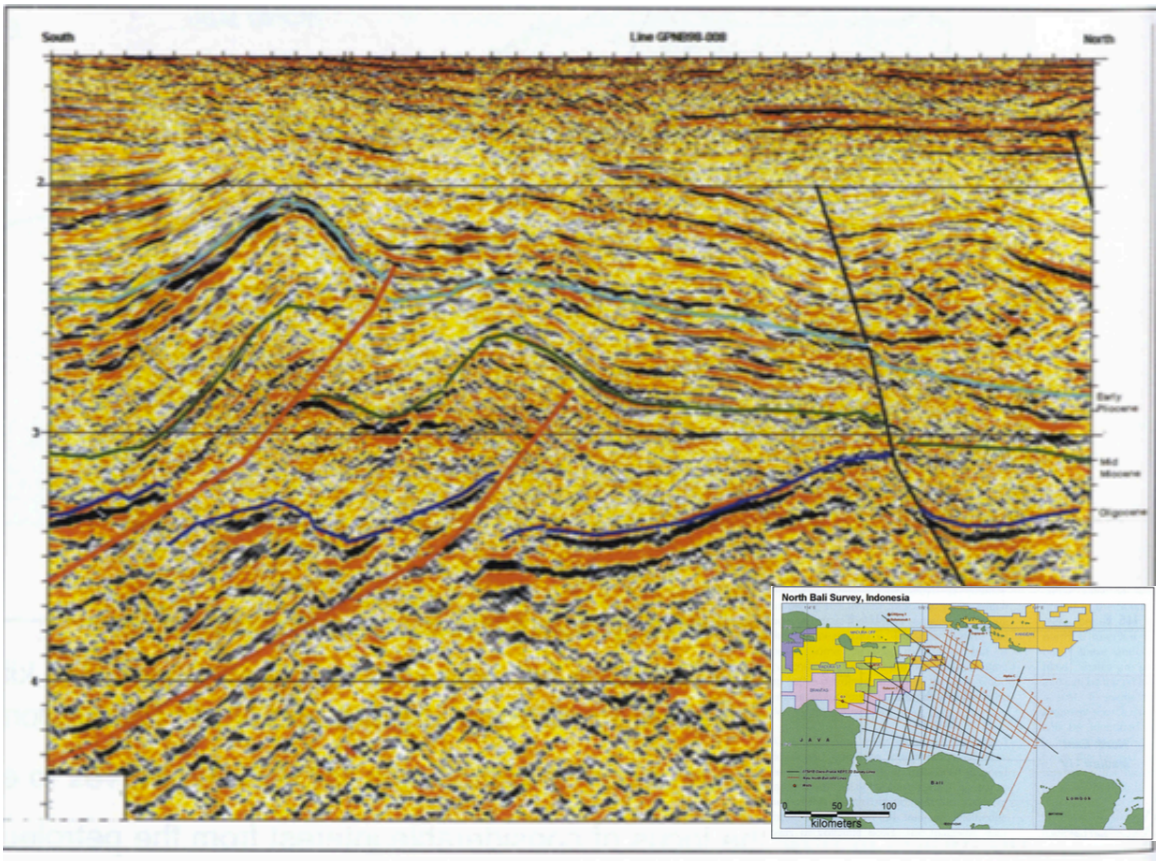

Figure 10) Seismic cross section of the Java Sea just north of Bali, inset shows the survey area. The blue and green horizons represent Cenozoic strata and the pink horizon represents the top of the Mesozoic basement. Thick red lines represent normal faults generated during an earlier extensional regime that were later inverted by regional compression (Xue et al., 2002).

Stratigraphy

The Bali Basin fill consists of Cenozoic carbonate and siliciclastic sequences that accumulated in the downthrown areas of Paleocene rift systems. These strata range from Eocene to Pliocene in age and unconformably overlie a Late Cretaceous basement complex consisting of siliciclastic, volcanic, and low-grade metamorphic rocks. The following formations are listed in order from youngest to oldest:

<u>"GL" Group</u>

The Upper Miocene to Pliocene "GL" Group includes the Lidah, Paciran, Ledok, and Wonocolo Formations.

Lidah Formation

Biostratigraphic studies reveal the Lidah Formation to be Pliocene in age (Susilohadi, 1995). The Lidah Formation consists of unstratified blue-grey mud and claystone; these deposits are interpreted as lacustrine and tidal in origin and are referred to by some literature as the Blue Clays (van Bemmelen, 1949). The Lidah Formation is more prevalent in the Kendeng Zone of the Northeast Java Basin, where it conformably overlies the Atasangin Formation, a series of marginal marine marl that is absent in the Bali Basin (Susilohadi, 1995).

Paciran Formation

The Paciran Formation is divided into an upper foraminiferal limestone unit and a lower sandstone unit. Planktonic forams in the upper unit reveal the formation to be Lower Pliocene in age (Susilohadi, 1995). Nomenclature for this formation varies geographically; termed the Mundu Formation (Aziz et al., 1993) on Madura Island and the Paciran (Pringgoprawiro, 1983) or Karren Formation (van Bemmelen, 1949) in the Tuban area of north Java. In the Mundu area, 10km west of Cepu, Java, the Paciran Formation manifests as an unstratified yellowish-white to greenish-grey calcareous clay; to the east, Paciran limestones act as a primary reservoir in the South East Madura Block (Pringgoprawiro, 1983).

Ledok Formation

The Ledok Formation conformably overlies the Wonocolo Formation; the presence of planktonic foraminiferal species *Globorotalia plesiotumida* indicates an age of Upper Miocene (Pringgoprawiro, 1983). In northeast Java the Ledok Formation is represented by calcareous clay with calcarenite intercalations that

increase up section. This shallowing up sequence indicates the Ledok Formation in this area to have been deposited in a high energy, neritic environment (Susilohadi, 1995). An observed decrease in the planktonic/benthic ratio from 47% to 30% upwards through the formation further supports this interpretation (Pringgoprawiro, 1983). In the Java Sea, a reefal limestone unit represents the Ledok Formation (Najoan, 1972).

Wonocolo Formation

The presence of forminiferal species *Cycloclypeus annulatus* in the Wonocolo Formation indicates its age to be Upper Miocene (Sharaf et al., 2006). The Wonocolo Formation is represented by thick successions of shale and unstratified calcareous clay with minor sandstone intervals underlain by a basal carbonate layer consisting of paralic grain and wackestone called the Bulu Member (Sharaf et al., 2006; Susilohadi, 1995). In the Northeast Java Basin, sandy fossiliferous limestone and well-bedded carbonate containing large amounts of benthic foraminifera and planar corals represent the Bulu Member (Sharaf et al., 2006). The Bulu Member is the primary representation of the Wonocolo Formation in the Bali Basin and is similarly represented by well-bedded, sandy, fossiliferous carbonate with interbedded calcareous clay and rare calcarenite intercalations. The Wonocolo Formation was mostly deposited on an inner to outer shelfal environment during a highstand period immediately following a mid-Miocene sea level drop (Susilohadi, 1995).

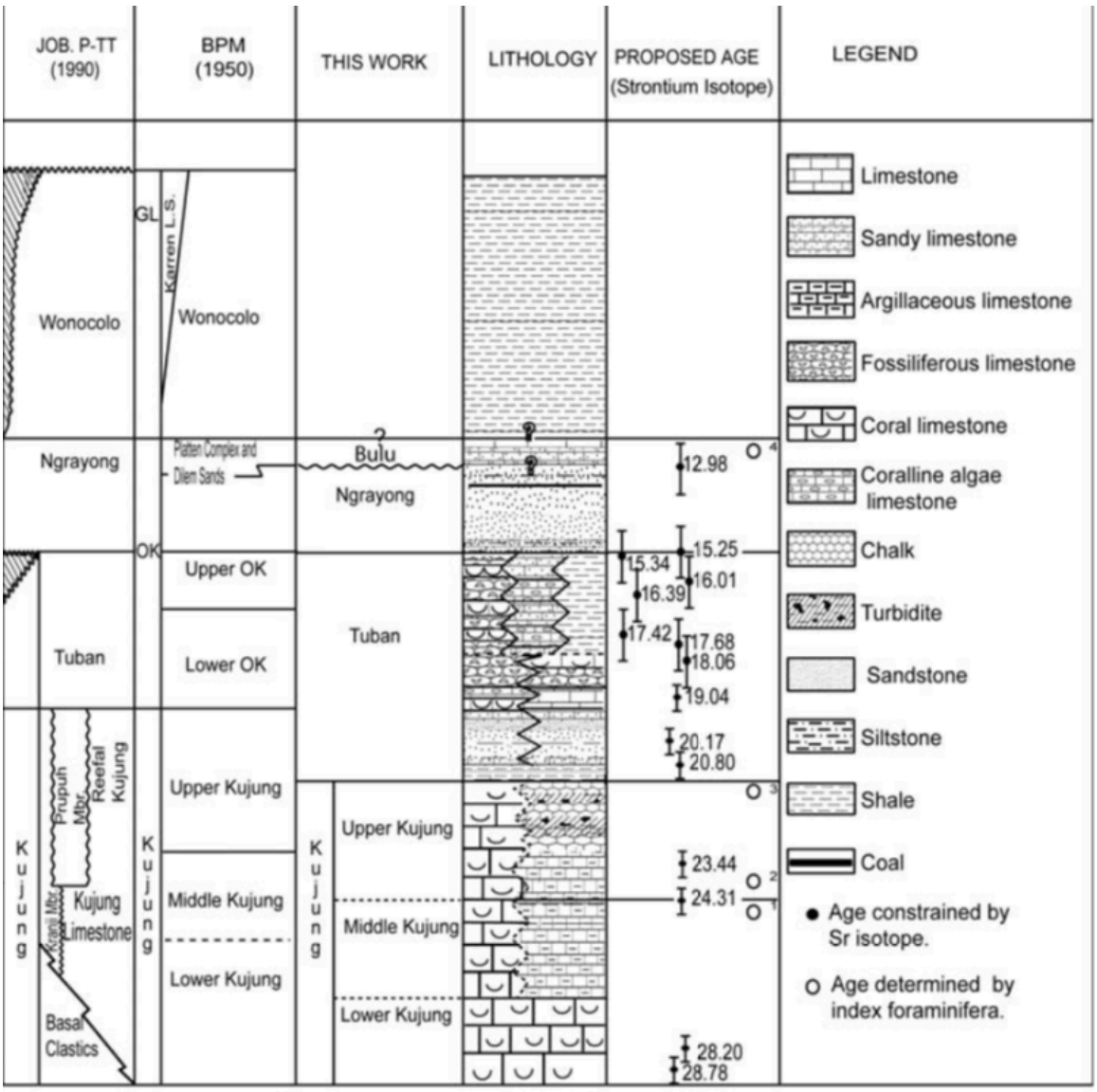

Figure 11) Stratigraphic column from Sharaf et al. (2006) comparing formation ages and nomenclature with previous works. Note the distinction of the Bulu Member.

Orbitoid Kalk ("OK") Group

The Late Oligocene to Early Miocene "OK" Group consists of the Ngrayong, Tuban, and Prupuh Formations and is divided into an upper and lower member. The Ngrayong Formation represents the Upper “OK” Member, whereas the Tuban and Prupuh Formations represent the Lower “OK” Member.

Ngrayong Formation

The Ngrayong Formation consists of argellacious, fine sandstone and shale that coarsens upwards to interbedded medium sandstone and mudstone with minor coal seams. Based on biostratigraphic studies, the Ngrayong Formation is Early to Middle Miocene in age (Ardhana et al., 1993). The shale contains benthic foraminiferal skeletal fragments and the sandstone shows planar cross-stratification, bioturbation, and contains calcareous concretions. The uppermost portion of the Ngrayong Formation consists of coarse, friable sandstone beds (Sharaf et al., 2006).

North of Madura, laterally extensive beds of quartzarenite represent the Ngrayong Formation, which indicates a large siliciclastic influx to the area; these deposits are heavily bioturbated, well sorted, and contain sedimentary structures such as tabular bedding and asymmetric ripples (Sharaf et al., 2005). The Ngrayong Formation is interpreted to be a prograding tidal delta (Sharaf et al., 2006). Well log data show the Ngrayong Formation's contact with the underlying Tuban Formation to be gradational, but observations of this contact in outcrops of Northeast Java reveal the contact to be represented by a few centimeters of glauconitic and broken skeletal grains, suggesting possible sediment starvation (Sharaf et al., 2005).

Tuban Formation

The Tuban Formation can be broken into three lithologies: (i) A carbonaceous shale unit that represents transgressive flooding over limestone of the underlying Kujung Formation, (ii) a subtidal to intertidal bioturbated sandstone unit representing a regressive period, and (iii) a fossiliferous, sandy carbonate unit characterized by massive coral beds and defined by the foraminifera species *Lepidocyclina formosa* and *Miogypsina tani*, which indicate an age of Lower Miocene (Ardhana et al., 1993). The three lithologies of the Tuban Formation have been broken into six cycles, each of which begins with a basal deep marine shale layer and shows a shallowing upward trend as the formation transitions to overlying calcareous mudstone and siltstone, followed by shallow marine and sandy carbonate and fossiliferous sandstone units (Sharaf et al., 2005; Sharaf et al., 2006).

In the Northeast Java Basin, the basal Tuban shale unit thickens to the east, whereas the sand and carbonate units are more prevalent to the west (Sharaf et al., 2006). Shale of the Tuban Formation can act as a source rock in some areas of the Northeast Java Basin (Satyana and Djumlati, 2003). In the North Madura Platform, just north of the Bali Sea, Tuban shale acts as a top-seal to Kujung reef plays (Fainstein, 1997; Johansen, 2003; Satyana and Djumlati, 2003).

Prupuh Formation (*Member)

Some well logs designate this Oligo-Miocene high-energy, clean limestone as its own formation; however, literature (Doust and Noble, 2007; Satyana and Djumlati, 2003; Sharaf et al., 2006) refers to the Prupuh Formation as a member of

the Kujung I Unit, since it was deposited during the same tectonically quiescent transgressive period as the Kujung Formation and contains a similar lithology.

Kujung Formation

Two major carbonate units deposited during a period of prolonged transgression represent the first two units of the Kujung Formation, whereas the third unit was deposited in regressive conditions (Satyana and Djumlati, 2003). Foraminiferal assemblages in the Kujung Formation indicate an age of Oligocene to Lower Miocene (Najoan, 1972). The Kujung I Unit consists entirely of limestone and represents a complete transgressive carbonate facies; it is related to the change from NW-SE extension to basin inversion in the Miocene (Bransden and Matthews, 1992). The Kujung II Unit is a transgressive sequence of shallow water carbonate and calcareous shale, which can act as an intraformational seal in some areas. This shale is described as yellowish-brown to grey-green in outcrop, in some places glauconitic, and rich in planktonic foraminifera. The Upper Kujung carbonate units contain alternating thin chalk beds and thick carbonate successions that fine upward. The bases of these successions contain large benthic foraminifera and other fauna (rhodoliths, echinoids, and corals) that indicate a high-energy depositional environment, whereas the overlying sections deepen upward to a gradational top (Sharaf et al., 2005). This indicates an aggregating carbonate facies attempting to keep up with transgressive conditions.

The basal Kujung III Unit contains a higher amount of siliciclastics and represents a regressive period (Satyana and Djumlati, 2003). Shallow water coral and coralline algae mounds that show evidence of constant wave reworking

characterize the Lower Kujung. This high-energy environment may have been drowned around 28Ma by the transgressive period that deposited the Upper Kujung carbonates (Sharaf et al., 2005). In the area north of Madura, shale found in the Kujung III Unit contain >1% TOC (Fainstein, 1997).

The Kujung I and II Units make excellent oil and gas reservoirs in the East Java Basin, particularly where widespread exposure to meteoric water caused dissolution of the carbonates, which developed excellent secondary porosity (Satyana and Djumlati, 2003; Mudjiono and Pireno, 2001; Park et al., 1995). Porosity of 20-25% has been observed in these reefs with porosity as high as 38% recorded in coral packstones of the Poleng field offshore Madura (Welker-Haddock et al., 2001). Sharaf et al. (2005) regard the Kujung Formation as the most important hydrocarbon reservoir in the Northeast Java Basin, where significant hydrocarbon plays exist in areas where hydrocarbons migrated from the underlying organic rich shales and coals of the Ngimbang Formation by carrier beds laterally, or by faults vertically. The Tuban Formation acts as a regional seal to the Kujung Formation; however, shale in the Kujung II & III units can behave as an intraformational seal (Mudjiono and Pireno, 2001). Interfaces between the Kujung Formation and overlying organic-rich shale in the Lower Tuban Formation can also help to charge Kujung reservoirs (Satyana and Djumlati, 2003).

Ngimbang Formation

The Ngimbang Formation is recorded as three distinct units. From youngest to oldest they are: the Ngimbang Shale, Ngimbang Carbonate, and Ngimbang Clastic Units. The Ngimbang Shale Unit is a thick sequence of lacustrine deltaic and

marginal marine Eocene shale (Fainstein, 1997). The Ngimbang Carbonate Unit is a blocky mudstone with silty lime interbeds and a calcareous content of 30-40%. The Ngimbang Clastic Unit is a foraminiferal mud and siltstone with sandstone stringers and coal seams. Ngimbang and Kujung III shales act as long-distance source rocks on the North Madura Platform and are critical to Kujung reef plays in that area (Johansen, 2003).

Geochemical analyses performed on oil seeps in the Northeast Java Basin correlated the seeps to the Ngimbang Formation. Studies on petroleum quality and origin reveal Ngimbang sourced hydrocarbons to contain 0.40-70.88% TOC and kerogen types II and III (Wiloso et al., 2009). It is postulated that the Ngimbang Formation is the main hydrocarbon source for the entire Northeast Java Basin (Wiloso et al., 2009). Because of this formation, the Northeast Java Basin contains a massive amount of highly productive, oil-prone wells. Potential Ngimbang offshore hydrocarbon plays east of Java may be found in stratigraphic wedges and in areas where the formation onlaps basement rocks (Fainstein, 1997).

Pre-Tertiary Basement

Basement rocks of the Bali Basin consist of sand, silt, and claystone mixed with basalt and metamorphic rocks typical to the metasedimentary and volcanic basement of the region (Prasetyo, 1992). Given the Bali Basin's position in Sundaland, it can be extrapolated that its basement rests on crust accreted from the Australian allocthon in the Late Jurassic (Hall, 2014) (Figure 3).

It is generally accepted that the basement of the Bali Basin is oceanic; however, the exact origin of the Bali Basin's basement is unknown. To address this uncertainty, three possible mechanisms are offered (Prasetyo, 1992):

1. Mid-Cretaceous oceanic crust from the Indian Ocean was trapped as the Bonerote submarine ridge, a chain of islands and bathymetric highs south of Sulawesi, separated the Banda Basin from the Bali-Flores Basin.
2. Oceanic crust was generated in the basin by back-arc spreading caused by subduction of Indian Ocean crust along the Eastern Sunda Trench.
3. Rifting of the Southeast Doang Boarderland, a series of ridges and intervening troughs located between Suluwesi and Borneo that was previously located along a triple junction, formed the oceanic crust.

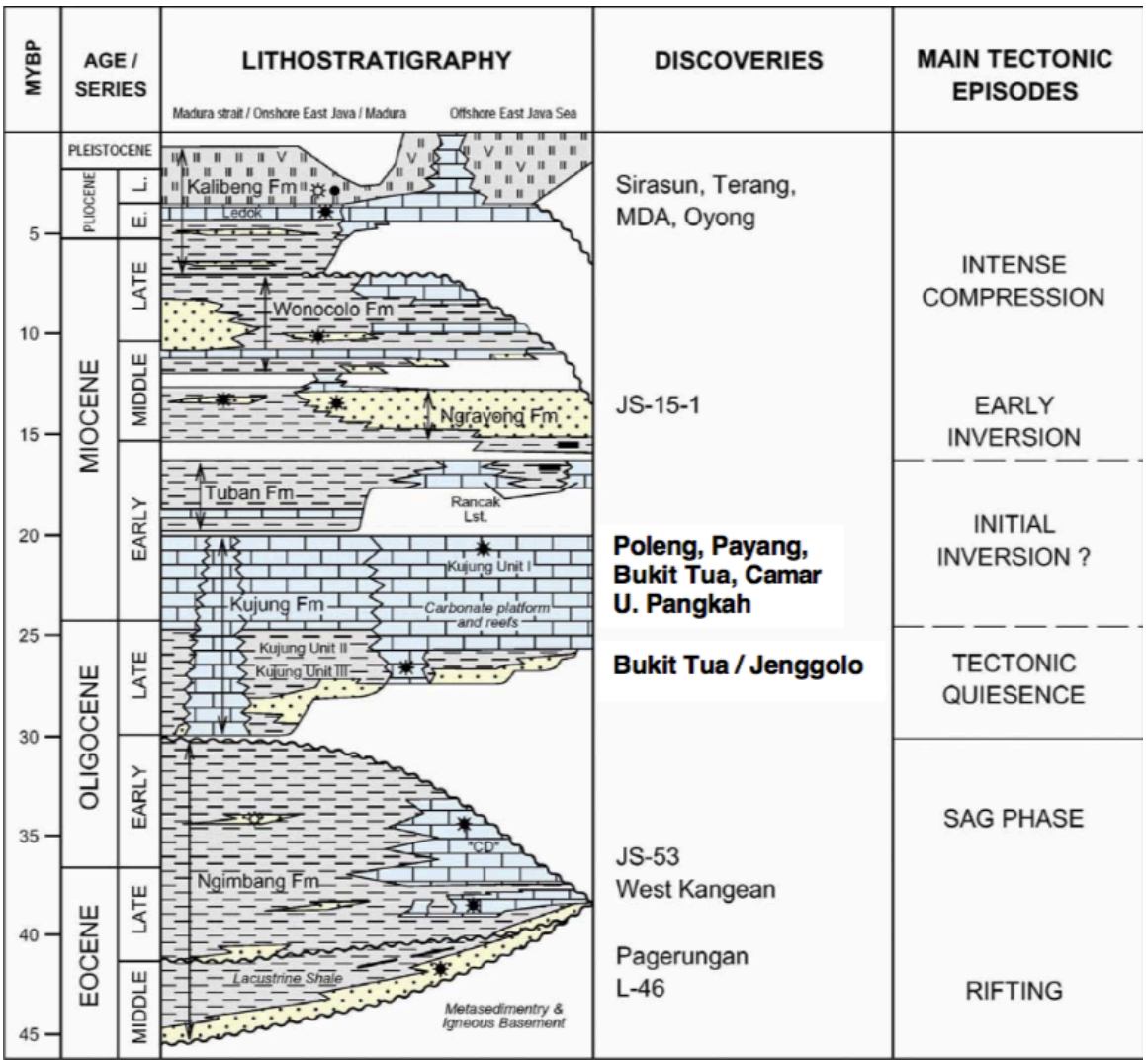

Figure 12) Lithostratigraphic column showing the spatial relationship of formations from onshore to offshore East Java (Johansen, 2003).

Methods

Ball State University is in possession of the largest privately owned collection of well log data covering the Southeast Asia Pacific Region. Donated to the university by L. Bogue Hunt and referred to as the L. Bogue Hunt database (LBH), this external hard drive contains thousands of drilling reports, seismic data,

lithostratigraphic and biostratigraphic columns, as well as sonic, gamma ray, neutron and density logs. The information contained in the LBH database is accessible via Geologic Information Systems 6 (GIMS 6) software on a department owned laptop. GIMS 6 supplies production information and geographic context to the LBH wells, placing them on a global map by symbols representing what has been recovered from each well, e.g. oil, gas, condensate, dry hole, etc.

Well logs stored in the LBH database generally contain information recorded in the 1970's and 80's from a wide range of operators. All LBH logs and reports have been physically scanned and stored in the database, but have not been digitized. For these reasons, LBH well logs contain variable information. Additionally, poor scanning and software issues have rendered some logs illegible or unviewable. This inconsistency in available data means the number of usable wells in a given study will vary depending on what information is needed. If available, the following information was recorded from each well: well name, latitude, longitude, kelly bushing or drill floor elevation, total depth (TD), circulating mud temperature (Rm), bottom hole temperature (BHT), lithology and formation name, basin name, operator name, and the source of acquired samples, e.g. mud pit, flowline, circulation, etc.

2D Modeling

Data was recorded from 35 wells across the northern margin of the Bali Basin in the LBH database in order to construct a 2D stratigraphic correlation model in IHS Petra. The latitude and longitude of each well was recorded in decimal degrees and then converted to UTM coordinate format for the model. This

information was recorded in an excel spreadsheet along with the calculated depth of each well, i.e. the difference between the total depth as recorded by the driller and the kelly bushing elevation. This information was then saved as a wellheads file in ASCII format and uploaded to Petra to establish the spatial relationship of the wells. The depth to each formation in every well was recorded in a separate well tops file, also in ASCII format. In combination, the wellheads and well tops files allow Petra to show the location of each well and create a 2D surface between the wells for each formation.

Effective Porosity Calculations

Effective porosity is a value that represents the "true" porosity of a formation, i.e. the percentage of the formation that is open pore space, as opposed to the percentage of the formation that is actual rock. First order porosity calculations, not accounting for the volume of shale present in a formation, only show a vague estimation of the formation's porosity (Asquith and Krygowski, 2004). In order for effective reservoir porosity to be determined from a well, sonic, neutron, or bulk density information must be recorded and used in conjunction with gamma ray records through a series of calculations.

Effective porosities in this study were calculated using sonic log records because sonic logs are the most consistently recorded well logs in the Bali Basin. Sonic logs record interval transit time as the reciprocal velocity of a compressional sound wave moving along the borehole axis in feet per second. This transit time is dependent on lithology and porosity, so interval transit times recorded in the well (Δt_{log}) were used with the known interval transit times of the borehole fluid (Δt_f)

and surrounding rock (Δtma) to calculate an initial porosity value (Φi) using the following equation (Asquith and Krygowski, 2004):

$$\Phi i = (\Delta tlog - \Delta tma)/(\Delta tf - \Delta tma) \quad (1)$$

Drilling reports indicate saltwater mud to be the drilling fluid used in wells throughout the Bali Basin and the reservoirs are limestone and sandstone. Given this information the appropriate Δtma and Δtf values are (Asquith and Krygowski, 2004):

Δtma (limestone) = 49 μsec/ft

Δtma (sandstone) = 56 μsec/ft

Δtf (saltwater mud) = 185 μsec/ft

Reservoir porosity can be calculated from density or neutron records alone; however, until the volume of shale in the reservoir is calculated the recorded porosity will be erroneously greater than the actual porosity of the reservoir, i.e. effective porosity. Sonic log data is affected by shale because shale is typically very porous but its small grainsize renders the rock impermeable, thus increasing the porosity value recorded by sonic logs, without actually allowing the movement of formation fluids. Neutron log porosity measurements are misrepresented by the presence of shale because the recording equipment senses hydrogen in the shale, in addition to hydrogen in the pore spaces. The inability to differentiate between shale and pore space hydrogen artificially increases the porosity reading and is called the "shale effect" (Asquith and Krygowski, 2004).

Shale is more radioactive than sand or carbonate, so gamma ray readings of the borehole walls are used to locate shale stratigraphically. In order to calculate

the volume of shale present in a formation, the gamma ray index (GRi) must first be determined. Gamma ray logs from the Bali Basin were used to calculate the gamma ray index using the following equation (Asquith and Krygowski, 2004):

$$GRi = (GRlog-GRmin)/(GRmax-GRmin) \quad (2)$$

where:

GRlog = gamma ray reading from the formation

GRmax = maximum gamma ray reading

GRmin = minimum gamma ray reading

Shale volume (Vsh) in Tertiary rocks can be calculated by (Larionov, 1969):

$$Vsh = 0.083(2^{(3.7-GRi)}-1) \quad (3)$$

The gamma ray index determined in equation (2) was used in equation (3) to calculate the shale volume for reservoir rocks in each well. This shale volume was then applied to the initial porosity (Φi) calculated in equation (1) in order to calculate effective porosity (Φef) (Asquith and Krygowski, 2004):

$$\Phi ef = \Phi i(1-Vsh) \quad (4)$$

Well Log Digitization

Logs for each well that penetrated a reservoir formation and contained both gamma ray and sonic data were digitized using WebPlotDigitizer 3.8. This program allows the user to upload an image file, define two axes, and then plot data points within the defined plane. These points are recorded by the program with up to 12

significant digits and are then exported to Microsoft Excel as comma delineated (CSV) files.

JPEG images of each reservoir well log containing both gamma ray and sonic data were uploaded to WebPlotDigitizer. The x and y axes were defined to constrain the given reservoir by the respective log's left-most margin and the formation bottom. Data points were aligned with the Δtlog and GRlog measurements at 10-foot intervals throughout the entire formation and then exported to Excel, where Φef was calculated at each interval to determine the average reservoir Φef value for each well.

Effective Porosity Map Creation

A map showing the effective porosity of each potential reservoir in the Bali Basin was created using the calculated average Φef values of each respective well and ArcMap 10.4.1. Each well was placed on a world ocean reference base-map according to the longitudinal and latitudinal information in the drilling report and specified to the WGS 1984 world geographic coordinate system. The space between the wells was contoured using the inverse distance weighted spatial analysis tool by setting the x, y and z-axes to longitude, latitude, and Φef, respectively.

Heat Flow Calculation

Geothermal heat flow (Q) measures the amount of Earth's latent formational heat reaching the surface at a given location. This value can be calculated by (Batir et al., 2013):

$$Q = (\Delta T/\Delta z)k \quad (5)$$

where:

Q = heat flow, mW/m^2

ΔT = change in temperature (T-To), °C

Δz = depth, km

k = thermal conductivity, W/m*K

In order to calculate ΔT, the surface temperature (To) and the temperature at depth (T) must be recorded. This study used bottom hole temperatures (BHT) and thermal readings from mud resistivity tests at the surface (Rm) recorded in drilling reports to represent (T) and (To) respectively. ΔT, when divided by well depth (z), represents the thermal gradient of the well. The thermal gradient describes the direction and rate that heat travels in a given location, and is vital to the calculation of heat flow. Depth measurements (Δz) were also obtained from LBH reports.

Thermal conductivity (k) can be described as the quantity of heat transmitted through a unit thickness of a material, in a direction normal to a surface of unit area, due to a unit temperature gradient under steady state conditions. It is a materials ability to conduct heat, and every lithology has a specific calculated thermal conductivity value (Eppelbaum et al., 2014). Thermal conductivity values were adapted from Shim et al. (2010) and assigned to well sections based on recorded lithologies. The well section thermal conductivity values were then normalized in order to reach a single thermal conductivity value for each well. These values were then multiplied by the calculated thermal gradient for each well, per equation (5).

Bottom Hole Temperature Correction

Bottom hole temperatures recorded from well log headers are generally biased lower than actual formation temperatures at depth (Peters and Nelson, 2009). This is due to a combination of short static times, re-circulation between measurements, inaccurate or illegitimate recordings, and the Joule-Thompson effect; a thermodynamic mechanism by which heat is lost from a liquid when forced through an insulated valve (in this case, the borehole). Because of these issues, bottom hole temperatures must be corrected via "Horner correction" methodologies (Horner, 1951).

A full Horner correction is the most accurate adjustment of bottom hole temperature and requires total circulation time, records of time since circulation, and bottom hole temperatures. A reliable Horner correction will contain a minimum of three logging runs recording temperature and time, temperature extrapolation less than the range of temperature data, and deviations from the least squares regression line that are less than the measurement uncertainty (Horner, 1951). If total circulation time is not available, a simpler correction using only time since circulation and bottom hole temperature can be performed. If only bottom hole temperature data is available, then a last resort correction can be done by simply adding 18°C to the recorded bottom hole temperature. This study used an online calculator by Zetaware to determine all Horner corrections. The calculator used for these corrections can be found at (http://www.zetaware.com/utilities/bht/horner.html).

Heat Flow Map Creation

Q values were calculated using equation (5) for each of 857 wells obtained from the LBH database. These Q values were then used in ArcMap 10.5.1 to construct a map showing the change in geothermal heat flow throughout Indonesia. Each well was placed on a world ocean reference base-map according to the longitudinal and latitudinal information in the drilling report and specified to the WGS 1984 world geographic coordinate system. The space between wells was contoured using the inverse distance weighted (idw) spatial analysis tool by setting the x, y and z axes to longitude, latitude, and Q, respectively. The idw layer was then restricted to areas proximal to wells, minimizing extrapolation and increasing the accuracy of the map. Layer restrictions were performed using ArcMap's polygon creation feature in combination with the data management clipping function. For maps illustrating the Bali Basin, the transparency of the idw contour fill colors was adjusted to 30% so the base-map is visible beneath the idw layer. Adjusting the z value of the idw layer to the appropriate attribute allows the creation of additional maps plotting bottom hole temperature, thermal gradient, thermal conductivity and depth.

Results

2D Petroleum Systems Model

Geographic information obtained from coordinates recorded in drilling reports stored in the LBH database was used to define the spatial relationship between wells in Petra and to render a well location map in ArcMap.

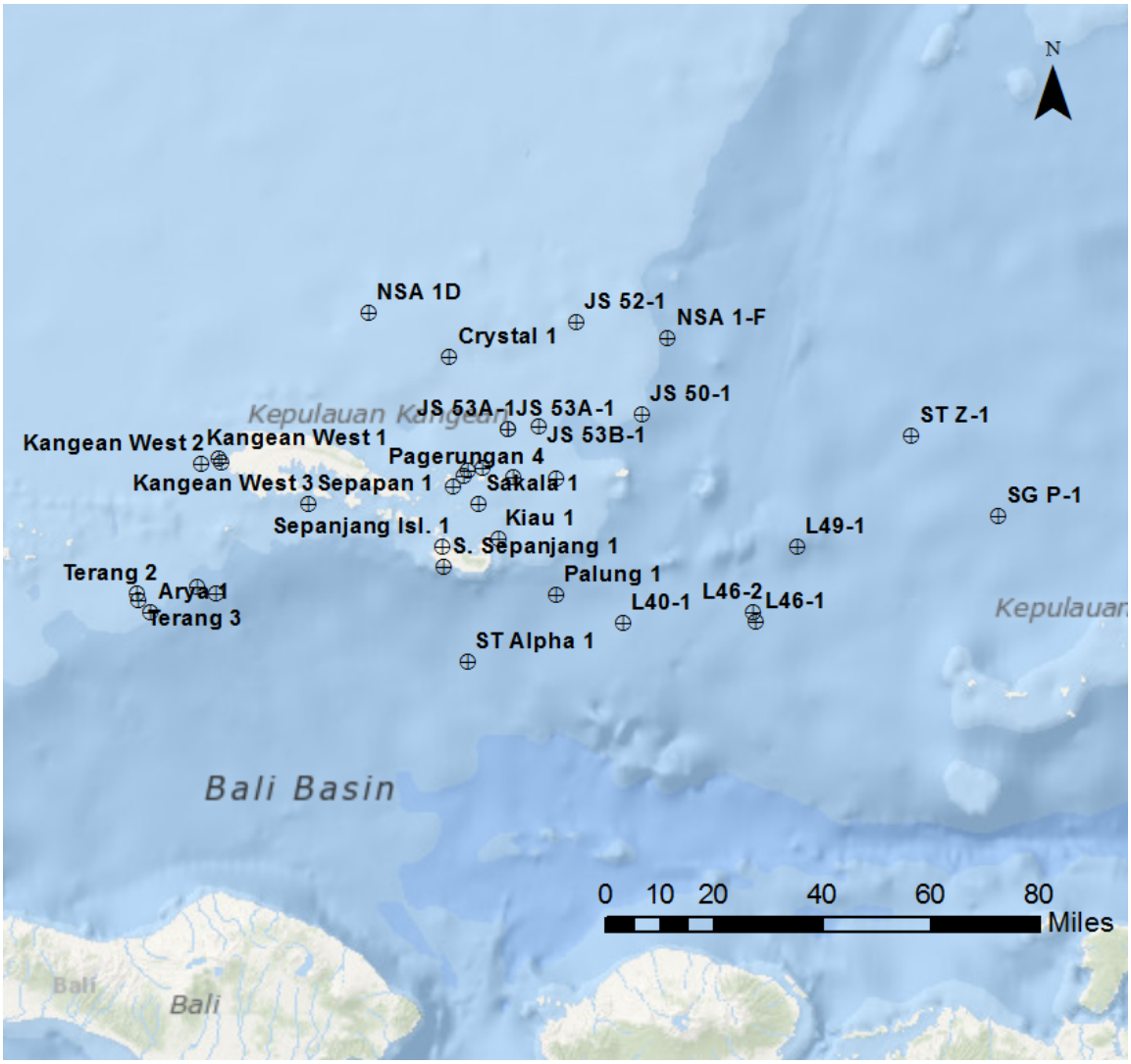

Figure 13) Map showing the geographic location of the wells used to render the Bali Basin model. Map produced in ArcMap; the proximity of some wells prevents the program from displaying their label feature.

From this base map a 2D model of the study area was constructed in IHS Petra, beginning with the basement and moving up through the stratigraphic section. Basement depths were collected from LBH well logs; however, not all wells had total depths reaching basement rock. This is shown by the restricted nature of the basement surface rendered in Petra.

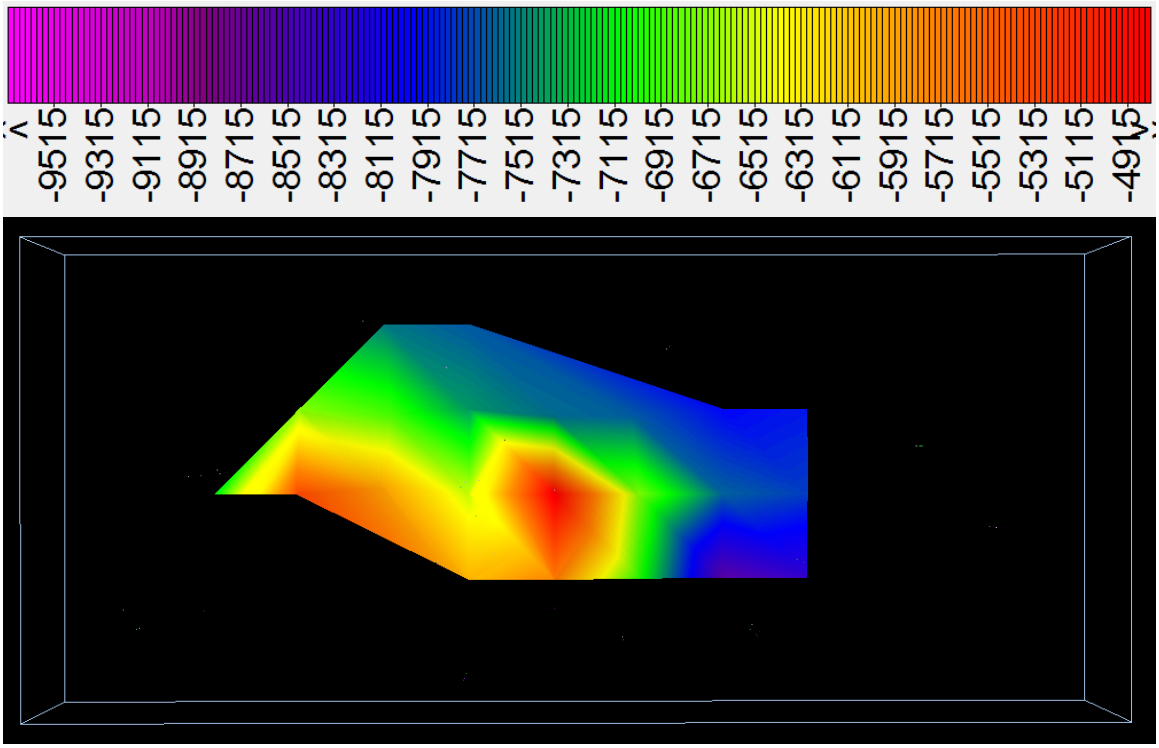

Figure 14) Map view of the study area's basement. Extent of the basement is misrepresented by this surface due to the shallow depth of some wells. North is toward the top of the image; legend represents depth in feet. VE=20.

A two-dimensional rendering of the basement is important because structures in the basement can affect the geometry of overlying layers. It should be noted that the structural nature of the stratigraphic section up to but not including the Ngrayong Formation resembles that of the basement. Additionally, knowing the basement depth in the study area can help determine the overall sediment infill of the basin.

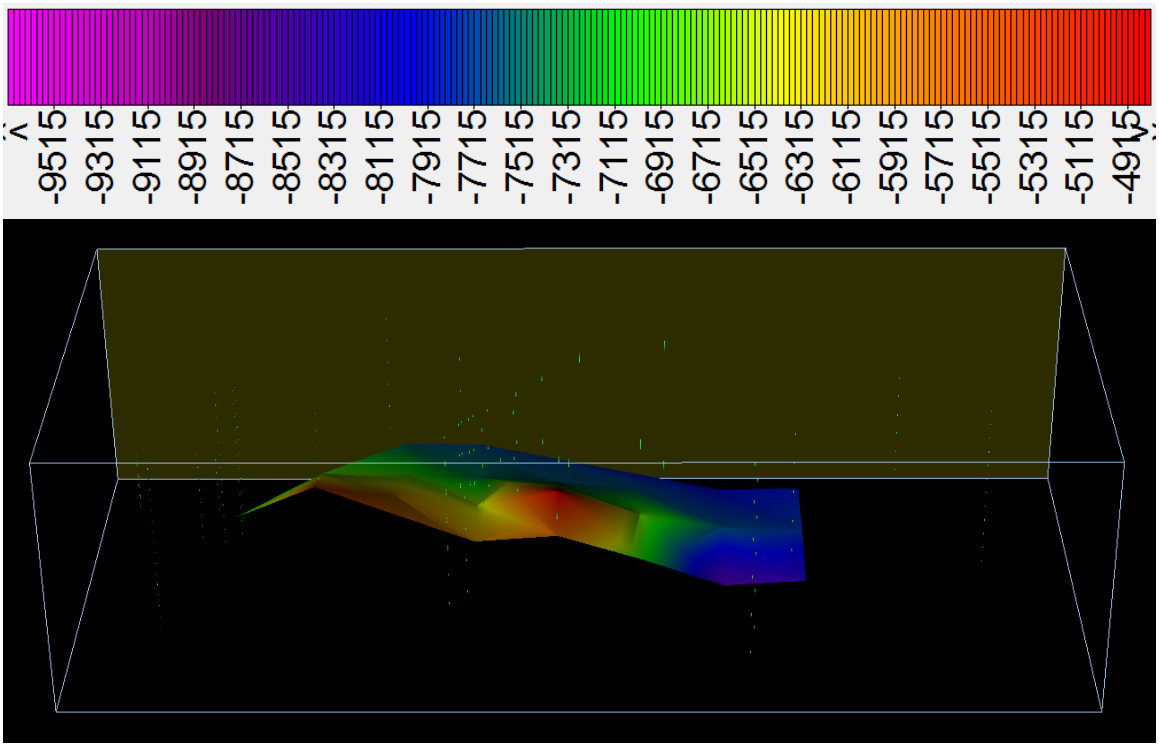

Figure 15) 2D surface representing the basement of the study area. Shaded box indicates north; legend represents depth in feet. VE=20.

The Ngimbang Formation unconformably overlies the basement and includes a lacustrine, deltaic, and marginal marine shale unit, a fine-grained, blocky carbonate unit, and a clastic unit composed of mudstone, siltstone, sandstone, and coal seams. The Ngimbang Formation acts as a major source to plays in the Northeast Java Basin (Wiloso et al., 2009) and on the North Madura Platform (Johansen, 2003). Geochemical analyses reveal the Ngimbang Formation to have TOC levels of up to 70.88% in some areas of the Northeast Java Basin (Wiloso et al., 2009).

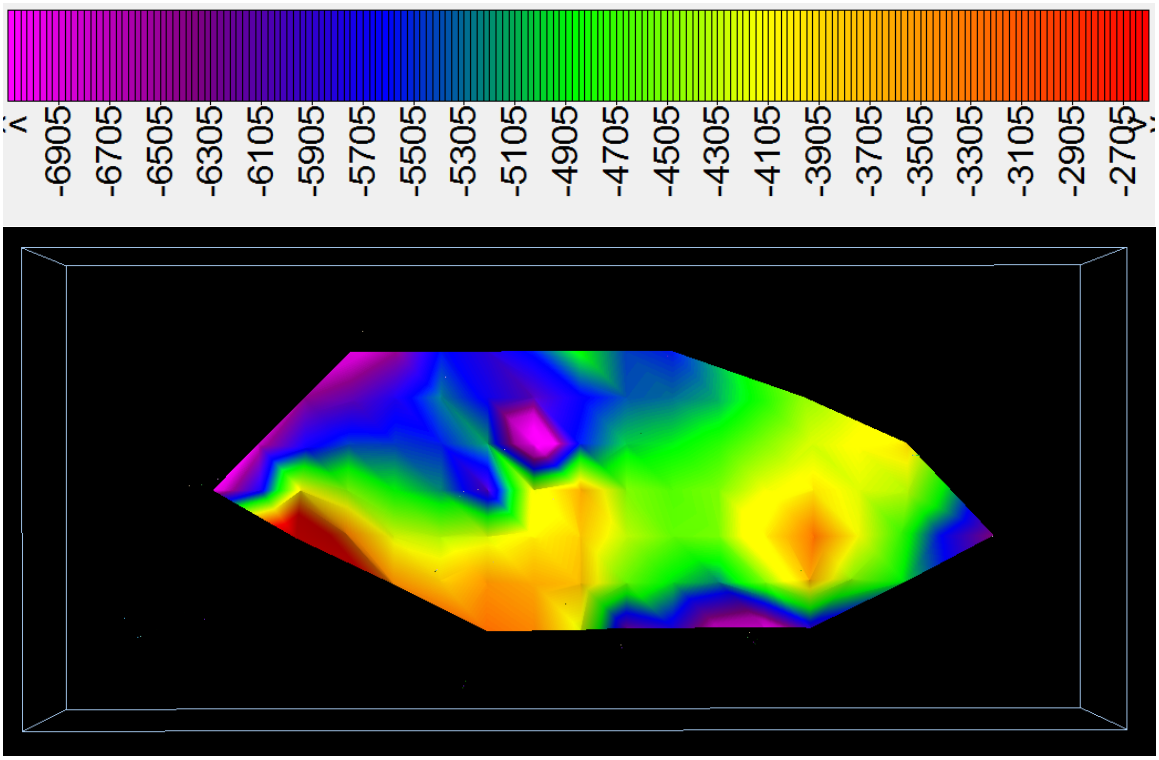

Figure 16) Map view of the Ngimbang Formation. North is toward the top of the image; legend represents depth in feet. VE=20.

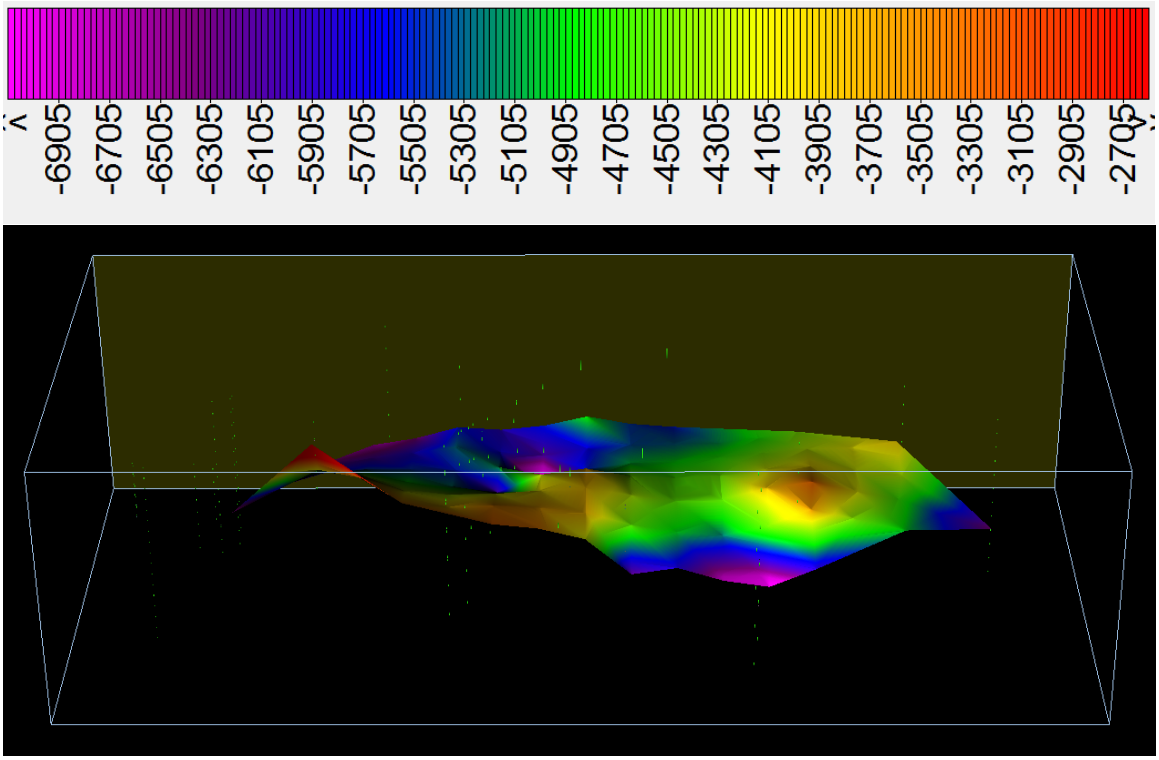

Figure 17) 2D surface representing the Ngimbang Formation. Shaded box indicates north; legend represents depth in feet. VE=20.

The Kujung III Unit conformably overlies the Ngimbang Formation. This unit is unique because it has the potential to be both a source and a reservoir; in areas where regressive shales dominate the carbonate facies, the Kujung III unit may charge the overlying Kujung I & II Units, as it has done in petroleum systems northwest of the study area (Johansen, 2003; Satyana and Djumlati, 2003). Porous carbonate sections of the Kujung III Unit can act as reservoirs both to hydrocarbons generated by the Ngimbang Formation, and potentially to hydrocarbons generated by interfingering shales within the Kujung III Unit itself. In this way, the Kujung III Unit may contain pockets of hydrocarbon trapped in limestone that is surrounded or stratigraphically pinches out into impermeable shales of the same formation (Satyana and Djumlati, 2003).

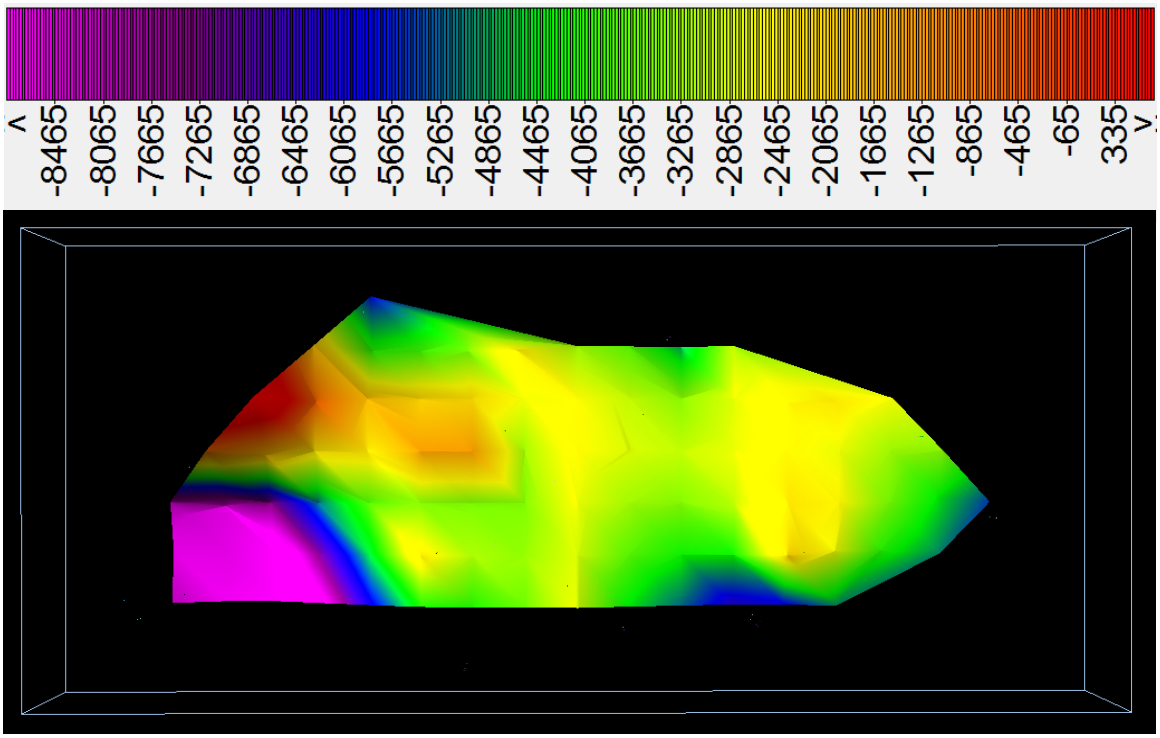

Figure 18) Map view of the Kujung III Unit. North is toward the top of the image; legend represents depth in feet. VE=20.

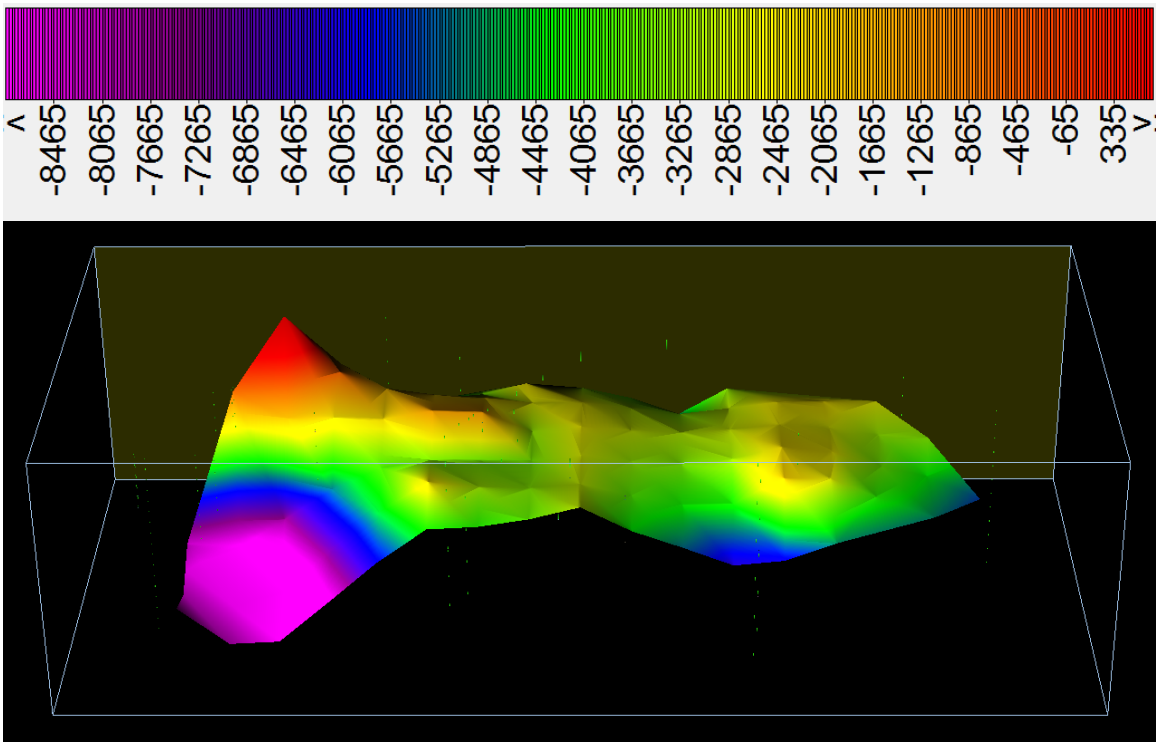

Figure 19) 2D surface representing the Kujung III Unit. Shaded box indicates north; legend represents depth in feet. VE=20.

The Kujung I and Kujung II Units are composed mostly of clean, high-energy limestone with some calcareous clay; they share very similar lithologies and were both formed during transgressive periods following a regional regression. Given their similar depositioal history, lithology, and reservoir potential (Satyana and Djumlati, 2003; Mudjiono and pireno, 2001; Park et al., 1995; Sharaf et al., 2006; Welker-Haddock et al., 2001) the Kujung I & II Unit surfaces have been amalgamated to promote simplicity in the 2D model.

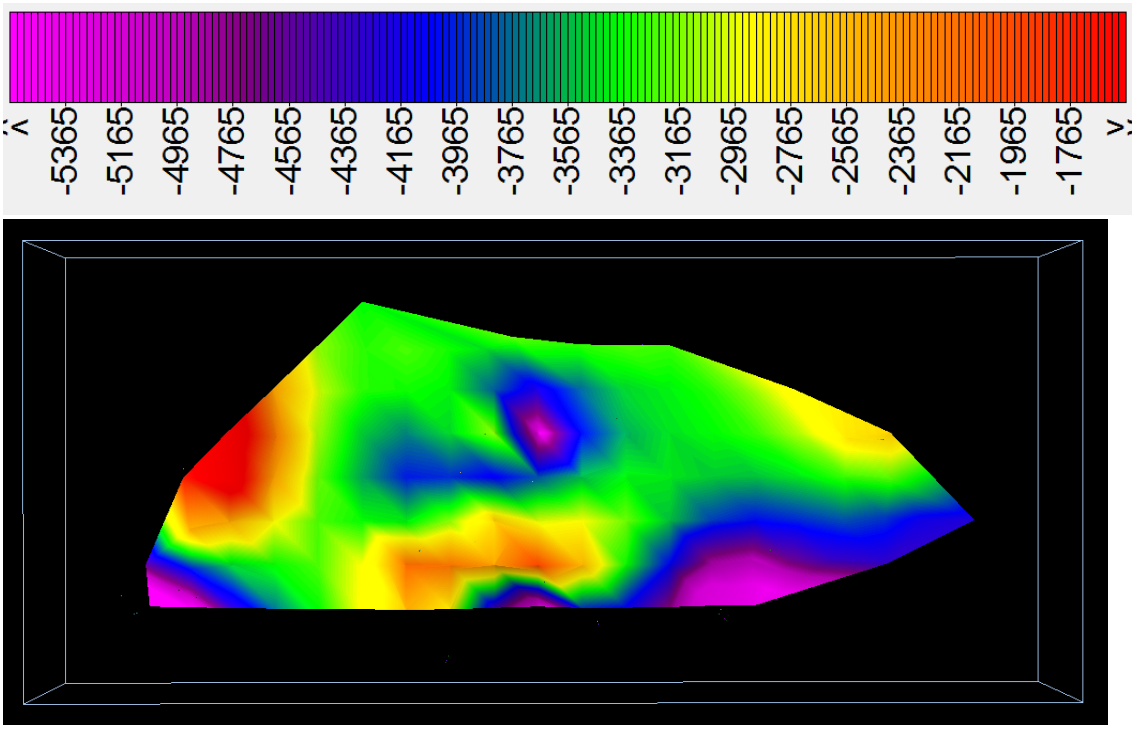

Figure 20) Map view of the Kujung I & II units. North is toward the top of the image; legend represents depth in feet. VE=20.

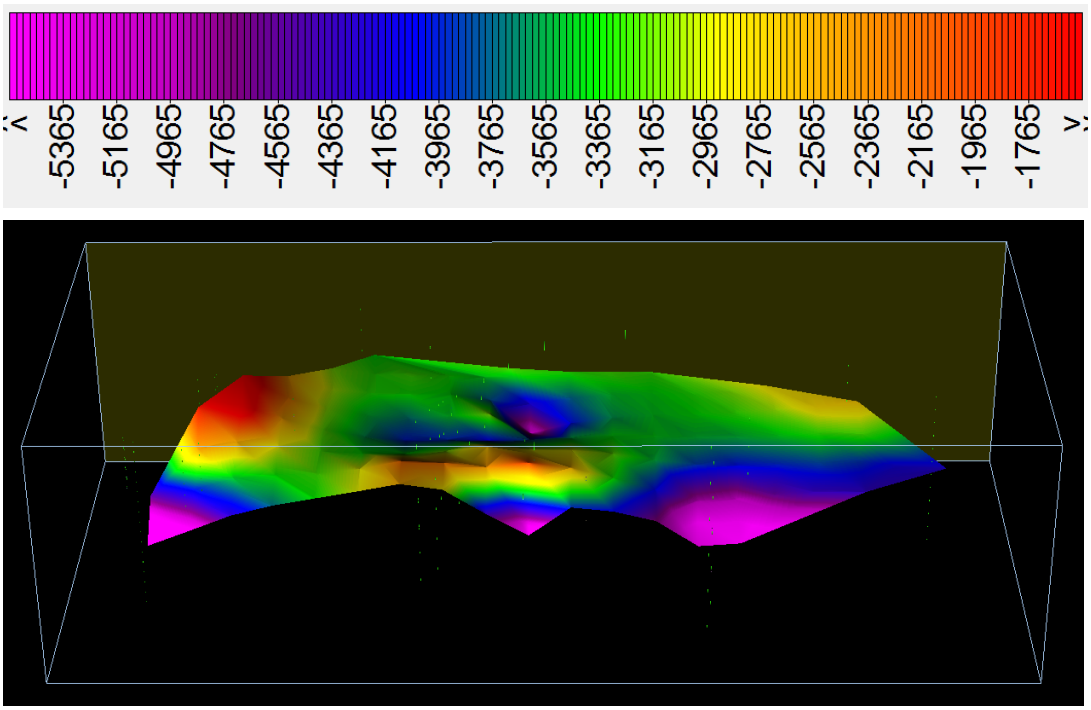

Figure 21) 2D surface representing the Kujung I & II units. Shaded box indicates north; legend represents depth in feet. VE=20.

A transgressive, carbonaceous shale unit, a subtidal to intertidal, regressive sandstone unit, and a fossiliferous carbonate unit represent the Tuban Formation, which conformably overlies the Kujung I & II Units (Sharaf, et al., 2006). The Tuban Shale Unit can act as both a source (Satyana and Djumlati, 2003) and seal (Fainstein, 1997; Johansen, 2003; Satyana and Djumlati, 2003).

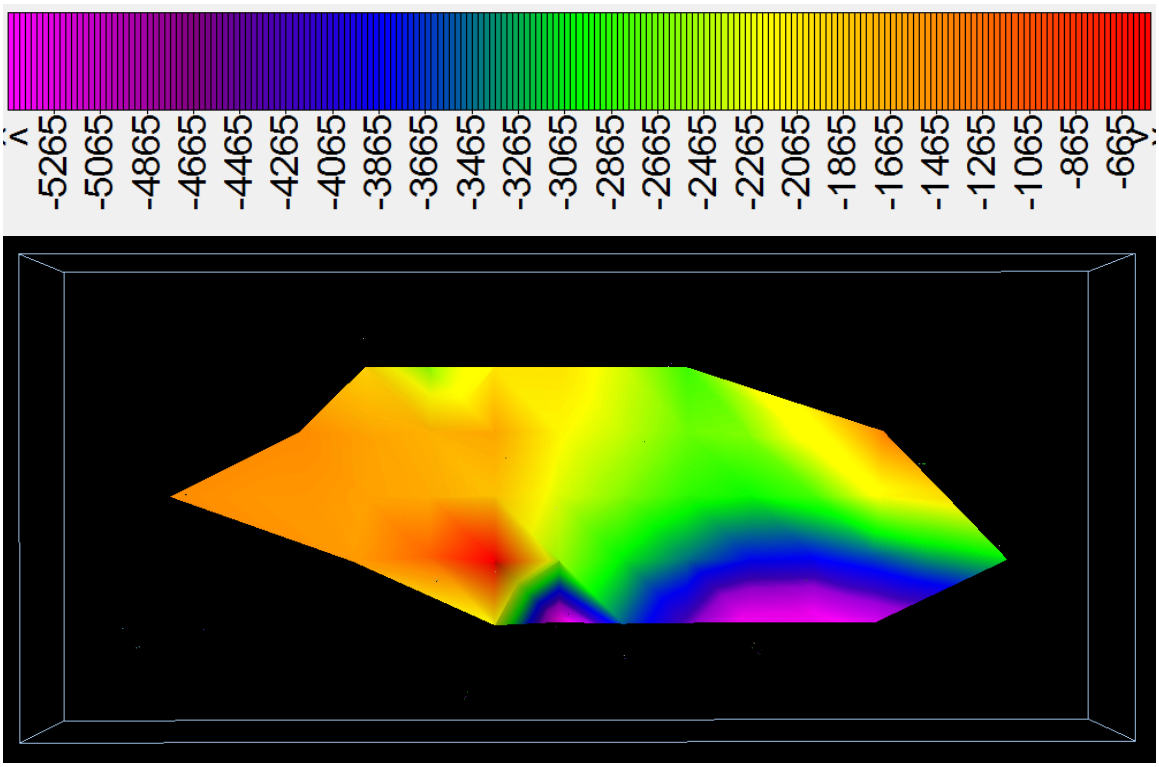

Figure 22) Map view of the Tuban Formation. North is toward the top of the image; legend represents depth in feet. VE=20.

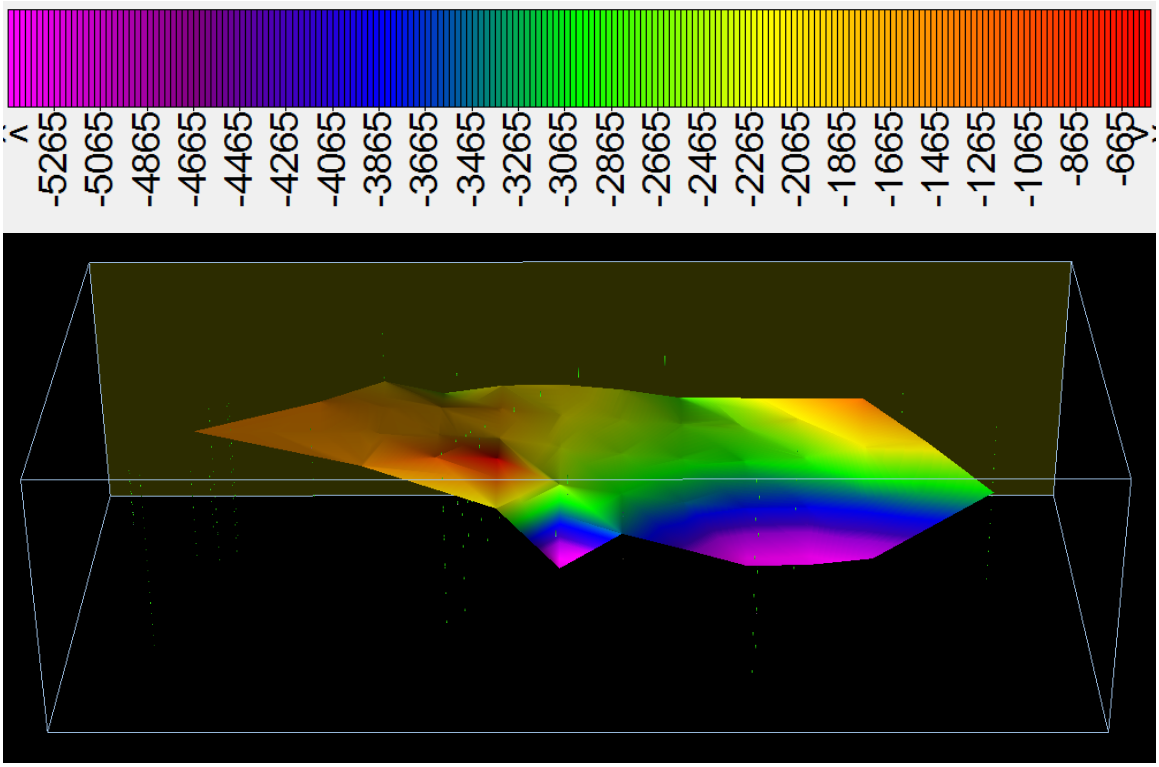

Figure 23) 2D surface representing the Tuban Formation. Shaded box indicates north; legend represents depth in feet. VE=20.

The Ngrayong Formation conformably overlies the Tuban Formation. This transition from bioturbated sandstones and fossiliferous carbonates of the Upper Tuban Formation to high-engery, progradational tidal delta deposits of the Ngrayong Formation represent continued regression through the early to mid-Miocene (Sharaf et al., 2005; Sharaf et al., 2006).

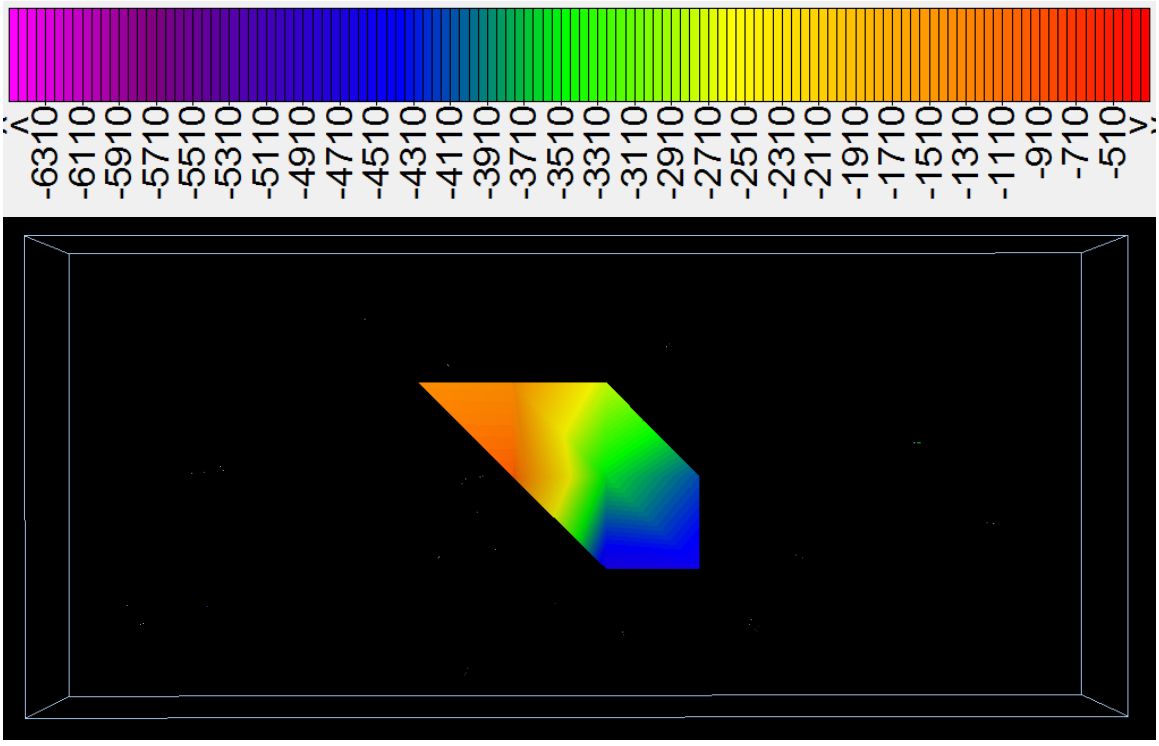

Figure 24) Map view of the Ngrayong Formation. North is toward the top of the image; legend represents depth in feet. VE=20.

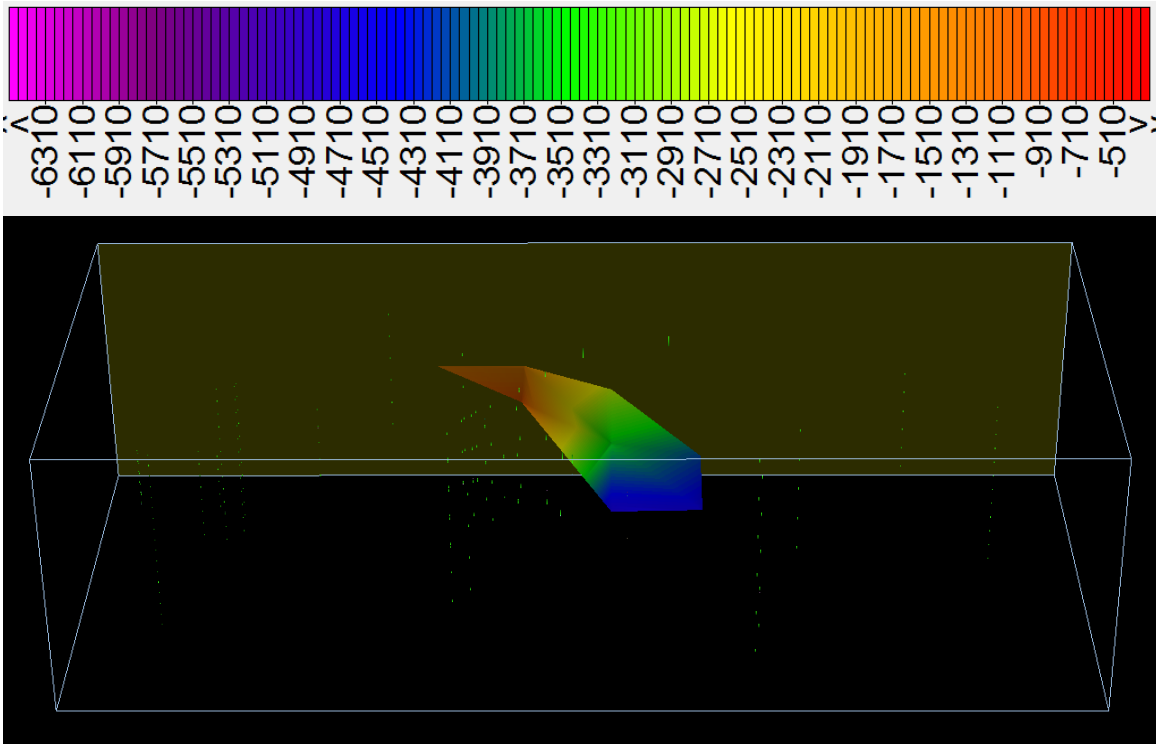

Figure 25) 2D surface representing the Ngrayong Formation. Shaded box indicates north; legend represents depth in feet. VE=20

The Wonocolo Formation conformably overlies the Ngrayong Formation. Sandy limestone and calcareous clay beds of the formation's Bulu Member (Sharaf et al., 2006) are the primary lithology present in the Bali Basin, localized to the center of the study area.

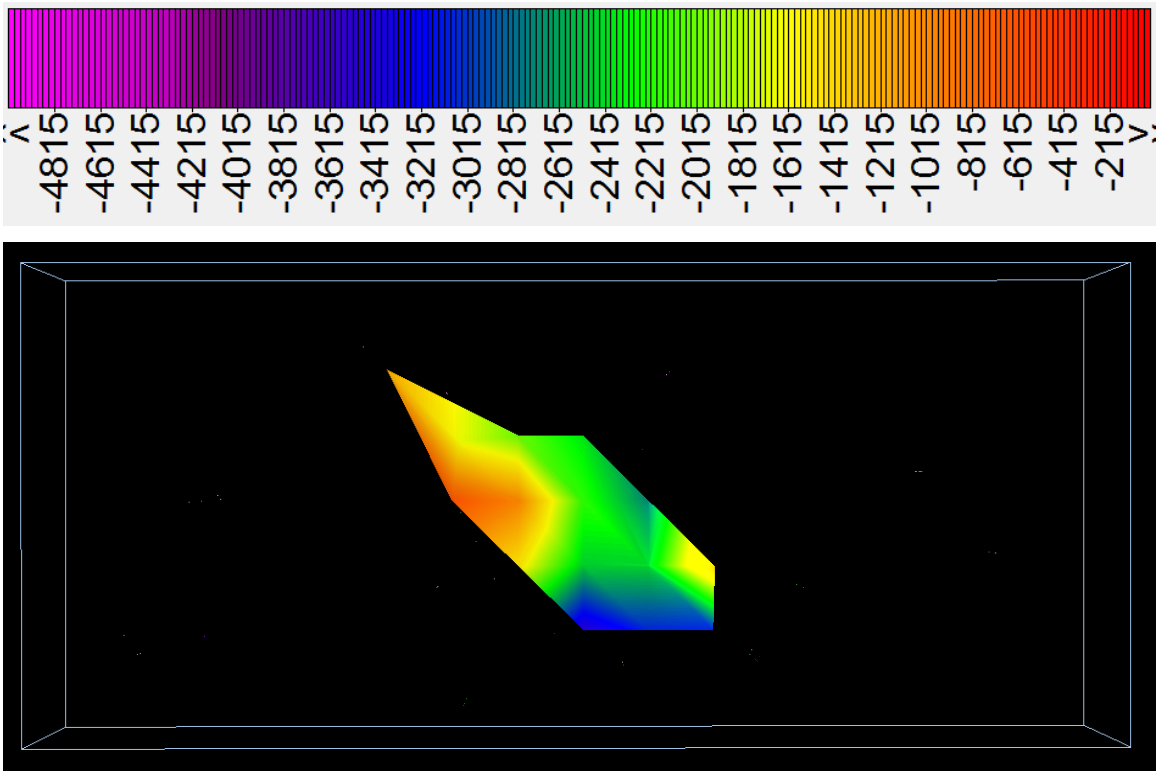

Figure 26) Map view of the Wonocolo Formation. North is toward the top of the image; legend represents depth in feet. VE=20

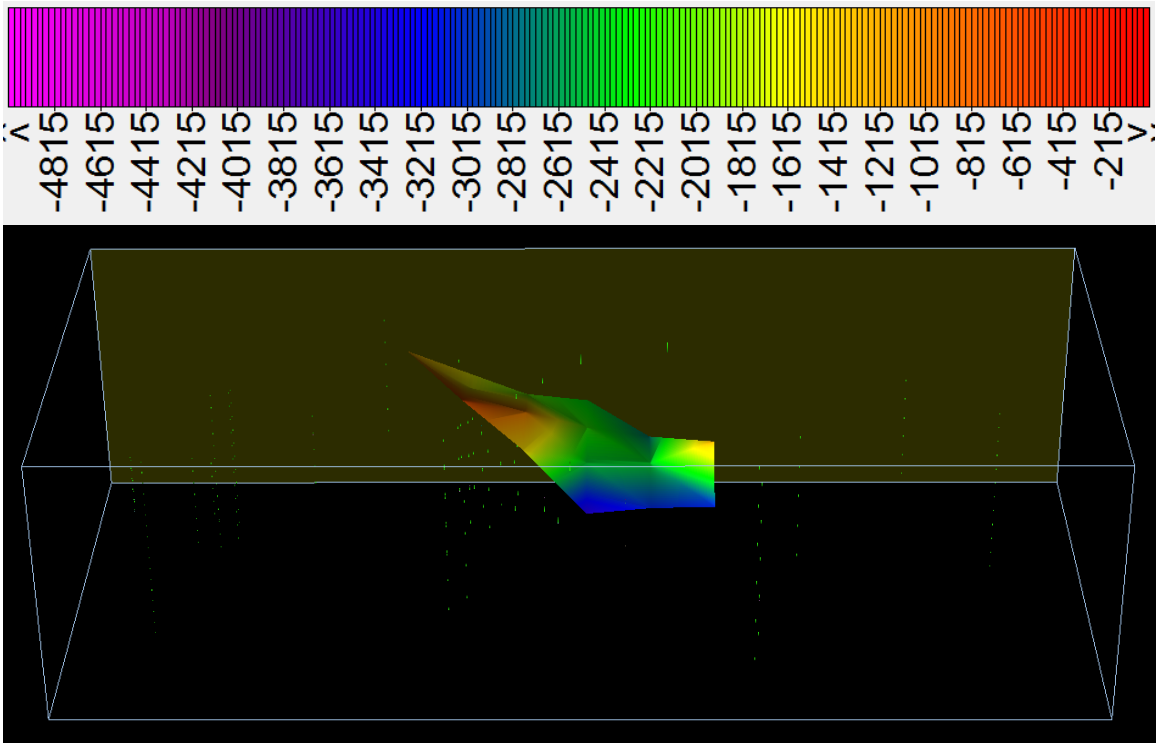

Figure 27) 2D surface representing the Wonocolo Formation. Shaded box indicates north; legend represents depth in feet. VE=20

The Ledok Formation conformably overlies the Wonocolo Formation. Shallowing up sequences in the Ledok Formation represent persistently regressive conditions through the Upper Miocene (Susilohadi, 1995).

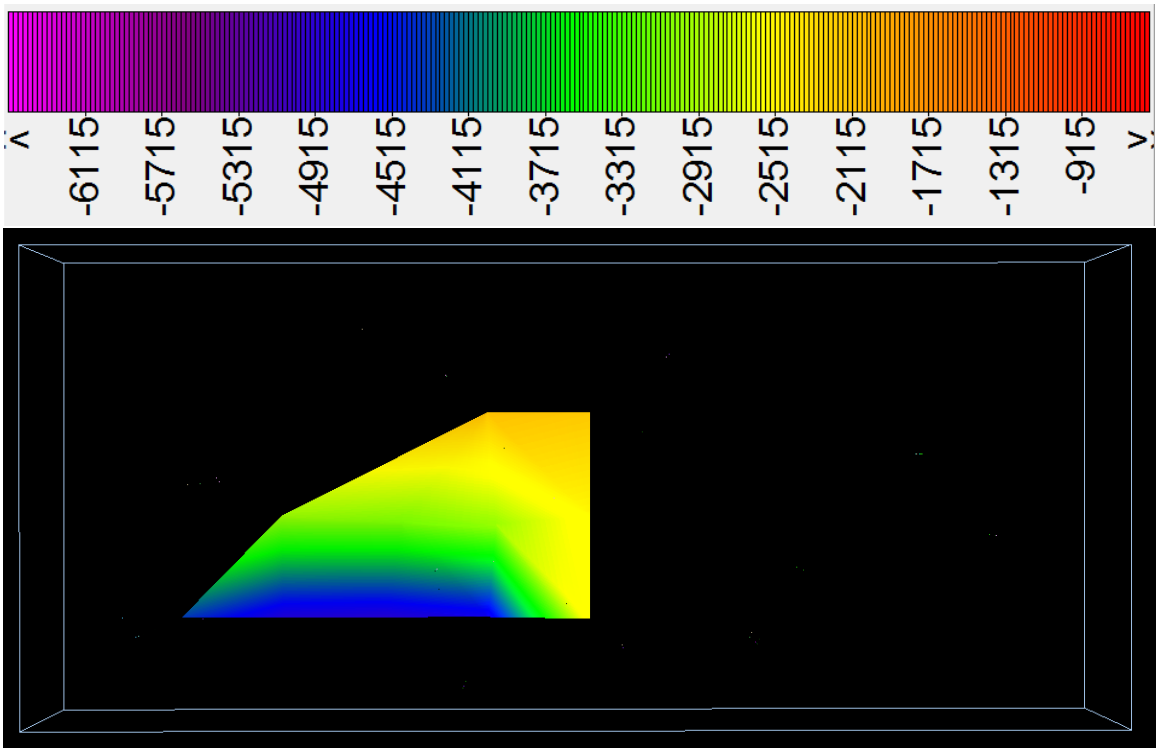

Figure 28) Map view of the Ledok Formation. North is toward the top of the image; legend represents depth in feet. VE=20.

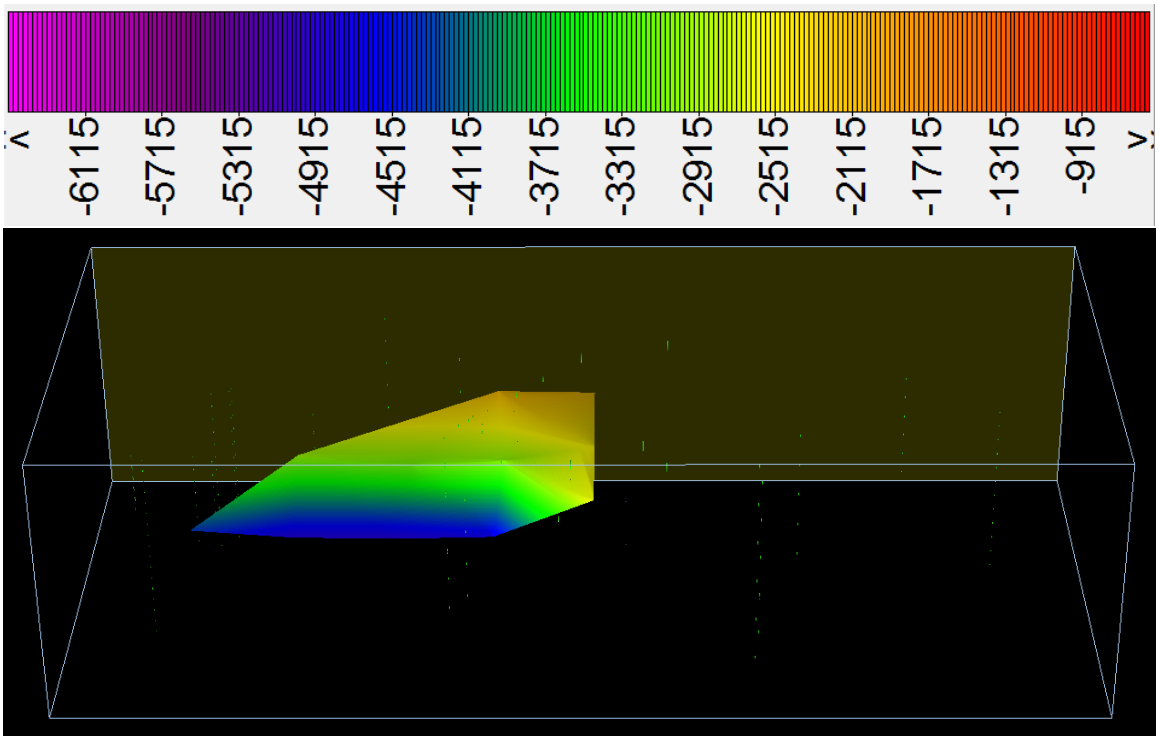

Figure 29) 2D surface representing the Ledok Formation. Shaded box indicates north; legend represents depth in feet. VE=20.

The Paciran formation is broken into an upper limestone and a lower sandstone unit, each of which is stratigraphically adjacent and has excellent reservoir characteristics (Susilohadi, 1995). For simplicity in the 2D model the Upper and Lower Paciran Units are regarded collectively as the Paciran Formation and represented by a single surface.

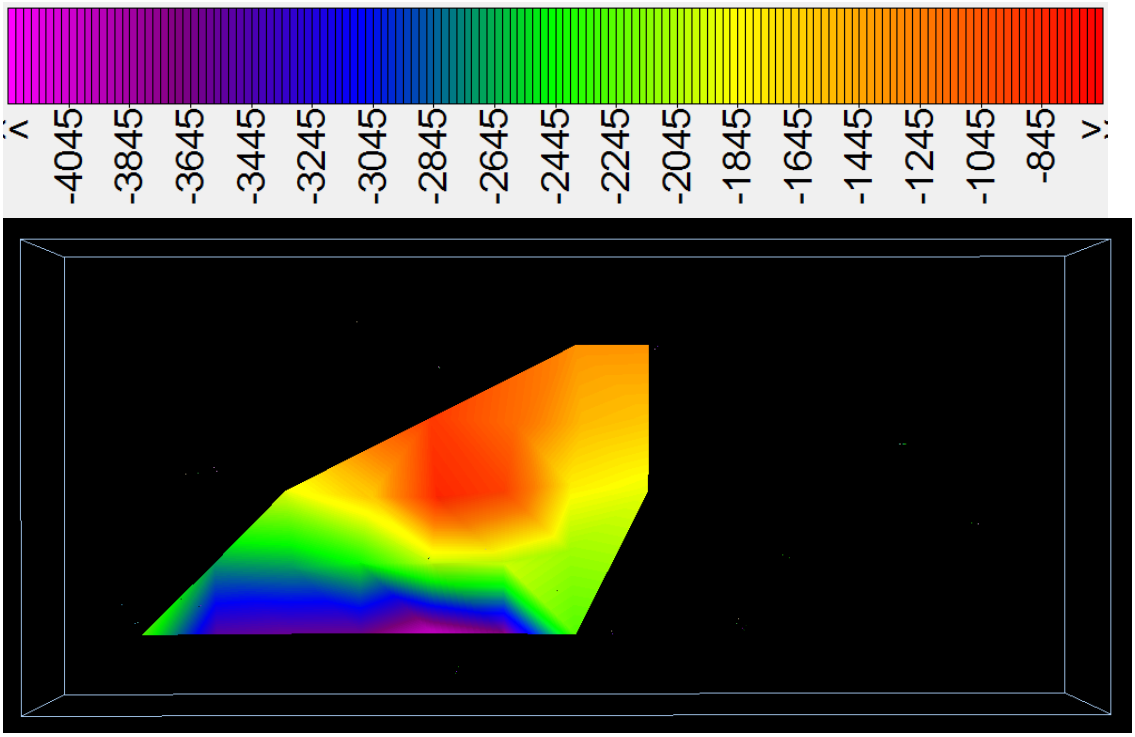

Figure 30) Map view of the Paciran Formation. North is toward the top of the image; legend represents depth in feet. VE=20.

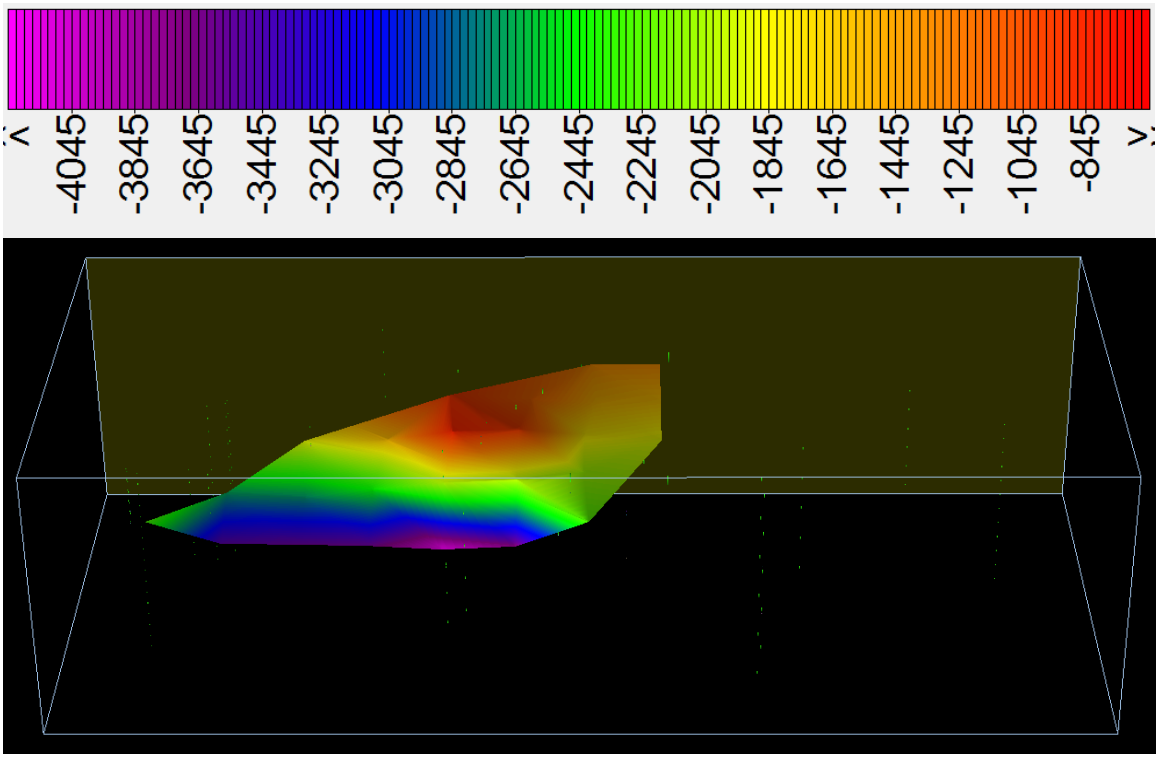

Figure 31) 2D surface representing the Paciran Formation. Shaded box indicates north; legend represents depth in feet. VE=20.

The upper-most layer in the Bali Basin fill is the Lidah Formation, which unconformably shares an erosional contact with the Paciran Formation. The Lidah Formation is composed of lacustrine-tidal claystones and mudstones (Susilohadi, 1995).

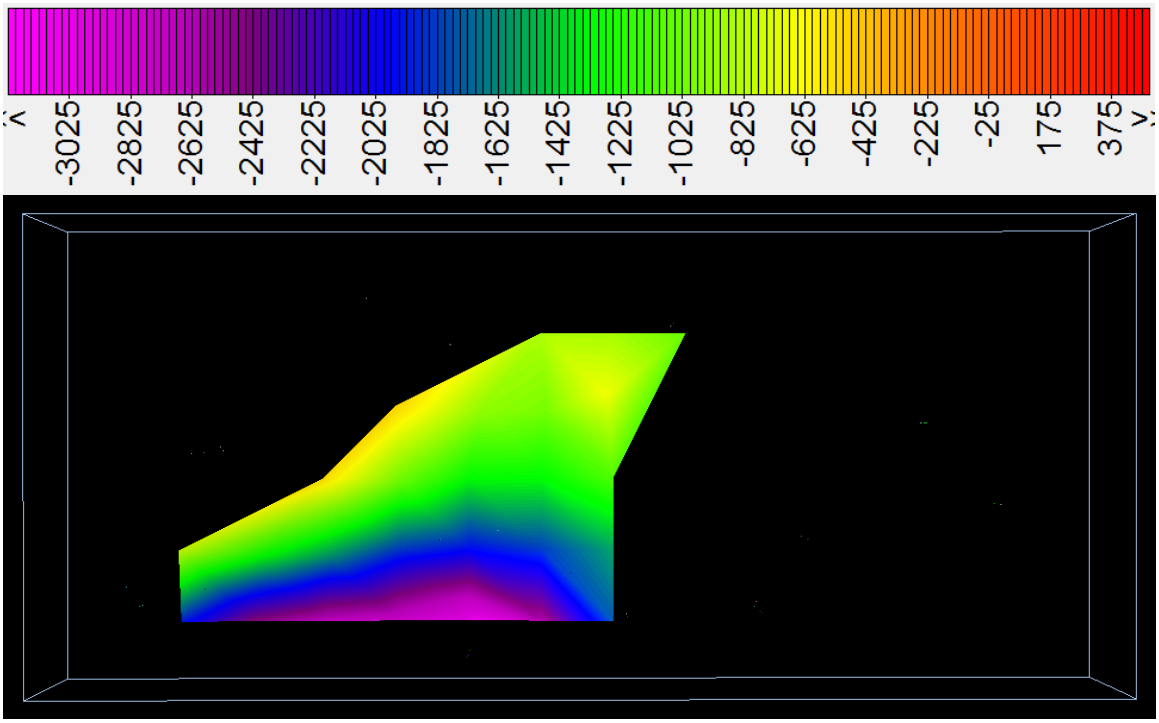

Figure 32) Map view of the Lidah Formation. North is toward the top of the image; legend represents depth in feet. VE=20.

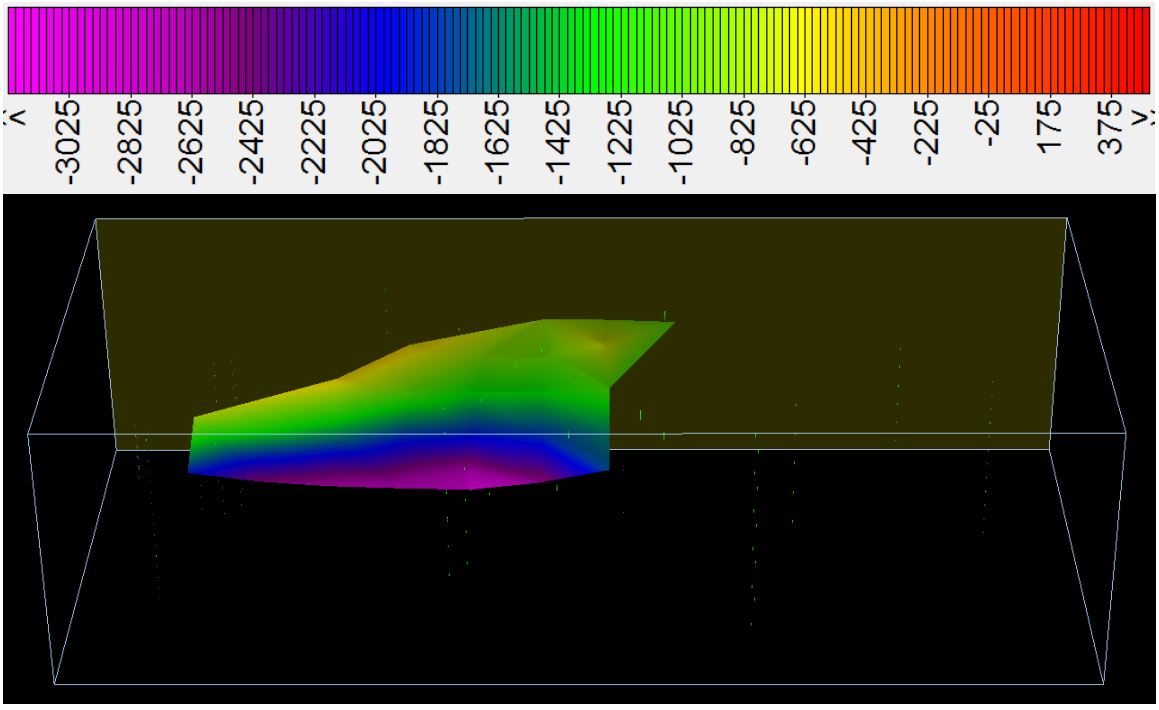

Figure 33) 2D surface representing the Lidah Formation. Shaded box indicates north; legend represents depth in feet. VE=20.

Together, the Ngimbang, Kujung, and Tuban Formations make up the Bali Basin's primary petroleum system. Hydrocarbons potentially generated by the upper Ngimbang shale unit would migrate into the overlying Kujung Formation. Impermeable, carbonaceous shales of the Tuban Formation act as a top seal to porous, underlying carbonate sequences. Self-contained petroleum systems may exist where Ngimbang Shales form stratigraphic wedges and/or onlap basement rocks. Additional, intraformational petroleum systems may exist where hydrocarbons are captured by carbonate "pockets" surrounded by shales within the Kujung III unit. Out of sequence overlap between formations in the study area is more prevalent in the primary petroleum system.

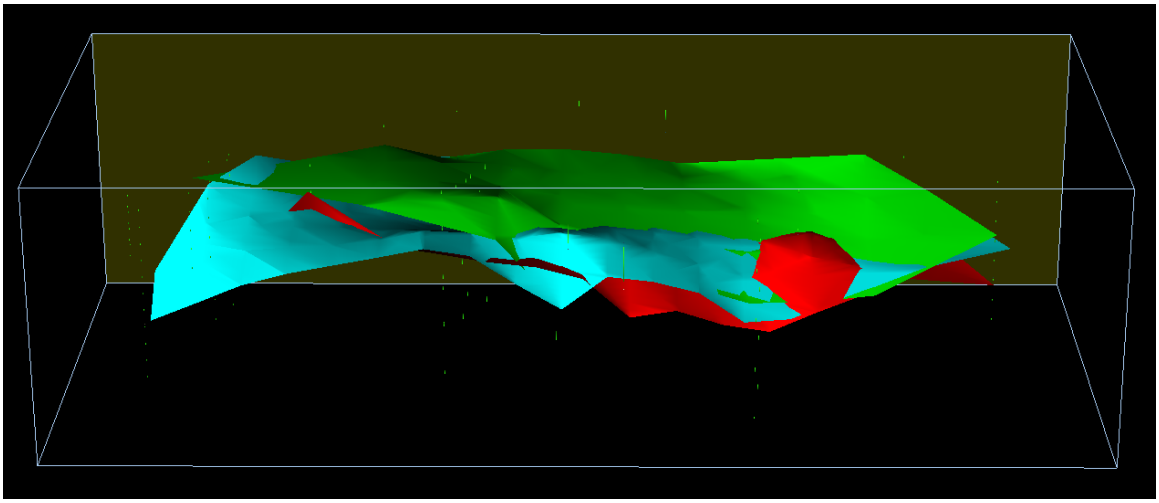

Figure 34) 2D surfaces representing the Ngimbang, Kujung I & II, and Tuban Formations simultaneously rendered. This provides a picture of the primary petroleum system in the north Bali Basin. Surface colors have been altered to more easily distinguish between surfaces; Ngimbang (source): Red, Kujung I & II (reservoir): Blue, Tuban (seal): Green. Shaded box indicates north. VE=20.

The Tuban, Paciran, and Lidah Formations compose the Bali Basin's secondary petroleum system. In this model, carbonaceous shales of the basal Tuban Formation seal underlying hydrocarbons, while producing hydrocarbons of their

own which are then stored in the overlying Paciran Formation and sealed by impermeable clays of the Lidah Formation. Overlap of formation surfaces exists in the secondary petroleum system, but not to the significance observed in the primary system.

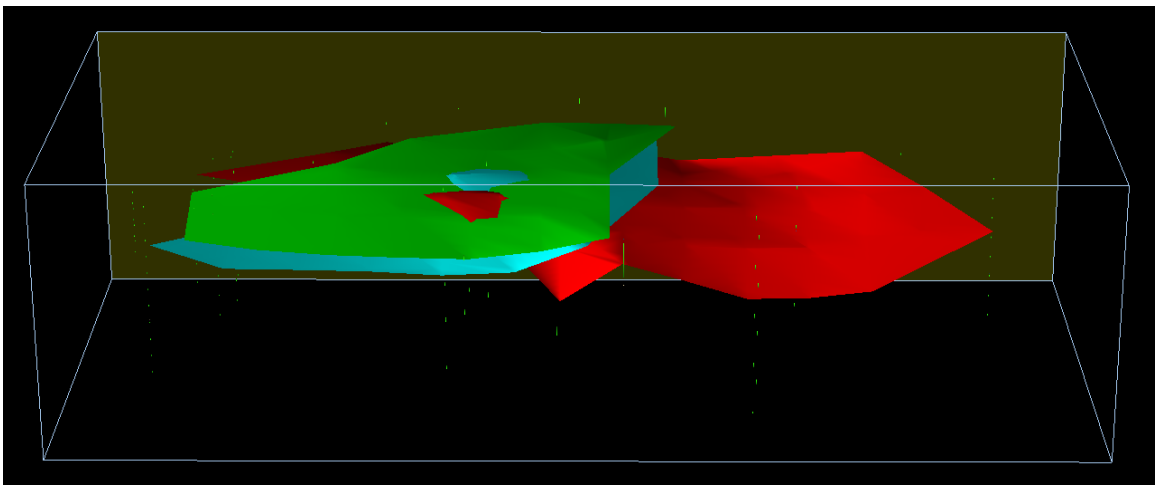

(Figure 35) 2D surfaces representing the Tuban, Paciran, and Lidah Formations simultaneously rendered. This provides a picture of the secondary petroleum system in the north Bali Basin. Surface colors have been altered to more easily distinguish between surfaces; Tuban (source): Red, Paciran (reservoir): Blue; Lidah (seal): Green. Shaded box indicates north. VE=20.

Reservoir Characterization

With an average effective porosity (Φef) of 17.5%, the Kujung I & II Units show good reservoir characteristics; additionally, their stratigraphic position, directly above the Ngimbang Formation, makes the migration of hydrocarbons into these units very likely. The Kujung III Unit showed an average Φef value of 15.4%. While this makes the unit the least porous of the assessed lithologies, it is still well within the parameters expected from good reservoirs and lies stratigraphically adjacent to the source rocks. The Paciran Formation contained the highest average effective porosity of 21.5%; however, its distance from the primary source interval

makes it a secondary reservoir. Maps showing changes in Φef throughout these reservoirs can be found in Appendices G-I.

Source Interval Depths

In assessing the maturity of source rocks in the Bali Basin, the depth to each source interval was compared to the same interval depths in productive wells of the Northeast Java Basin. In the Bali Basin, the Tuban Formation has an average depth of 2,880 feet and the Ngimbang Formation has an average depth of 5,097 feet. In the Northeast Java Basin, the Tuban Formation has an average depth of 3,103 feet and the Ngimbang Formation has an average depth of 9,103 feet. This means the Tuban and Ngimbang source intervals in the Bali Basin are respectively 223 and 4,006 feet shallower than the same intervals in the Northeast Java Basin.

Heat Flow Analyses

In order to assess the thermal maturity of potential hydrocarbons in the Bali Basin, a heat flow analysis was conducted for the study area using bottom hole temperature, lithology, and well depth information recorded in LBH drilling reports. This information was used with equation (5) to calculate a Q value for each well. These values were then spatially plotted and contoured in ArcMap. Heat flow data collection and analysis was expanded to include all of Indonesia in order to give more breadth to this aspect of the study.

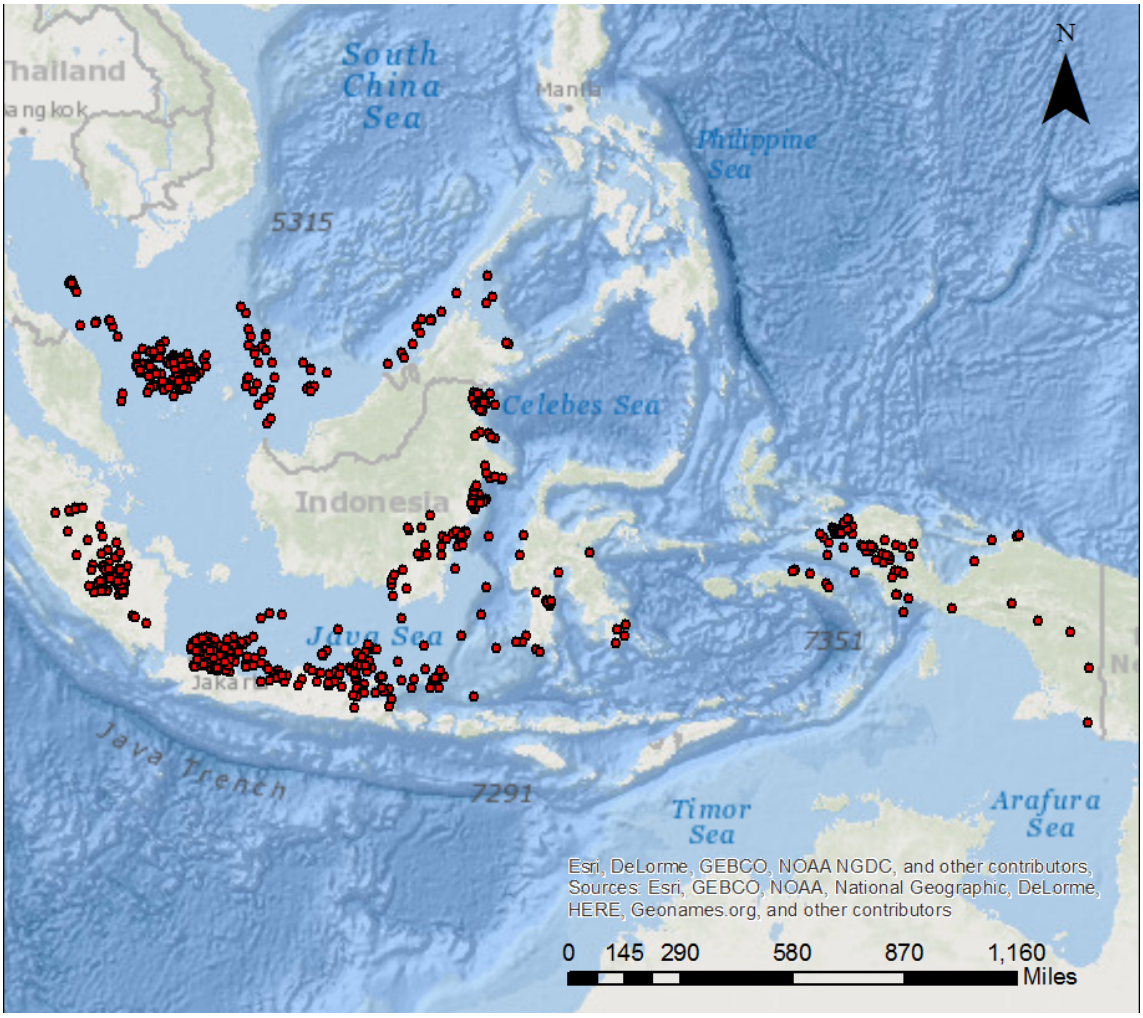

Figure 36) Map showing the locations of wells used to construct the regional heat flow map.

Expanding the heat flow analysis to include most of Sundaland allows heat flow data recorded in the Bali Basin to be viewed with regional context. By restricting the heat flow layer in ArcMap only to areas containing wells, extrapolation by the software is minimized because areas missing data are removed; this ensures the heat flow map is as accurate as possible.

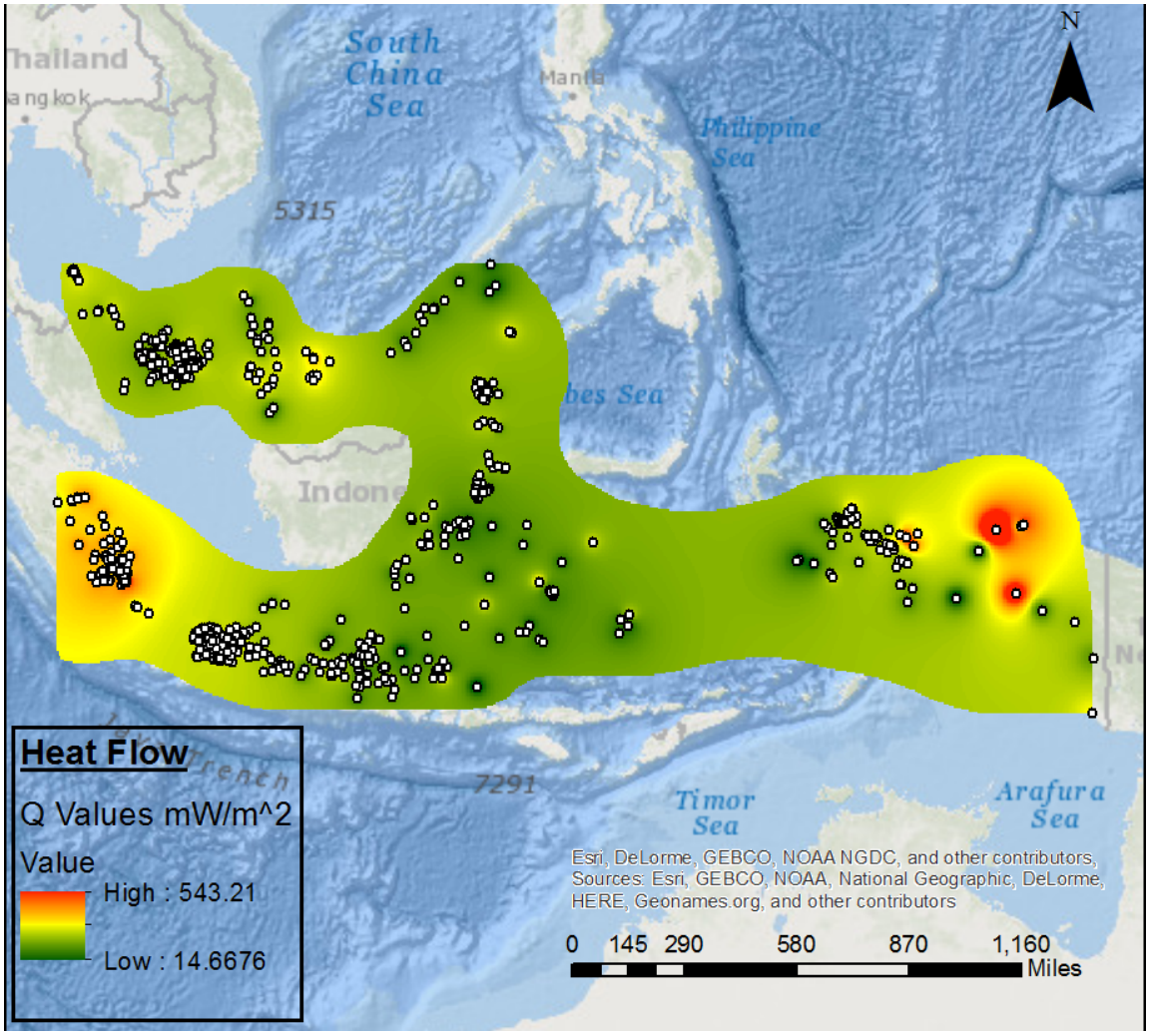

Figure 37) Map plotting Q values across Sundaland. Polygonal restriction minimizes extrapolation by the program and increases accuracy between wells. Well dots are colored white to contrast the heat flow layer.

In the Bali Basin, discrepancies between wells used for 2D modeling and wells used for heat flow analysis exist because some wells that do contain stratigraphic data do not contain information regarding the thermal conditions of the well.

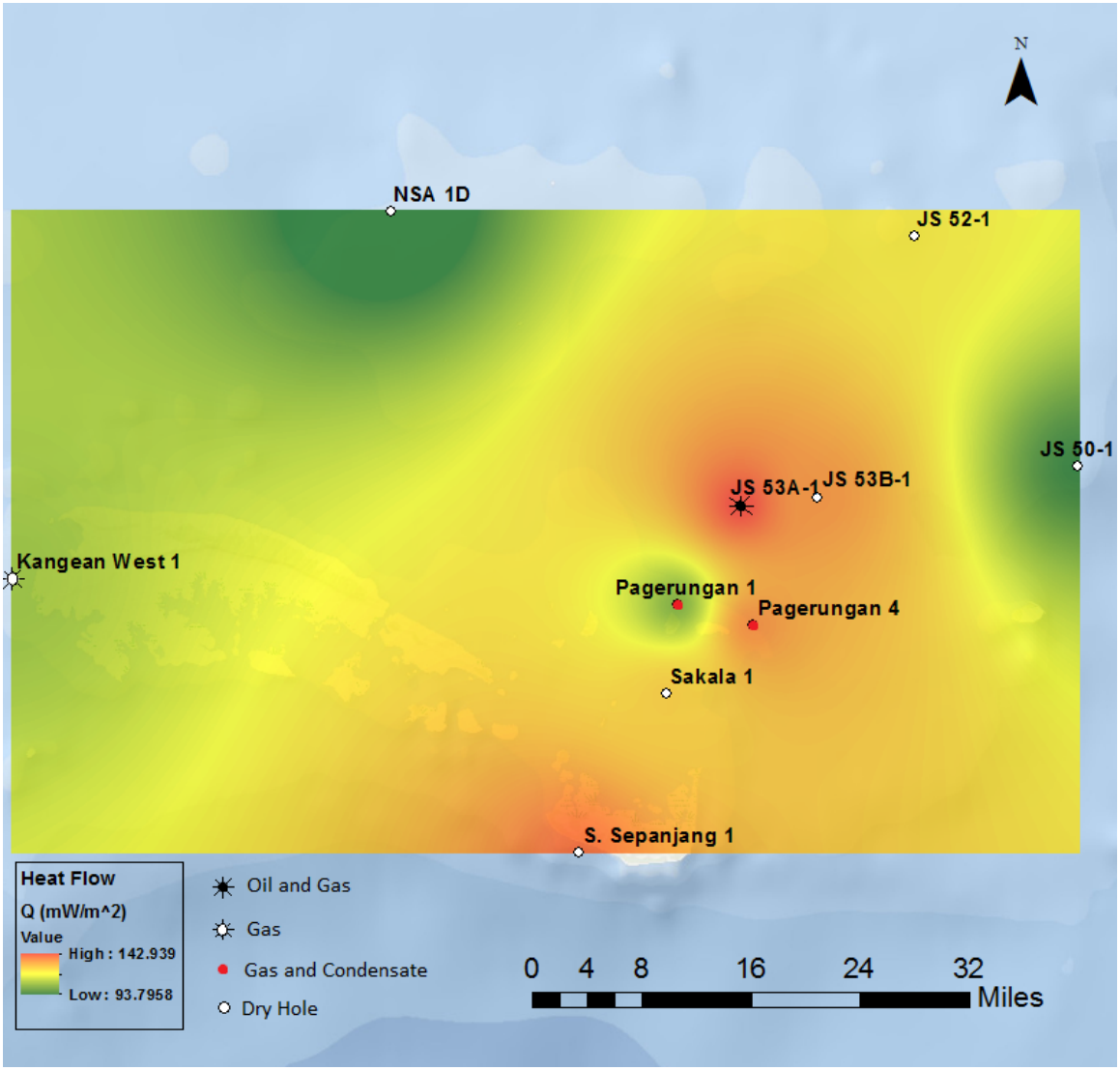

Figure 38) Map plotting the heat flow (Q) values and production of wells in the study area. A list of oil and gas shows in dry holes can be found in appendix F.

Average heat flow in the Bali Basin is 122.3 mW/m^2 with an average bottom hole temperature of 78.0°C. Heat flow is directly affected by temperature and thermal conductivity and is affected inversely by depth. In order to better understand the influences behind heat flow in the Bali Basin, maps plotting bottom hole temperature, well depth, thermal conductivity, and thermal gradient were created (Appendices J-M).

Discussion

Although the Bali Basin longitudinally occupies the area from the northern shores of Bali and Lombok to the Kangean Ridge, the LBH database only contains wells located along the southern shores of the Kangean Islands; this area only represents the mid-northern portion of the basin. The lack of wells south of "ST Alpha 1" (Fig. 15) means the Bali Basin is empirically represented only by its shallowest, most deformed region and that information regarding the center of the basin must be hypothesized and extrapolated. Source rocks located in the center of the basin would be located at greater depths and are more likely to have reached thermal maturity. Additionally, strata in the basin's center lie further from sources of deformation along the Bali Basin's northern and southern margins. Such a location may allow for the formation of thrust faults necessary to the entrapment of hydrocarbons without excessive displacement, which may release otherwise trapped hydrocarbons. Exploration of the Bali Basin's center would greatly enhance our knowledge of this poorly understood feature and could yield a high payout if significant hydrocarbon stores were discovered.

Petroleum Systems Elements

Primary System: Oligo-Miocene Reef Play

Source

- The Ngimbang Shale Unit is the main source rock in the Bali Basin; it contains high TOC levels and type II and III kerogen, making it prone to producing oil and primarily gas. Gas production is seen in the Pagerungan field on the Kangean Ridge, along the Bali Basin's northern margin.
- Secondary hydrocarbon generation may occur in particularly shaly portions of the Kujung III Unit, as observed in the Northeast Java Basin and in the Java Sea, northwest of the study area. The Kujung III Unit shallows up so the generation of hydrocarbons would be most likely to occur near the base of the unit, close to its boundary with the underlying Ngimbang Formation.

Reservoir

- The Kujung Formation shows very good porosity and directly overlies the Ngimbang Formation, giving it excellent stratigraphic position for the capture and storage of hydrocarbons generated at depth.
- Additional reservoirs may exist where hydrocarbons become trapped by intraformational pinchouts of carbonate and shale in both the Ngimbang Clastic and Kujung III Units.

Seal

- The widespread, impermeable Tuban Shale Unit overlies and behaves as a top-seal to the Kujung Formation.

- Intraformational seals may exist in the Kujung III Unit, where interfaces between shale and limestone create pockets of hydrocarbon in the unit.
- The Ngimbang Shale Unit can act as a seal to hydrocarbons stored in the Ngimbang Clastic Unit.

Timing

- Eocene deposition of the Ngimbang Formation (source).
- Oligocene-Early Miocene deposition of Kujung Formation (reservoir).
- Early Miocene deposition of Tuban Formation (seal).
- Miocene-present basin inversion (trap formation, migration pathway creation, and thermal sourcing).
- Late Miocene-present back-arc subduction (additional thermal sourcing and uplift).

Advantages

- The source, reservoir, and seal are all stratigraphically adjacent. This leaves a smaller distance for generated hydrocarbons to migrate through the rock column, leaving fewer opportunities for deviation from their path to the reservoir (primary migration).
- The Ngimbang Formation is a proven producer in the North East Java Basin and may possess self-contained hydrocarbon plays where the Ngimbang Carbonate Unit acts a reservoir to Ngimbang Clastic generated hydrocarbons. Additional plays may exist where the formation onlaps basement.
- The Kujung Formation occupies a large portion of the stratigraphic column, allowing the formation to act as a high-volume reservoir.

- This system is stratigraphically deeper than the secondary system, making adequate thermal maturity more likely.

Disadvantages

- 2D modeling shows high levels of deformation and overlap between layers. Tectonic inversion in this area may have exceeded the creation of structural traps and facilitated the escape of hydrocarbons to the surface.

Secondary System: Miocene Sourced Shallow Carbonate and Clastic Play

Source

- The Tuban Formation has the potential to generate hydrocarbons, as it has in some areas of the Northeast Java Basin, provided the proper depths and thermal conditions are met.

Reservoir

- The Paciran Formation shows excellent porosity, can store hydrocarbons generated by both sources, and is directly overlain by a sealing unit.

Seal

- Impermeable clays of the Lidah Formation directly overlie the Paciran Formation and act as the sealing unit.

Timing

- Early Miocene deposition of the Tuban Formation (source).
- Miocene-present basin inversion (trap formation, migration pathway creation, and thermal sourcing).
- Upper Miocene-present back-arc subduction (additional thermal sourcing and uplift).

- Early Pliocene deposition of the Paciran Formation (reservoir).
- Pliocene deposition of the Lidah Formation (seal).

Advantages

- The secondary system overlies both source intervals. This increases the amount of hydrocarbons it can potentially capture, as hydrocarbons that may have bypassed the Tuban Formation via fault systems would have the chance to be stored in the Paciran Formation.
- The Lidah and Paciran Formations show less deformation than the primary petroleum system and lie uniformly in sequence.

Disadvantages

- Their shallow depths make the reservoir and seal more susceptible to uplift and erosion, as evidenced by the Lidah-Paciran unconformity.
- Occupying a shallow depth in an already shallow basin could result in a lack of source rock maturity.
- If the Tuban Formation has not entered the oil window, hydrocarbons stored in the Paciran Formation would have to be sourced by Ngimbang Formation due to the lack of alternative shallower sources. The greater distance from the Ngimbang Formation means generated hydrocarbons would have more opportunities to become trapped in non-Paciran strata or escape via deep reaching faults. Additionally, Ngimbang sourced hydrocarbons stored in the Paciran Formation would have to have bypassed the Tuban seal entirely.
- The Lidah and Paciran Formations are not as laterally extensive as the primary petroleum system elements and were deposited after thermal

sourcing and trap formation; however, ongoing subduction and basin inversion, coupled with the Tuban Formation's shallower depth, may mitigate this issue.

Unconventional System: Intraformational Eocene Clastic and Carbonate Play

There is potential for the Ngimbang Formation to behave as an intraformational petroleum system. In this case coal seams and any organic-rich mudstones located in the basal Ngimbang Clastic Unit could source the overlying sandstones of the same unit and limestones of the overlying Carbonate Unit. The Ngimbang Shale Member would then seal the system. However, coal seams alone could not produce an adequately voluminous and high quality column of hydrocarbon. Additionally, even if more appropriate sources in the Ngimbang Clastic Unit were able to generate significant hydrocarbons, the primary and secondary petroleum systems outlined by this study would remain relevant. As evidenced by Kaldi et al. (1997), any significantly productive interval of the Ngimbang Clastic Member would produce hydrocarbons in excess of the capillary capacity of the Ngimbang Shale Member, estimated to withhold 700 feet of gas. These excess hydrocarbons would migrate upwards into shallower reservoirs, i.e. the Kujung and Paciran Formations, creating a columnar system of stacked hydrocarbon pools. This pattern of hydrocarbon generation and storage followed by capillary failure and breeching of the seal would continue until the system reached equilibrium.

Trap Assessment

Both the primary system (Fig. 38) and secondary system (Fig. 39) show out-of-sequence overlap between their constituent formations. This overlap is caused by regional compression resulting in the thrusting of lower lying strata on top of overlying layers. These thrust systems supply the mechanics for effective trap creation by which hydrocarbons are captured in between the imbricated thrust sheets; however, excessive thrusting has the potential to release hydrocarbons through deep reaching fault planes.

The primary system is more affected by this deformation, which matches that seen in the basement. This is to be expected as the older rocks in the primary system have been exposed to compressional forces for a greater amount of time. The first formation to not share deformational characteristics with the basement is the Ngrayong Formation (Figs. 28, 29). This indicates that the episodes of thrusting that affected the stratigraphic section from the basement to the Tuban Formation did not affect the section from the Ngrayong and up.

Deformation due to thrusting can be expected to decrease to the south as distance from the Flores Thrust Zone increases. This decrease in thrusting deformation would continue until a point at which influences of the Bali Fold would cause deformation to increase once more. Thrusting and uplift is greatest at the basin's margins and smallest in the center. If convergent motions of the Flores Thrust Zone exceeded the necessary amount for trap creation in the study area, it is likely that effective traps may exist further south.

The formation of hydrocarbon traps and migration pathways was facilitated by basin inversion that was initiated in the Miocene and has continued to present day; a subduction zone that initiated in the Late Oligocene drives this basin inversion. Further uplift, deformation, and thermal sourcing is supplied by the development of an Upper Miocene back-arc subduction zone along the Flores Thrust.

Heat Flow Analyses and Source Interval Depths

In a model subduction zone and back-arc system, the greatest heat flow can be expected to be in the arc itself (80±10mW/m^2), closely followed by the back-arc basin (75±15mW/m^2) (Fig. 8). Heat flow analysis reveals the Bali Basin to be comparatively hot, exhibiting an average Q value 32.3mW/m^2 higher than the upper range predicted by this model. This can be expected, given the additional heat provided by subduction along the Flores Thrust (Prasetyo, 1992; Zubaidah et al., 2013). It is not likely that subduction along the Flores Thrust (Figure 7) is deep reaching, given its relative youth compared to the primary subduction zone, and since it is only a secondary feature of compressive forces along the plate boundary to the south, as opposed to subducting by its own mechanism (Zubaidah et al., 2013). Even so, shallow melting of oceanic crust subducted along the Bali Basin's northern margin, in addition to Indo-Australian Plate subduction to the south, is the most likely cause for the basin's higher than average heat flow.

Expression of heat flow in the Bali Basin is variable. Heat flow is affected directly by temperature and thermal conductivity and inversely by depth. By isolating these constituent values, the way in which heat flow in the study area

manifests can be more accurately observed. For example, well "JS 53 A-1" shows high heat flow, a high BHT, and a deep TD, but only moderate thermal conductivity. This information shows the high Q value of "JS 53 A-1" to be primarily driven by bottom hole temperature, rather than thermally conductive country rock or a reduction of the denominator in equation (5) by shallow depth. The opposite is observed in "Sakala 1", which exhibits moderately high heat flow but a low bottom hole temperature. In this example, Q is driven by thermal conductivity and depth. Variances in the proportions of this constituent data can reveal the nature of heat flow in the study area.

It is generally understood that the "oil window" exists in the temperature range of about 60-160°C at depths of around 6,500-18,000 feet (Levorsen, 1954; Hyne, 2001; Rullkötter, 1993). The study area has an average adjusted bottom-hole temperature of 78.0°C and an average well depth of 7,972 feet**,** placing the it in the lower range of the oil window; however, the Ngimbang Formation lies at an average depth of 5,097 feet. Using the mean thermal gradient of 32°C/km**,** a calculated temperature of ~51.2°C can be assumed at this depth. This places the primary source interval just outside the oil window. In the Northeast Java Basin, which shows an average Q value of 147.6mW/m^2 and average bottom-hole temperature of 87.4°C, the Ngimbang Formation has an average depth of 9,103 feet which places it well within the oil window. This 4,006-foot deviation in source interval depth may be reason for the lack of hydrocarbon production in the Bali Basin

In the study area, the Tuban Formation has an average depth of 2,880 feet. According to the local thermal gradient, a temperature of ~28.2°C can be expected

at this depth, placing the secondary source interval significantly outside the oil window. This interval is also well outside the oil window in the Northeast Java Basin, where the Tuban Formation has an average depth of just 3,103 feet. The Tuban Formation's shallow depth makes the success of the secondary petroleum system unlikely. In the center of the Bali Basin, where the Tuban Formation may lie in low lying depressions or downthrown fault blocks, depths approaching the oil window may be reached; in either case, the primary petroleum system would make a more desirable target.

In comparing the Northwest Java and Bali Basins, the difference in depth to the Ngimbang Formation is far greater (4,006') than the Tuban Formation (223'), which is at about the same depth. This indicates a significant increase in sedimentation after deposition of the Ngimbang Formation in the Northeast Java Basin and/or greater uplift during the Early Miocene inversion, as compared to regions immediately east.

Petroleum System Chronology

The Bali Basin's primary source and reservoir were deposited conformably during a period of Paleocene extension in which organic rich, marginal marine shales of the Ngimbang Formation and transgressive carbonates and siliciclastics of the Kujung Formation were subsequently deposited in local depressions. This extensional regime was reversed by convergence and subduction between the Indo-Australian and Eurasian Plates in the Late Oligocene to Early Miocene. Melting and upwelling of mantle material caused by this subduction zone became the initial source of heat necessary to crack the kerogen stored in the Ngimbang Formation.

The sealing Tuban Formation was deposited concurrent to the early stages of the new compressional regime, which would soon reactivate pre-existing normal faults to cause widespread basin inversion and the creation of potential hydrocarbon traps. Although occurring in rapid succession, initial thermal sourcing predates seal deposition and trap creation by a geologically minor amount of time. Because of this, the possibility of hydrocarbons stored in the Ngimbang Shale maturing before the completion of a functioning seal and trap cannot be ruled out. However, the same mechanism by which hydrocarbon traps were created also formed the primary migration pathways. In order for this scenario to have taken place, catagenesis would need to have occurred rapidly and alternative pre-inversion migration pathways would need to be utilized.

Continued convergence through the Late Miocene to recent time propagated the Flores Thrust Zone into the northern margin of the Bali Basin. This formed a back-arc subduction zone in which oceanic crust of the Sunda Shelf began to subduct beneath the Bali Basin, toward the plate boundary, supplying the petroleum system with an additional heat source. Continued sedimentation through the Neogene led to the deposition of thick siliciclastic and carbonate sequences. The Paciran and Lidah Formations were deposited during the Pliocene and respectively behave as a potential secondary reservoir and seal to hydrocarbons that may have migrated to shallower intervals.

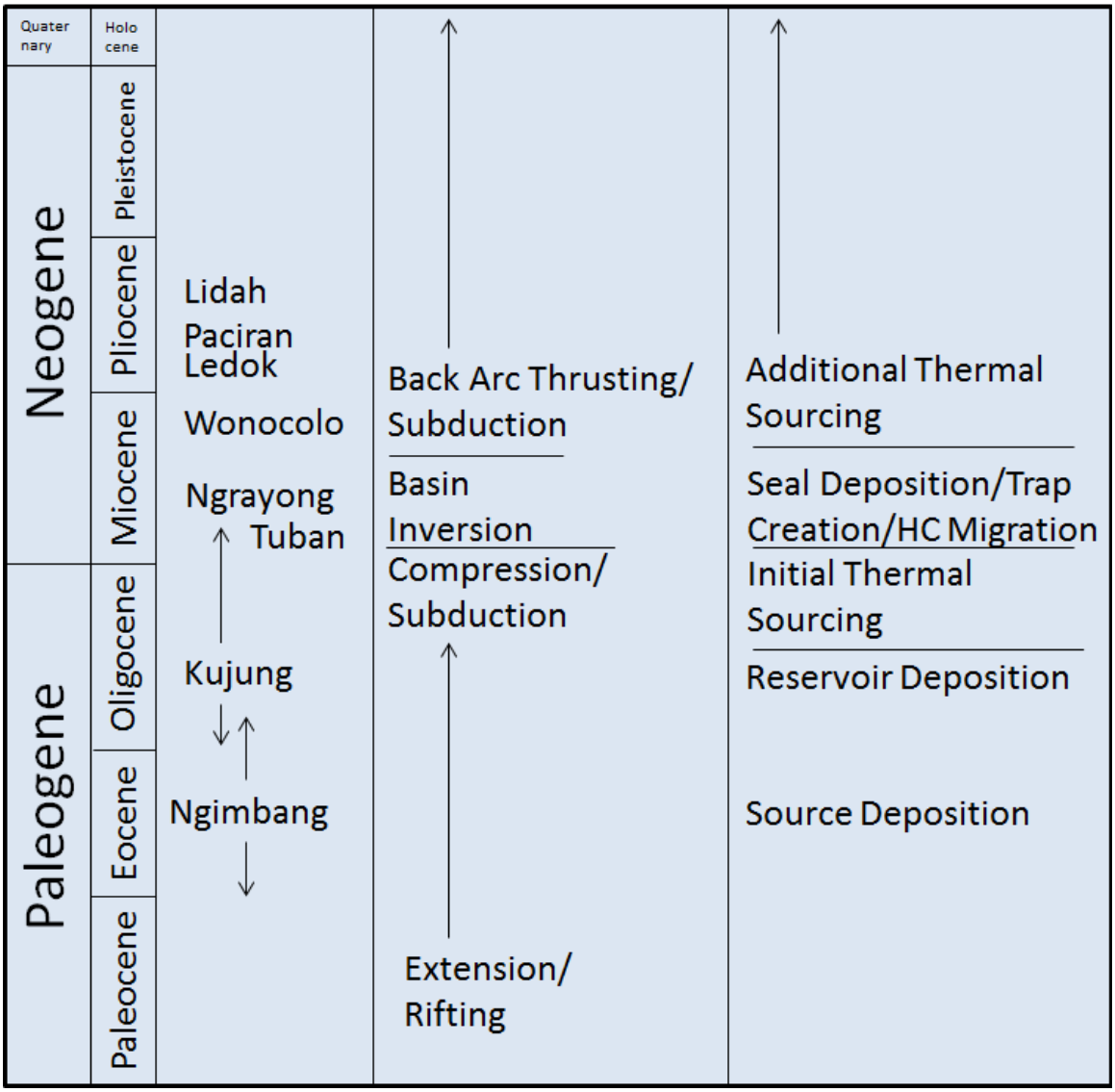

Figure 39) Chart illustrating the timing of petroleum system elements and tectonic history relative to one another.

Given its position over two opposing subduction zones, the Bali Basin can be expected to exhibit higher than average heat flow values. While this expectation is realized, closer investigation of the local thermal regime reveals source intervals in the study area to be just outside the oil window. Broadening the lens, productive areas are found directly west of the study area with deeper source intervals and greater temperatures. This observation fits in with the westerly trend of increasing

heat flow that continues into Sumatra (Figs. 41, 42). This trend generally matches previous heat flow studies conducted by Hall (2002 (a)) (appendix N). While dual subduction brought thermal conditions in the Bali Basin to levels appropriate for hydrocarbon generation, the two opposing convergent margins also formed large thrust belts that caused significant uplift. This uplift may have been great enough to remove the source interval from the oil window during the maturation process before sufficient maturity could be reached. This would explain the limitation of hydrocarbons in the Bali Basin to just a few productive wells. The presence of gas in some areas, namely the Pagerungan field, could be the result of kerogen type as opposed to thermal maturity (Kaldi et al., 1997; Wiloso et al., 2009).

The Bali Basin possesses the necessary qualities of a productive basin. It shares proven source, reservoir, and seal formations with nearby productive fields, the depositional history and trap formation chronology is favorable to the creation of an effective petroleum system, and there is a viable heat source for the cracking of kerogen into petroleum and natural gas. Even given these qualities, the Bali Basin lacks the production seen immediately west. The most likely cause for this lack in production is the concentration of exploratory wells drilled along the basin's northern margin. The Bali Basin's northern margin is directly adjacent to the Flores Thrust Zone, making this area the most susceptible to uplift and deformation. It is along this margin that thrusting may exceed the amount required for trap creation and instead allow the release of previously trapped hydrocarbons. The northern margin marks the shallowest area of the basin, where uplift of the source interval from the oil window is most likely. Heat flow analyses indicate the source interval

along the Bali Basin's northern margin to lie just outside of the oil window. It stands to reason that this interval would lie at greater depths, well within the oil window, in the basin's center; however, this area remains unexplored. The diminished returns offered by wildcat wells along the Bali Basin's northern margin might have deterred petroleum companies from further investments in the area or Bali's illustrious tourism industry may prevent near-shore petroleum exploration. Barring municipal restrictions, exploratory well logging and seismic survey of the Bali Basin's center could supply petroleum explorationists with the information needed to turn this frontier basin into a major producer.

Conclusions

1) Three potential petroleum systems are identified in the Bali Basin, listed here in stratigraphic order:

- The first is internally contained within the Ngimbang Formation, where coals and shales of the Ngimbang Clastic Unit source overlying sandstones of the same member and porous limestone of the Ngimbang Carbonate Unit. The Ngimbang Shale Unit seals this system. If significant hydrocarbon generation occurred in this system, it is likely that excess hydrocarbons would pass through the seal, having breeched its capillary capacity, and charge shallower reservoirs; however, sizable generation of quality hydrocarbons from the Ngimbang Clastic Unit is not likely given the poor source rock quality of coal.
- The second is the primary petroleum system described by this paper, in which hydrocarbons sourced by the Ngimbang Shale and Kujung III Units migrate through reactivated normal faults into the Kujung I & II Units where

they are captured in structural traps created by the reactivated fault systems and sealed by the Tuban Formation. The effective source, reservoir, and seal of this system, in combination with favorable timing of trap creation and hydrocarbon maturation and migration, makes this petroleum system the most likely to contain hydrocarbons.

- The final petroleum system consists of carbonaceous Tuban shales sourcing sandstones and limestones of the Paciran Formation to be sealed by impermeable clays of the overlying Lidah Formation. This system is likely too shallow for adequate petroleum maturation and contains unfavorable timing, particularly that of the reservoir and seal deposition.

2) Depositional history with respect to the timing of trap formation is favorable in the Bali Basin's primary petroleum system: the Oligo-Miocene reservoir was conformably deposited on top of Eocene source rocks, followed by the deposition of a sealing formation and concurrent structural trap development in the Miocene. Heating of the system began in the Late Oligocene by plate boundary subduction. This heat source was augmented in the Late Miocene with the formation of an additional, opposing subduction zone along the Bali Basin's northern margin.

In the unlikely case of hydrocarbons lacking from the Bali Basin entirely, their absence could be explained by two hypotheses: (i) the subduction zones along the Bali Basin's northern and southern margins, while supplying the heat necessary for source rock maturation, concurrently uplifted and removed the source rocks from the oil window; (ii) initiation of plate boundary subduction in the Late Oligocene could have matured the source rocks and facilitated the escape of

hydrocarbons to the surface prior to adequate trap and seal formation in the Early Miocene. This would require rapid catagenesis and the existence of pre-inversion migration pathways.

3) Heat flow in the Bali Basin is high relative to typical back-arc basins (Q = 122.3 mW/m^2); this is expected given its position over opposing zones of subduction. Source interval depth and thermal gradient data indicate the primary source rocks to lie just outside the oil window; however, this is according wells drilled along the basin's highly uplifted and deformed northern margin. In the center of Bali Basin, it is likely for the primary source interval to have reached depths well within the oil window. For this reason, exploratory well logging and seismic survey in the center of the Bali Basin would prove advantageous to those seeking oil and gas in this region.

References

Ardhana, W., Lunt, P., and Burgon, G.E., 1993, The deep marine sand facies of the Ngrayong Formation in the Tuban Block, East Java Basin, Indonesian Petroleum Association, Clastic Core Workshop, p. 118-175.

Asquith, G., and Krygowski, D., 2004, Porosity Logs, *in* Asquith, G., and Krygowski, D., eds., Basic Well Log Analysis: AAPG Methods in Exploration 16, p. 37-76.

Asquith, G., and Krygowski, D., 2004, Gamma Ray, *in* Asquith, G., and Krygowski, D., eds., Basic Well Log Analysis: AAPG Methods in Exploration 16, p. 31-35.

Aziz, S., Sutrisno, Noya, Y., and Brata, K., 1993, Geology of the Tanjungbumi and Pamekasan Quadrangle, Jawa, Bandung: Geological Research and Development Center, p. 11.

Batir, J.F., Blackwell, D.D., and Richards, M.C., 2013, Updated heat flow of Alaska, new insights into the thermal regime: Final Report to the Alaska Energy Authority and Alaska Center for Energy and Power, June 15, 2013.

Baumann, P.H., Suminta, O., and Wibisono, 1972, The Cenozoic of Java and Sumatra: Proceedings of the Indonesian Petroleum Association, 1st Annual Convention, p. 31–42.

Ben Avraham, Z., and Emery, K.O., 1973, Structural Framework of Sunda Shelf: American Association of Petroleum Geologists, v. 57, p. 2323-2366.

Bishop, M.G., 2000, Petroleum systems of the Northwest Java Province, Java, and offshore Southeast Sumatra, Indonesia: United States Geological Survey, Open-File Report 99-50R.

Bransden, P.J.E., and S.J. Matthews, 1992, Structural and stratigraphic evolution of the East Java Sea, Indonesia: Proceedings of Indonesian Petroleum Association, 21st Annual Convention, October 1992, p. 417–453.

Coron, C.A., 1994, Wrench fault control on sedimentation in the East Java, Madura, Sakala, and Bali Basins: American Association of Petroleum Geologists, Annual Convention, Denver, Colorado, June 12-15, 1994, Abstract, v. 1994, p. 126, 1994.

Curray, J.R., Moore, D.G., Lawver, L.A., Emmel, F.J., Raitt, R.W., Henrey, M., and Kieckhefer, R., 1978, Tectonics of the Andaman Sea and Burma: American Association of Petroleum Geologists, Mem., 29, p. 189-198, 1978.

DeMets, C., Gordon, R.G., and Argus, D.F., 2010, Geologically current plate motions: Geophysical Journal International, v. 181, p. 1–80, doi:10.1111/j.1365-245X.2009.04491.x.

Doust, H., and Noble, R.A., 2007, Petroleum systems of Indonesia: Marine and Petroleum Geology, v. 25, p. 103-129.

Doust, H., and Sumner, S.H., 2007, Petroleum systems in rift basins-a collective approach in Southeast Asian basins: Petroleum Geoscience, v. 13, p. 127-144.

Downey, M. W., 1984, Evaluating seals for hydrocarbon accumulations: AAPG Bulletin, v. 68, p. 1752-1763.

Eppelbaum, L., Kutasov, I., and Pilchin, A., 2014, Thermal Properties of Rocks and Density of Fluids: Applied Geothermics: Ó Springer-Verlag Berlin Heidelberg 2014, p. 99-130, doi: 10.1007/978-3-642-34023-9_2.

Fainstein, R., 1997, Seismic prospects offshore North Madura, East Java Sea: Society of Exploration Geophysicists, 67th Annual Meeting, v. 16, p. 643-646.

Hall, R., 1997, Cenozoic plate tectonic reconstructions of SE Asia, *in* S. J. Mathews and R. W. Murphy, eds., Petroleum Geology of Southeast Asia: Geological Society, London, Special Publication 126, p. 11–23.

Hall, R., 2002 (a), SE Asian Heatflow: call for new data: IPA Newsletter, June 2002, p. 20-21; SEAPEX Press, April 2002, v. 5(2), p. 54-56.

Hall, R., 2002 (b), Cenozoic geological and plate tectonic evolution of SE Asia and the SW Pacific, Computer-based reconstructions, model, and animations: Journal of Asian Earth Sciences, v. 20, no. 4, p. 353–431.

Hall, R., 2011, Australia–SE Asia collision: plate tectonics and crustal flow, *in* Hall, R., Cottam, M. A. & Wilson, M.E.J., eds., The SE Asian Gateway: History and Tectonics of the Australia–Asia Collision: Geological Society, London Special Publication 355, p. 75– 109. doi: 10.1144/SP355.5.

Hall, R., 2014, The origin of Sundaland: Proceedings of Sundaland Resources 2014, MGEI Annual Convention, 17-18 November 2014, Palembang, South Sumatra, Indonesia.

Hamilton, W., 1979, Tectonics of the Indonesian region: United States Geological Survey, Professional Paper 1078.

Horner, D.R., 1951, Pressure build-up in wells: Proceedings of the Third World Petroleum Congress, The Hague.

Hutchinson, C.S., 1992, The Eocene unconformity on Southeast and East Sundaland: Geological Society of Malaysia, Bulletin 32, p. 69-88, November 1992.

Hyndman, R.D., Currie, C.A., and Mazzotti, S.P., 2005, Subduction zone backarcs, mobile belts, and orogenic heat: GSA Today 15, 4- 10.

Hyne, N.J., 2001, Nontechnical Guide to Petroleum Geology, Exploration, Drilling, and Production: 2nd ed, Pennwell Books.

Johansen, K.B, 2003, Depositional geometries and hydrocarbon potential within Kujung carbonates along the North Madura Platform, as revealed by 3D and 2D seismic data: Proceedings of the Indonesian Petroleum Association, Twenty-Ninth Annual Convention & Exhibition, October 2003.

Junghuhn, F., 1854, Java, its shape, plant cover, and interior design: v. 2, Leipzig, Arnoldische Buchhandlung, 1854.

Kaldi, J.G., Macgregor, D., and O'Donnell, G.P., 1997, Seal capacity in dynamic petroleum systems: Example from Pagerungan Gas Field, East Java Sea, Indonesia: Proceedings of the Petroleum Systems of SE Asia and Australasia Conference, May 1997.

Keep, M., Longley, L., and Jones, R., 2003, Sumba and its effect on Australia's northwestern margin: Geological Society of Australia Special Publication, v. 22, p. 303-312.

Kohar, A., 1985, Seismic expression of Late Eocene carbonate build-up features in the JS25 and Sepanjang Trend, Kangean Block: Proceedings Indonesian Petroleum Association, Fourteenth Annual Convention, October 1985.

Krishna, N.R., and Sanu, T.D., 2002, Shallow seismicity, stress distribution and crustal deformation pattern in the Andaman-West Sunda arc and Andaman Sea, northeastern Indian Ocean: Journal of Seismology, v. 6, p. 25-41.

Kundu, B., and Gahalaut, V.K., 2011, Slab detachment of subducted Indo-Australian plate beneath Sunda arc, Indonesia: Journal of Earth Systems Science, v. 120, n. 2, p. 193-204.

Kusnida, D., Silalahi, I.R., Yuningsih, A., and Sudjona, E.H., 1995, Geological transition between southeast Sunda Shelf and Bali Trough: revealed by quantitative magnetic interpretation: Bulletin of the Marine Geological Institution of Indonesia, v. 10, issue 1, p. 1-12.

Larionov, V.V., 1969, Radiometry of Boreholes: NEDRA, Moscow.

Levorsen, A.I., 1954, The Geology of Petroleum: W.H. Freeman, San Francisco, California.

Longley, I.M., 1997, The tectonostratigraphic evolution of SE Asia, *in* Fraser, A. J., Matthews, S. J., and Murphy, R. W., eds., Petroleum Geology of Southeast Asia: Geological Society Special Publication no. 126, p. 311-339.

Lüschen, E., Müler, C., Kopp, H., Engels, M., Lutz, R., Planert, L., Shulgin, A., and Djajadihardja, Y.S., 2011, Structure, evolution and tectonic activity of the eastern Sunda forearc, Indonesia, from marine seismic investigations: Tectonophysics, v. 508, p. 6-21.

Matthews, S.J., and Bransden, P.J.E., 1995, Late Cretaceous and Cenozoic tectono-stratigraphic development of the East Java Sea Basin, Indonesia: Marine and Petroleum Geology, v. 12, no. 5, p. 499-510.

McGaffey, R., and Nabelek, J., 1987, Earthquakes, gravity and the origin of the Bali Basin: an example of a nacent continental fold-and-thrust belt: Journal of Geophysical Research, v. 92, no. B1, p. 441-460, January 10, 1987.

Metcalfe, I., 2011, Paleozoic–Mesozoic history of SE Asia, *in* Hall, R., Cottam, M. A. & Wilson, M. E. J., eds., The SE Asian gateway: history and tectonics of the Australia–Asia collision: Geological Society, London, Special Publications, v. 355, p. 7–34.

Mudjiono, R., and Pireno, G.E., 2001, Exploration of the North Madura Platform, offshore East Java , Indonesia: Proceedings of the Indonesian Petroleum Association, 28th Annual Convention, v. 1, p. 707-726.

Murphy, R.W., 1998, Southeast Asia reconstruction with a non-rotating Cenozoic Borneo: Geologic Society of Malaysia Bulletin 42, p. 85-94, December 1998.

Najoan, G.A.S., 1972, Correlation of Tertiary lithostratographic units in the Java Sea and adjacent areas: Proceedings of the Indonesian Petroleum Association, First Annual Convention, June 1972, p. 11-16.

Newcomb, K.R., and McCann, W.R., 1987, Seismic history and seismotectonics of the Sunda Arc: Journal of Geophysical Research, v. 92, no. B1, p. 421-439, January 10, 1987.

Pacey, A., Macpherson, C.G., and McCaffrey, K.J.W., 2013, Linear volcanic segments in the central Sunda Arc, Indonesia, identified using Hough Transform analysis: Implications for arc lithosphere control upon volcano distribution: Earth and Planetary Science Letters, v. 370, p. 24-33.

Pandito, R.H., Haris, A., Zainal, R.M., and Riyanto, A., 2016, Hydrocarbon potential assessment of Ngimbang formation, Rihen field of Northeast Java Basin: American Institute of Physics Conference Procedings 1862, 030191, 2017.

Park, R.K., Matter, A., and Tonkin, P.C., 1995, Porosity evolution in the Batu Raja carbonates of the Sunda Basin-windows of opportunity: Proceedings of the Indonesian Petroleum Association, 24th Annual Convention, v. 1, p. 163-184.

Peters., K., and Nelson, P.H., 2009, Criteria to determine borehole formation temperatures for calibration of basin and petroleum system models: American Association of Petroleum Geologists Annual Convention and Exhibition Proceedings, Denver, Colorado, June 7-10, 2009.

Posamentier, H.W., Priscilla, L., Alex, W., Meirince, P., and Dedan, D., 2010, Seismic stratigraphy and geomorphology of Oligocene to Miocene carbonate buildups, offshore Madura, Indonesia: Cenozoic Carbonate Systems of Australasia, SEPM Special Publication, no. 95.

Prasetyo, H., 1992, The Bali-Flores Basin: geological transition from extensional to subsequent compressional deformation: American Association of Petroleum Geologists, 21st Annual Convention Proceedings, v. 1, p. 455-478, October 1992.

Prasetyo, H., 1994, Marine geoscientific survey of the west-east Indonesia back arc transition zone, southeast Sulawesi margin: Proceedings of the Session of the Committee for Co-ordination of Joint Prospecting for Mineral Resources in Asian Offshore Areas (CCOP), v. 29, part 2, p. 127-146.

Prasetyo, H., 1995, Structural and tectonic development of eastern Indonesia: Proceedings of the Session of the Committee for Co-ordination of Joint Prospecting for Mineral Resources in Asian Offshore Areas (CCOP), Thirty-first CCOP annual session, Kuala Lumpur, Malaysia, 1995, Abstract, v. 30, Part 2, p. 204-231, 1995.

Prasetyo, H., Sarmili, L., 1994, Structural and tectonic development of west-east Indonesian back arc transition zone: implications for hydrocarbon prospect: Bulletin of the Marine Geological Institution of Indonesia, v. 2, Issue 2, p. 23-60, December, 1994.

Pringgoprwiro, 1983, Biostratigrafi dan paleogeografi Cekungan Jawa Timur Utara, Suatu Pendekatan Baru [Ph.D thesis]: Institut Teknologi, Bandung, Bandung, p. 239.

Rullkötter, J., 1993, The thermal alteration of kerogen and the formation of oil, *in* Engel, M.H., Macko, S.A., eds., Organic Geochemistry, Topics in Geobiology: v. 11, Springer, Boston, Massachusetts.

Satyana, A.H., and Purwaningsih, M.E.M., 2003, Geochemistry of the East Java Basin: New observations on oil grouping, genetic gas types and trends of hydrocarbon habitats: Proceedings of the Indonesian Petroleum Association, Twenty-Nineth Annual Convention and Exhibition, October 2003.

Satyana, A.H., and Djumlati, M., 2003, Oligo-Miocene Carbonates of the East Java Basin, Indonesia: Facies definition leading to recent significant discoveries: American Association of Petroleum Geologists International Conference, Barcelona, Spain, Sep. 21-24, 2003.

Silver, E.A., Reed, D., McCaffrey, R., and Joyowidiryo, Y., 1983, Back arc thrusting in the southern Sunda Arc, Indonesia: a consequence of arc continent collision: Journal of Geophysical Research, v. 88, p. 7429-7448, 1983.

Sharaf, E.F., Simo, J.A., Carroll, A.R., and Shields, M., 2005, Stratigraphic evolution of Oligocene-Miocene carbonates and siliciclastics, East Java Basin, Indonesia: American Association of Petroleum Geologists Bulletin, v. 89, no. 6, p. 799-819, June, 2005.

Sharaf, E.F., BouDagher-Fadel, M.K., Simo, J.A., and Carroll, A.R., 2006, Biostratigraphy and strontium isotope dating of Oligocene-Miocene strata, East Java, Indonesia: Stratigraphy, v. 2, no. 3, 2005.

Steinshouer, D.W., Qiang, J., McCabe, P.J., and Ryder, R.T., 1997, Maps showing geology, oil and gas fields, and geologic provinces of the Asia Pacific region: United States Geological Survey, United States Department of the Interior, Open File Report, 97-470F, 1997.

Shim, B.O., Park, J.M., Kim, H.C., and Lee, Y., 2010, Statistical analysis on the thermal conductivity of rocks in the Republic of Korea: Proceedings World Geothermal Congress, Bali, Indonesia, p. 25-29, April 2010.

Susilohadi, 1995, Late tertiary and quaternary geology of the East Java Basin, Indonesia [Ph.D. thesis]: University of Wollongong, p. 155.

Tikku, A.A., 2011, A revision to the tectonics of the Flores back-arc thrust zone, Indonesia?: American Geophysical Union Fall Meeting, San Francisco, California, December 2011, Abstract, v. 2011.

Tjia, H.D., 1978, Active faults in Indonesia: Geological Society of Malaysia, v.10, p. 73-92, 1978.

Tyrell, W.W., and Davis, R.G., 1982, Miocene carbonate shelf margin, Bali-Flores Sea, Indonesia: Amoco Production Company, Houston, Texas, 1982.

Van Bemmelen, R.W., 1949, The Geology of Indonesia: v. 1a: Government Printing Office, The Hague, p. 732.

Van Gorsel, V.T., 2016, Bibliography of the geology of Indonesia and surrounding areas: Bibliography of Indonesian Geology, part III, edition 6.0, September 2016.

Vavra, C. L., Kaldi, J. G., and Sneider R. M., 1992, Capillary Pressure, *in* D. Morton-Thompson, and A.M. Woods, eds., Development Geology Reference Manual: AAPG Methods in Exploration Series: American Association of Petroleum Geologists, Tulsa, Oklahoma, v. 10, p. 221-225.

Verbeek, R.D.M., R. and Fennema, 1896, Geologische beschrijving van Java en Madoera (geology of Java and Madura): Amsterdam, J. G. Stemler Cz, 2 volumes and atlas, p. 1135.

Welker-Haddock, M., Park, R.K., Asjhari, I., Bradfield, J., and Nguyen, B., 2001, The transformation of Poleng Field: Proceedings of the Indonesian Petroleum Association, 28th Annual Convention, v. 1, p. 681-698.

Widiyantoro, S., Pesicek, J.D., and Thurber, C.H., 2011, Subducting slab structure below the eastern Sunda arc inferred from non-linear seismic tomographic imaging, *in* Hall, R., Cottam, M. A. & Wilson, M. E. J., eds., The SE Asian Gateway: History and Tectonics of the Australia–Asia Collision: Geological Society, London, Special Publications 355, p. 139–155, doi:10.1144/SP355.7.

Wiloso, D.A., Subroto, E.A., and Hermanto, E., 2009, Confirmation of the Paleogene source rocks in the Northeast Java Basin, Indonesia, based from petroleum geochemistry: American Association of Petroleum Geologists International Conference and Exhibition, Cape Town, South Africa.

Xue, F., Broetz, R.J., and Sirodj, E., 2002, Seismic evolution of hydrocarbon prospectivity in offshore north Bali, Indonesia: WesternGeco Data Packages Acreage Review, Petroleum Exploration Society of Australia News, February/March 2002, http://archives.datapages.com/data/petroleum-exploration-society-of-australia/news/056/056001/pdfs/66.htm.

Zubaidah, T., Korte, M., Mandea, M., and Hamoudi, M., 2013, New insights into regional tectonics of the Sunda–Banda Arcs region from integrated magnetic and gravity modeling: Journal of Asian Earth Sciences, v. 80, p. 172–184.

Appendix

Appendix A

Well locations and depths.

Well ID	Latitiude	Longitude	Depth'
SG P-1	-7.05778	117.2542	8,950
ST Z-1	-6.84111	117.0217	5,725
Sakala East 1	-6.95472	116.0767	6,526
JS 50-1	-6.78333	116.3044	5,100
NSA 1-F	-6.58278	116.3742	9,035
Crystal 1	-6.63111	115.7903	7,403
JS 53A-1	-6.82444	115.9475	9,497
JS 53B-1	-6.81611	116.0289	9,412
Pagerungan 5	-6.93528	115.84	6,845
Sidulang 1ST	-6.97944	115.8022	6,286
Sakala 1	-7.02417	115.8681	5,792
Kiau 1	-7.11583	115.9217	4,600
ST Alpha 1	-7.44583	115.8397	7,579
Sepapan 1	-7.02417	115.4142	5,154
Kangean West 3	-6.91222	115.1833	8,245
Kangean West 2	-6.91778	115.1286	9,532
Sirasun 2	-7.26556	115.1683	4,000
Sirasun 1	-7.24778	115.1164	5,814
Arya 1	-7.31333	114.9928	10,015
Terang 3	-7.28	114.9594	3,252
Terang 2	-7.26306	114.9583	3,000
JS 52-1	-6.53972	116.1306	7,453
JS 53A-1	-6.82444	115.9475	9,497
Pagerungan 1	-6.92944	115.8797	9,092
S. Sepanjang 1	-7.19278	115.7753	10,000
L49-1	-7.13944	116.7189	8,176
L46-2	-7.31528	116.6033	11,348
L46-1	-7.33833	116.6103	11,325
L40-1	-7.34111	116.255	12,011
Palung 1	-7.26806	116.0767	7,618
Pagerungan 3ST	-6.94778	115.8281	7,755
Pagerungan 4	-6.95167	115.9606	6,460
NSA 1D	-6.51306	115.5764	7,762
Sepanjang Island 1	-7.13972	115.7717	7,209
Kangean West 1	-6.90194	115.1764	9,000

Appendix B

Thermal conductivities (Shim et al., 2010).

Igneous (Intrusive)	
Lithology	Thermal Conductivity (W/m*K)
Granite	3.33
Diorite	2.87
Feldspar Porphyry	3.23
Quartz Porphyry	3.44
Granite Porphyry	3.37
Acidic Dike	3.93

Igneous (Extrusive)	
Lithology	Thermal Conductivity (W/m*K)
Andesite	2.80
Tuff	2.95
Felsite	3.41
Rhyolite	3.51

Metamorphic (Crystalline)	
Lithology	Thermal Conductivity (W/m*K)
Gneiss	3.72
Schist	4.40
Quartz Schist	6.08

Metamorphic (Non-Crystalline)	
Lithology	Thermal Conductivity (W/m*K)
Phyllite	4.08
Quartzite	5.69
Hornfels	3.46
Amphibolite	3.68
Andesitic Porphyry	2.87

Sedimentary (Detrital)	
Lithology	Thermal Conductivity (W/m*K)
Sandstone	3.81

Breccia	3.13
Mudstone	3.69
Siltstone	3.49
Conglomerate	3.43
Shale	3.82

Sedimentary (Carbonate)	
Lithology	Thermal Conductivity (W/m*K)
Limestone	3.83

Appendix C

Well data used for heat flow calculations.

Well ID	Depth, (km)	Adj. BHT (°C)	Thermal Gradient (°C/km)	Thermal Conductivity (W/m*K)	Heat flow (Q) (mW/m^2)
JS 50-1	1.55448	42.35444	27.2467	3.72	101.3577
JS 53A-1	2.894686	108.3256	37.42222	3.82	142.9529
JS 53B-1	2.868778	101.7911	35.4824	3.81	135.1879
Sakala 1	1.765402	59.00444	33.42268	3.83	128.0088
JS 52-1	2.271674	74.88111	32.96296	3.77	124.2704
Pagerungan 1	2.771242	79.57667	28.71517	3.82	109.6919
S. Sepanjang 1	3.048	102.9767	33.785	4.13	139.532
Pagerungan 4	1.969008	70.10333	35.60338	3.82	136.0049
NSA 1D	2.365858	58.39667	24.68309	3.80	93.79573
Kangean West 1	2.7432	82.57222	30.10069	3.73	112.2756
AVG		**77.9982**			**122.308**

Appendix D

Calculated effective porosities of potential reservoirs.

Kujung I & II	
Well ID	Effective Porosity (Φef)
Crystal 1	9.5%
Kiau 1	26.9%
Pagerungan 5	11.3%
Pagerungan 1	12.1%
Sakala 1	11.4%
SG P-1	25.6%
ST Z-1	24.9%
S. Sepanjang 1	17.5%
Sidulang 1ST	10%
Kangean West 3	14.5%
Kangean West 2	22.4%
Arya 1	20.6%
L 46-2	15.0%
Palung 1	17.8%
Pagerungan 4	18.4%
Pagerungan 3ST	22.0%
AVG	**17.5%**

Kujung III	
Well ID	Effective Porosity (Φef)
Crystal 1	18.1%
SG P-1	18.3%
ST Z-1	0.0%
Sakala East 1	14.7%
Kiau 1	12.0%
S. Sepanjang 1	9.0%
Pagerungan 1	28.7%
Pagerungan 5	12.4%
Kangean West 3	16.4%
Kangean West 2	17.4%
Arya 1	10.9%
L 49-1	10.7%
L 46-2	13.0%
L 46-1	23.6%
L 40-1	17.7%
Pagerungan 4	22.9%
Pagerungan 3ST	17.5%
Sepanjang Island 1	14.2%

Kangean West 1	14.9%
AVG	**15.4%**

Paciran	
Well ID	Effective Porosity (Φef)
Terang 2	23.5%
Terang 3	23.4%
Sakala 1	20.1%
ST Alpha 1	22.5%
NSA 1-F	19.6%
Sirasun 2	22.9%
Sirasun 1	21.5%
Arya 1	22.9%
L 40-1	16.9%
AVG	**21.5%**

The following wells penetrate a reservoir formation, but were unable to be utilized in effective porosity calculations.

Well ID	Reservoir(s)	Reason for Omission
NSA 1-F	Kujung I,II,III	Sonic log not deep enough
JS 52-1	Kujung I,II,III; Paciran	No sonic log
JS 53 B-1	Kujung I,II	No sonic log
JS 53 A-1	Kujung I,II,III	No sonic log
L 40-1	Kujung I,II	No sonic log
JS 25-1	Kujung I,II,III	No sonic log
NSA 1-D	Kujung I,II,III	No sonic log

Appendix E

Source interval depths in the Northeast Java and Bali Basins.

Northeast Java Basin

Well ID	Production	Location	Producing Formation	Depth (ft)
JS 14 A-1	Oil & Gas	Northshore Madura	Tuban Ngimbang	2,280 7,961
Bunku 1A	Oil	Northshore Madura	Tuban	2,585
KE 23-1	Oil	Northshore Madura	Tuban Ngimbang	3,600 10,552
Poleng B-1	Oil & Gas	Northshore Madura	Tuban Ngimbang	3,148 11,000
Poleng B-2	Oil & Gas	Northshore Madura	Tuban	3,900
JS 19 W-1	Oil & Gas	Northshore Madura	Tuban Ngimbang	1,800 6,900
Bunku 1A	Oil	Northshore Madura	Tuban	2,585
JS 01-2	Oil	Northshore Madura	Tuban	2,000
Camar 1	Oil & Gas	Northshore Madura	Tuban	1,970
JS 01-1	Oil & Gas	Northshore Madura	Tuban	1,700
JS 19 W-3	Oil & Gas	Northshore Madura	Tuban	1,752
KE 02 B-1	Oil & Gas	Northshore Madura	Tuban	4,063
KE 02 B-3	Oil & Gas	Northshore Madura	Tuban	3,240
Mudi 01ST	Oil	Northeast Java	Tuban	9,328
Banyubang 1	Oil & Gas	Northeast Java	Tuban	2,592
AVG			Tuban Ngimbang	**3,103** **9,103**

Bali Basin

Well ID	Production	Location	Producing Formation	Depth (ft)

SG P-1	Dry Hole	Bali Basin	Tuban Ngimbang	3,172 6,315
ST Z-1	Dry Hole	Bali Basin	Tuban Ngimbang	1,476 3,937
NSA 1F	Dry Hole	Bali Basin	Tuban Ngimbang	3,060 5,508
Sakala East 1	Dry Hole	Bali Basin	Ngimbang	2,204
JS 53 B-1	Dry Hole	Bali Basin	Ngimbang	7,400
JS 53 A-1	Oil & Gas	Bali Basin	Tuban Ngimbang	1,840 4,600
Kiau 1	Dry Hole	Bali Basin	Tuban Ngimbang	250 3,540
Sakala 1	Dry Hole	Bali Basin	Tuban Ngimbang	1,000 4,194
Pagerungan 5	Gas	Bali Basin	Tuban Ngimbang	300 4,955
Pagerungan 1	Gas & Condensate	Bali Basin	Ngimbang	6,558
Sidulang 1ST	Dry Hole	Bali Basin	Ngimbang	5,260
Crystal 1	Dry Hole	Bali Basin	Tuban Ngimbang	3,114 5140
Sepapan 1	Dry Hole	Bali Basin	Ngimbang	1,550
Kangean West 3	Dry Hole	Bali Basin	Ngimbang	6,815
Kangean West 2	Gas & Condensate	Bali Basin	Tuban Ngimbang	1,700 7,003
S. Sepanjang 1	Dry Hole	Bali Basin	Ngimbang	3,890
JS 52-1	Dry Hole	Bali Basin	Tuban Ngimbang	2,300 4,850
L 49-1	Dry Hole	Bali Basin	Ngimbang	3,000
L 46-2	Dry Hole	Bali Basin	Tuban Ngimbang	6,240 7,000
L 46-1	Oil	Bali Basin	Tuban Ngimbang	6,700 7,500
L 40-1	Unknown	Bali Basin	Tuban Ngimbang	3,700 6,620
Palung 1	Dry Hole	Bali Basin	Tuban	6,040
JS 25-1	Dry Hole	Bali Basin	Ngimbang	3,150

Pagerungan 4	Gas and Condensate	Bali Basin	Tuban Ngimbang	2,888 4,700
Pagerungan 3ST	Gas	Bali Basin	Ngimbang	5,256
NSA 1D	Dry Hole	Bali Basin	Tuban Ngimbang	2,300 6,870
Sepanjang Island 1	Oil	Bali Basin	Ngimbang	3,000
Kangean West 1	Gas	Bali Basin	Ngimbang	6,810
AVG			Tuban Ngimbang	**2,880** **5,097**

Appendix F

Oil and gas shows in dry holes in the Bali Basin.

Well ID	Show(s)	Quality	Depths (ft)
SG P-1	None		
ST Z-1	Oil	Trace	3,400-3,500; 3,900-5,000
	Oil	Poor	3,900
	Oil	Fair	3,500-3,650; 5,000
NSA 1F	Oil	Trace	Throughout
	Oil	Poor	Throughout
Sakala East 1	Oil	Trace	4,846
JS 53 B-1	Gas	Poor	Throughout
	Gas	Fair	Throughout
Kiau 1	None		
Sakala 1	None		
Sidulang 1ST	None		
Crystal 1	None		
Sepapan 1	None		
Kangean West 3	Oil	Trace	4,600-6,400; 7,000-7,100; 7,700, 8,300, 8,900
S. Sepanjang 1	Oil	Fair	2,200
JS 52-2	Oil	Fair	7,000
L 49-1	None		
L 46-2	None		
Palung 1	None		
JS 25-1	Oil	Dead/Residual	Throughout
NSA 1D	None		

Appendix G

Map showing Φef, expressed in decimal percentages, in the Kujung I & II Units.

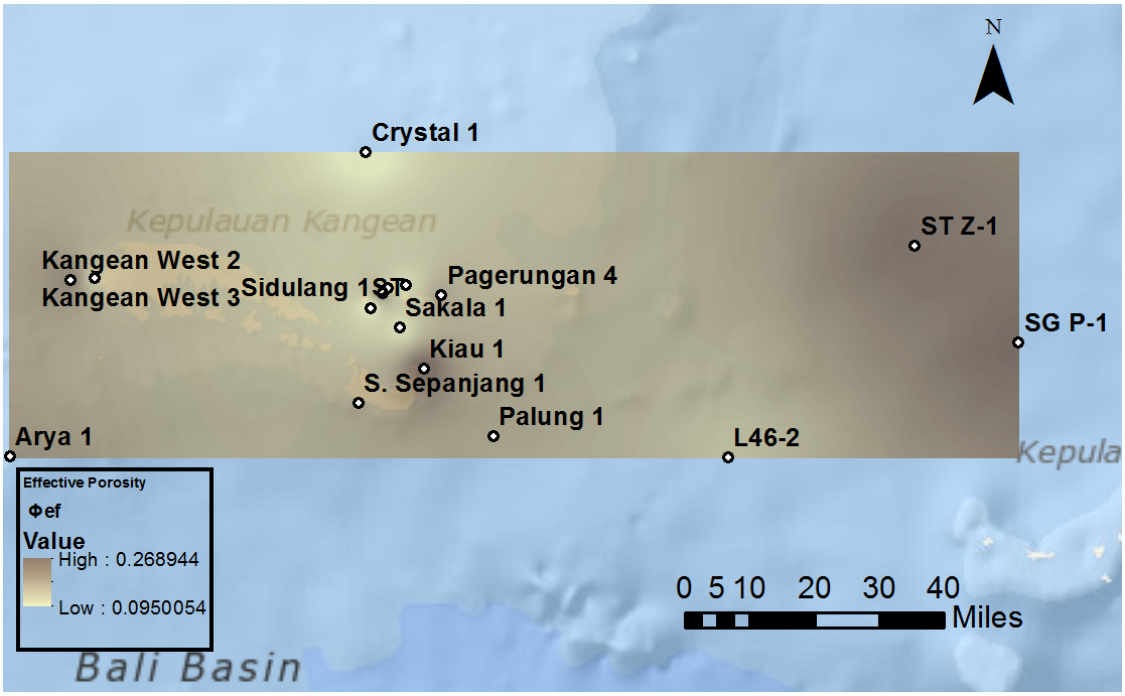

Appendix H

Map showing Φef, expressed in decimal percentages, in the Kujung III Unit.

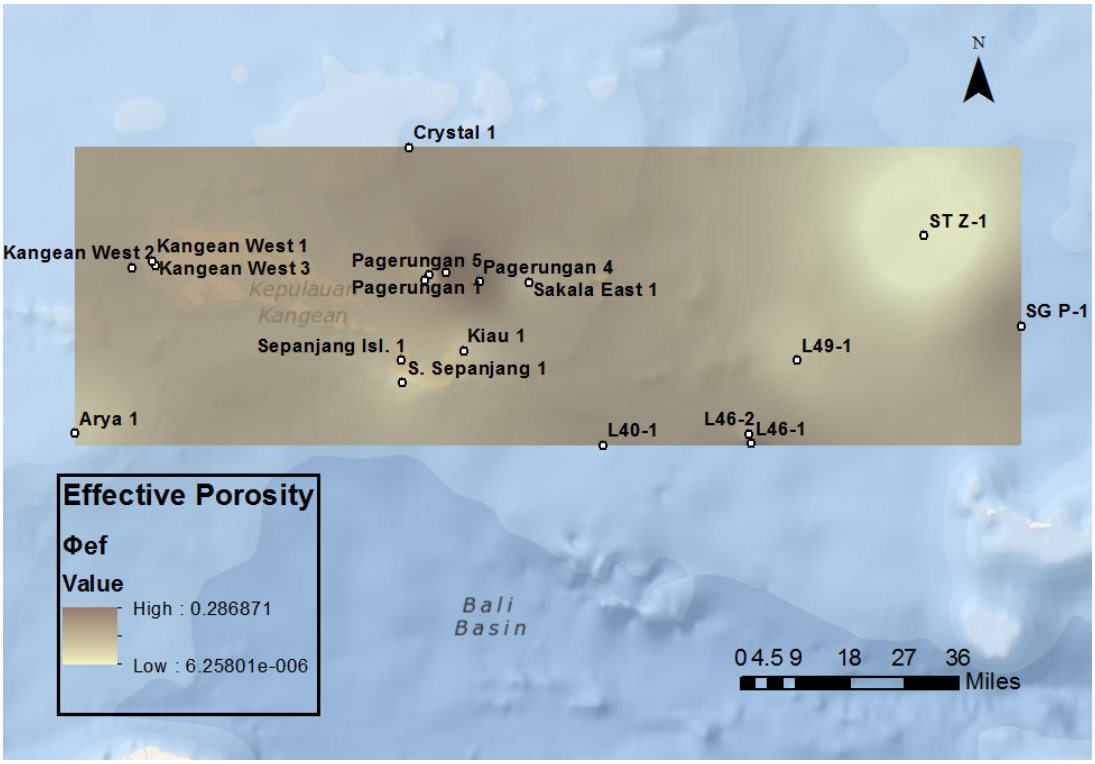

Appendix I

Map showing Φef, expressed in decimal percentages, in the Paciran Formation.

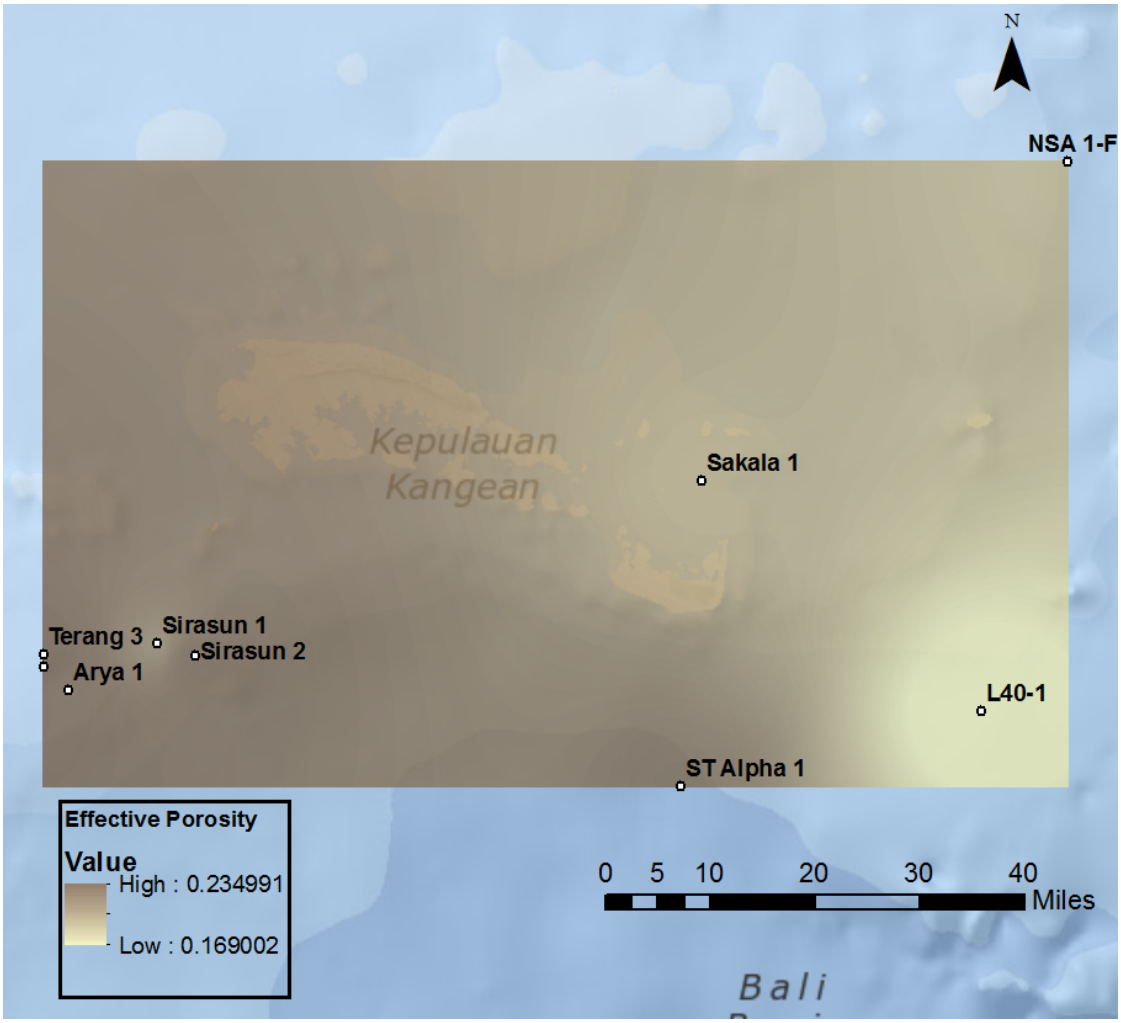

Appendix J

Map showing study area adjusted bottom hole temperatures (ΔT) in °C.

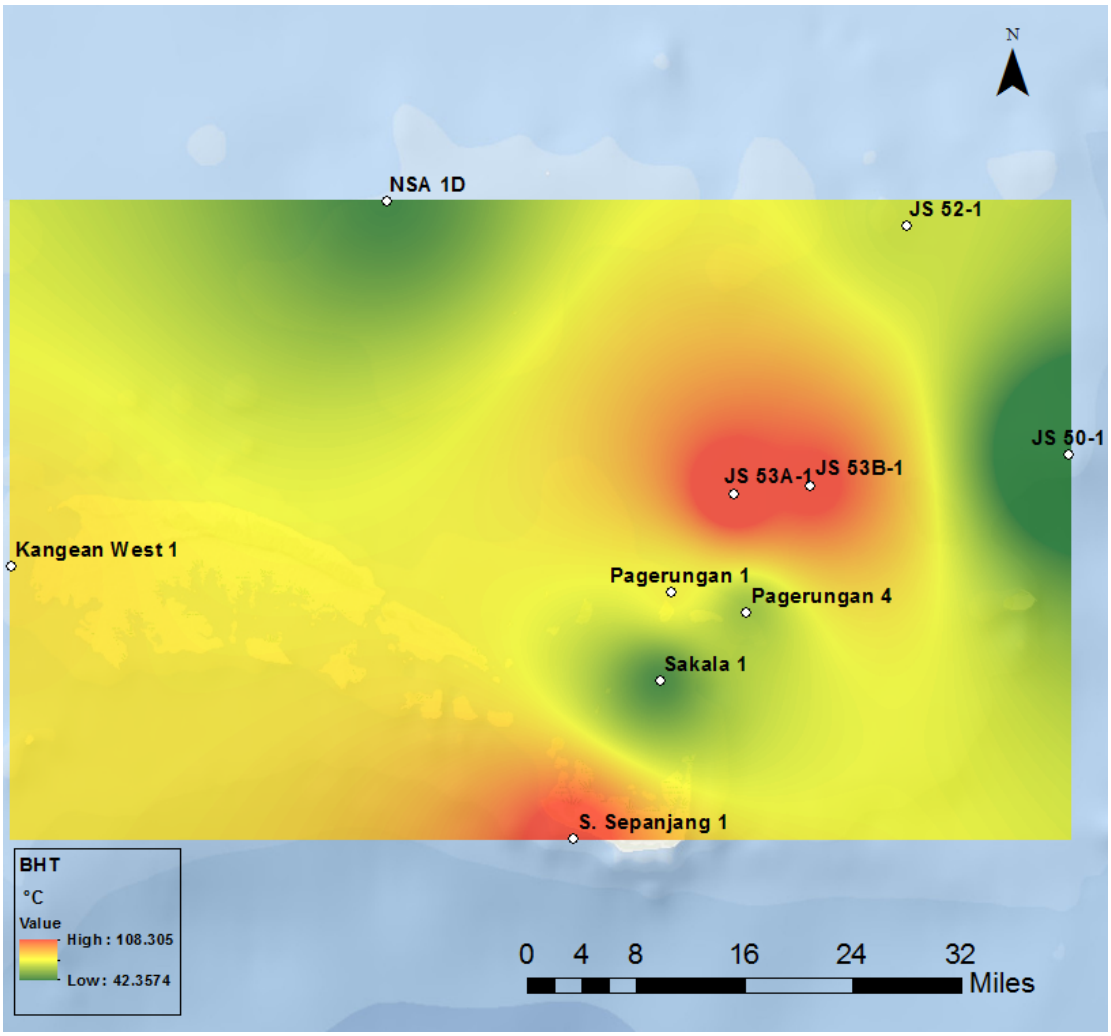

Appendix K

Map showing study area well depths (z) in km.

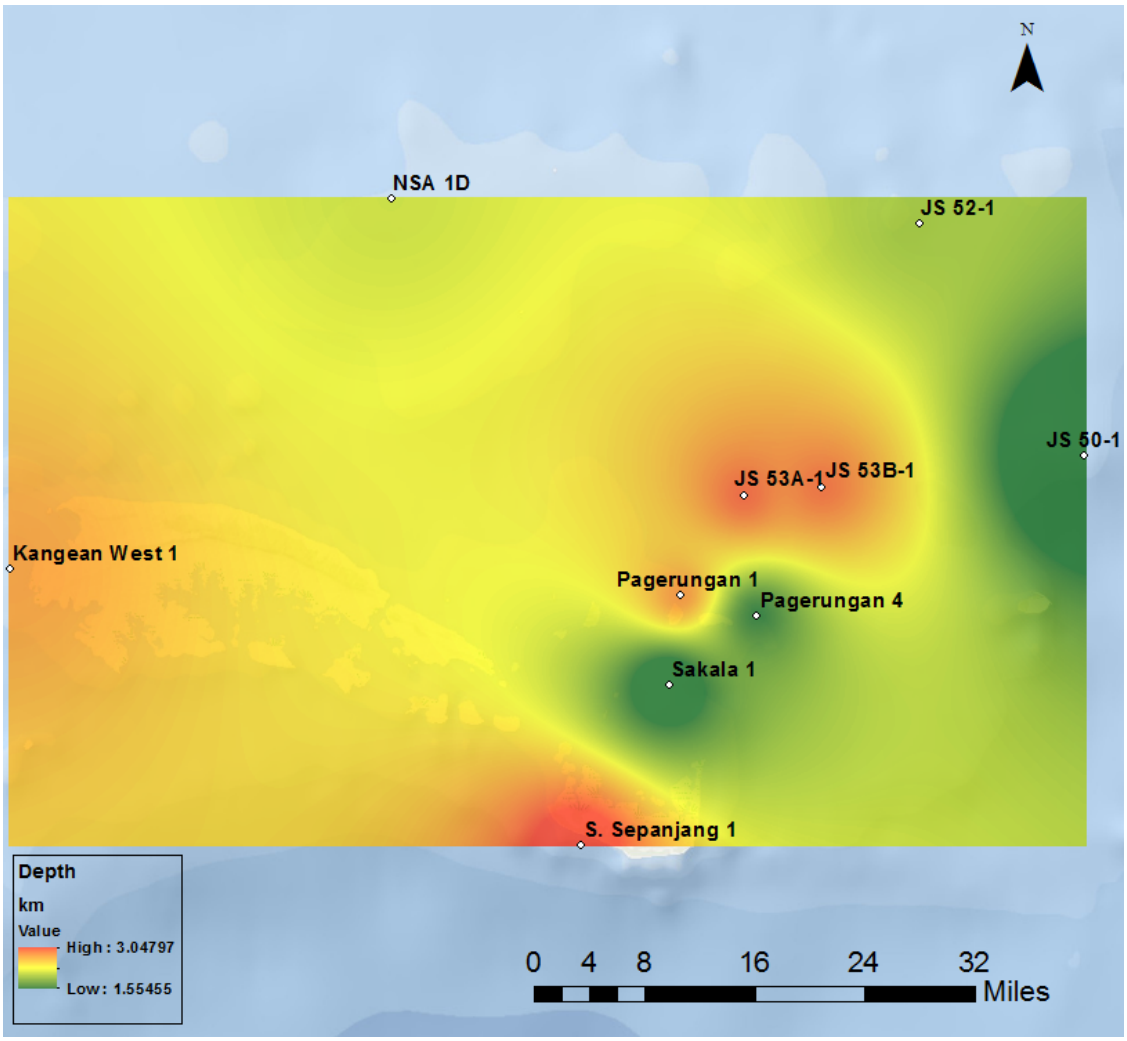

Appendix L

Map showing study area thermal conductivities (k) in W/m*K.

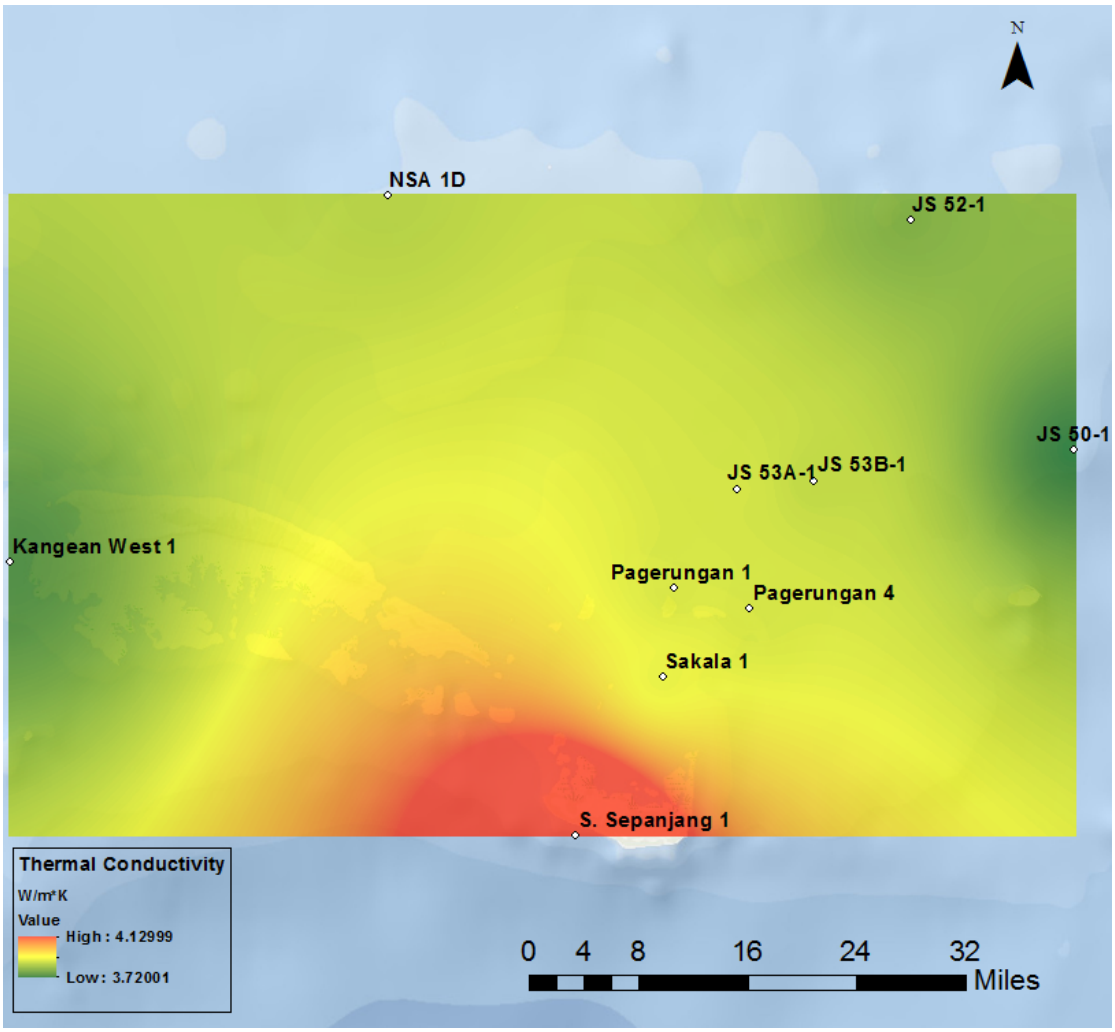

Appendix M

Map showing study area geothermal gradients (ΔT/z) in °C/km.

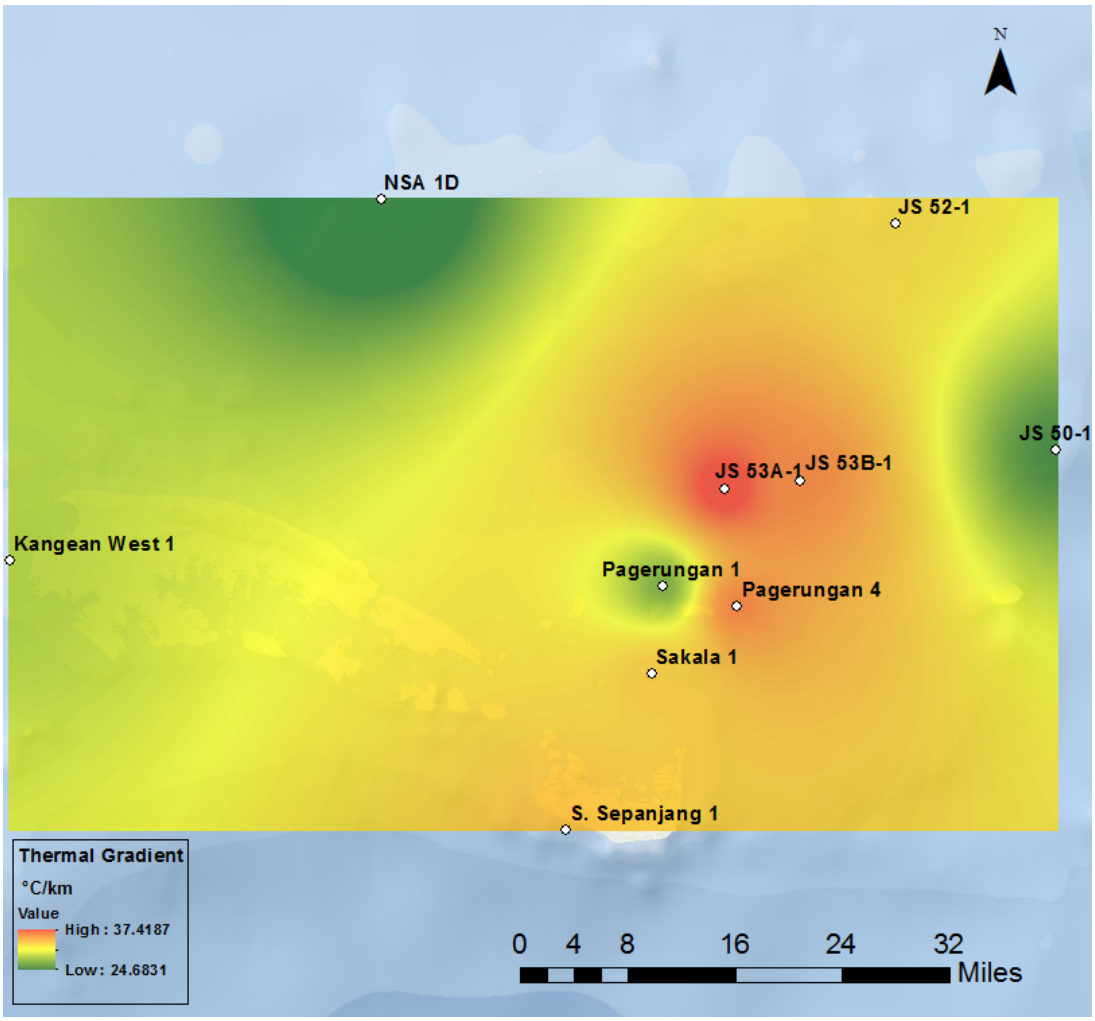

Appendix N

Heat flow map of Indonesia published by the Indonesian Petroleum Association and Southeast Asian Petroleum Exploration Society (Hall, 2002(a)).